Real-time power system oscillation monitoring using synchrophasor measurements

T. van Rooyen

22144153

Dissertation submitted in fulfilment of the requirements for the degree *Magister* in Electric and Electronic Engineering at the Potchefstroom Campus of the North-West University

Supervisor: **Prof. A.P.J. Rens**

November 2015

Declaration

I, T. van Rooyen hereby declare that the dissertation entitled "Real-time power system oscillation monitoring using synchrophasor measurements" and the material therein is my own original work except where specific reference is made by name or in the form of a numbered reference. The work herein has not been submitted to any other university or institution for examination.

TvRooyen

T. van Rooyen

Student number: 22144153

Signed on the 10th day of December 2015 at Potchefstroom.

Abstract

Advanced Measurement Infrastructure (AMI) constitutes one aspect necessary to realise a Smart Grid. Advanced monitoring is necessary for reliable operation and control of a modern power system.

Enabling measurement instrumentation to perform multiple measurement functions has benefits in creating versatile monitoring systems that is available to all levels of network management operations. Power system instrumentation that can record network coherent data with sufficient certainty in time-stamping to be within the IEEE C37.118.1 requirement for voltage and current synchrophasor has become affordable and accessible in general.

Methods for Low Frequency Oscillation (LFO) monitoring in power systems are evaluated from first principles. These monitoring functions are traditionally exclusively available through specialised hardware and software solutions in Wide Area Monitoring Systems (WAMS). Similar features can be made available cost-effectively by setting proper requirements to the signal analysis required to extract the LFO characteristics. Minimal sophistication should be required in the software needed for this purpose. This is demonstrated to be possible.

Two LFO monitoring methods, with vastly different mathematical underpinnings, were chosen according to their potential for real-time monitoring of LFOs. The modified Yule-Walker method fitting an ARMA model, and a wavelet method using orthogonal wavelet bases were used. The opportunity for real-time operational application of the LFO results from the two methods are comprehensively studied.

The two methods were first tested on simulated power system data. Results confirmed the ability of both methods to characterise LFOs in recorded data with sufficient accuracy and within reasonable processing time. Advantages and disadvantages are substantiated from the results obtained.

Field data were emulated and recorded by the synchrophasor recorders used in this research. Results obtained by the LFO analysis applied to this data, indicated that the measurement instruments used does not introduce additional inaccuracies in the two methods.

A case study of a Southern African transmission line validated the potential value of both methods in LFO monitoring of real power systems. Practical synchrophasor data were recorded over a 12-month period for this purpose.

It is shown that typical WAMS functions do not need to be the exclusive domain of data produced by PMUs at transmission level. Power system instrumentation that record network data coherently can also produce synchrophasor data and minimal sophistication is needed to extract LFO information. A cost-effective solution to obtain additional information on small signal stability performance of power systems is possible and can be deployed at all levels of power system operation.

Keywords: *Smart grid, Wide Area Monitoring Systems, Synchrophasor data, Low Frequency Oscillations*

Contents

List of Figures

List of Tables

List of Acronyms

AMI	Advanced Measurement Infrastructure
LFO	Low Frequency Oscillation
WAMS	Wide Area Monitoring System
PMU	Phasor Measurement Unit
PQ	Power Quality
ARMA	Auto Regressive Moving Average
MYW	Modified Yule-Walker
CSD	Cross Spectral Density
PSD	Power Spectral Density
CWT	Continuous Wavelet Transform

List of Symbols

Chapter 2

Power-Angle Relationship of a Synchronous Machine

P	Active power transferred over line
V_G	Voltage magnitude at generator
V_M	Voltage magnitude at motor
X_G	Reactance of generator
X_M	Reactance of motor
X_L	Reactance of line
X_T	Total reactance of two-machine system
δ	Angular separation of synchronous machine rotors

Small Signal Stability Analysis by State Space Model

$\overline{x}$	State vector
$\overline{u}$	Vector of inputs to state space system
$\overline{f}$	Vector of functions describing state space system
$\overline{g}$	Vector of functions relating input vector and state vector to system outputs.
$\overline{y}$	Output vector
$\overline{x_0}$	System state operating point

$\overline{x_0}$	System input operating point
$\Delta\overline{x}$	Small perturbation of system state vector
$\Delta\overline{u}$	Small perturbation of system input vector
A	State matrix
B	Input matrix
C	Output matrix
D	Feedforward matrix
λ_i	i-th eigenvalue of state matrix
f	Mode frequency in Hertz
ω	Mode frequency in radians
ζ	Mode damping
$\overline{\phi}_i$	i-th right-eigenvector
$\overline{\psi}_i$	i-th left-eigenvector
Φ	Modal matrix containing all right-eigenvectors
Ψ	Modal matrix containing all left-eigenvectors
$\overline{z}$	Decoupled state variables
Λ	Matrix containing all eigenvalues on the diagonal

Synchrophasor Measurements

$x(t)$	Arbitrary waveform
X_m	Maximum of waveform
ω	Frequency in radians
t	Time
ϕ	Instantaneous phase angle of waveform relative to cosine reference at nominal system frequency
f_0	Nominal system frequency
$f(t)$	System frequency as function of time
$g(t)$	Difference between system frequency and nominal frequency as function of time
$\boldsymbol{X}$	Synchrophasor representation of waveform

Chapter 3

Linear Ambient Method

$y(t)$	Measured dataset
$A(z)$	Polynomial of zeros for ARMA model in z-domain
$B(z)$	Polynomial of poles for ARMA model in z-domain
$e(t)$	White noise with variance σ^2
z^{-1}	Unit delay operator
$A(\omega)$	Polynomial of zeros for ARMA model in frequency domain
$B(\omega)$	Polynomial of poles for ARMA model in frequency domain
a_i	Coefficients of ARMA zero polynomial
b_j	Coefficients of ARMA pole polynomial
$r(k)$	Autocorrelation function of measured dataset $y(t)$
R	Matrix containing autocorrelation values for MYW equations
$\overline{a}$	Vector of ARMA pole polynomial coefficients
$\overline{r}$	Vector of autocorrelation values for MYW equations
$\widehat{r}(k)$	Estimated autocorrelation values for measured dataset $y(t)$
z_i	z-domain roots of ARMA pole polynomial
s_i	s-domain roots of ARMA pole polynomial
T	Sampling period of measured signal
B_{ji}	Residue of the z-domain root z_i for signal j
Z	Matrix containing z-domain roots for mode selection
$\overline{B}_j$	Vector of residues for mode selection
$\overline{r}_j$	Vector of autocorrelation values for mode selection
E_i	Pseudo energy of mode i
$\xi(\omega)$	PSD of rational signal
γ_k	Covariance sequence of MA part of ARMA model

$y_k(t)$, $y_l(t)$	Measured datasets
$Y_k(\omega)$, $Y_l(\omega)$	Fourier transformation of measured datasets
$S_{kl}(\omega)$	Cross-spectral density function of measured datasets $y_k(t)$ and $y_l(t)$
$S_{kk}(\omega)$	Power-spectral density function of measured dataset $y_k(t)$
$Z_i(\omega)$	Fourier transformation of decoupled state variable i
$\overline{U}_i(\omega)$	Fourier transformation of state space input vector
ω_i	Frequency of mode i
$\angle S_{kl}(\omega_i)$	Angle of CSD function at mode frequency
$S_{kk}(\omega_i)$	Power-spectral density function at mode frequency

Non-linear/Non-Stationary Method

$\varphi(t)$	Time domain mother wavelet
$\varphi_{u,s}(t)$	Scaled and translated daughter wavelet
$Wf(u,s)$	Continuous wavelet transform
C_{Φ}	Result of admissibility condition
$\Phi(\omega)$	Fourier transform of mother wavelet
$F(t)$	Time domain result of inverse CWT
$C(s,u)$	Wavelet coefficients of CWT
$C(s)$	Wavelet coefficients of CWT where translation effect is ignored
$W_s(t)$	Daughter wavelet function of wavelet used as new base for wavelet method
$\widehat{C}(s)$	Estimation of wavelet coefficients
f_s	Signal sampling frequency
$P(s)$	Matrix of wavelet coefficients of different signals
$P_{xy}(s)$	PSD matrix
$\widehat{\widehat{C}}(s)$	Result of averaging $\widehat{C}(s)$ over multiple analysis windows

R_i	Residues in Prony formulation of oscillatory signal
a_i	Coefficients of z-domain roots of oscillatory signal
$W_{Morlet}(t)$	Morlet wavelet in time domain
$w_{Morlet}(\omega)$	Morlet wavelet in frequency domain
ω_0	Central frequency of wavelet
s_j	Scales selected for use in wavelet method

Chapter 1

Introduction

... where topics regarding current trends and concepts in a modern power system is discussed to create context and motivation for the rest of the research.

1.1 Introduction

This chapter presents the context of the research. Trends in the modern power system are evaluated and opportunities to enhance Smart Grid functionality, identified.

1.2 Challenges in the Modern Power System

Most of the power system consists of ageing infrastructure. Power system design philosophies of earlier decades did not cater for the advances and trends that is seen in the modern power system. The power system was designed for largely centralised generation at transmission voltage level, with power flow in one direction.

A move towards distributed generation is seen currently. Sources of generation are typically of smaller capacity and more likely to be connected at distribution voltage level [1].

This is the case with many renewable sources of generation. Renewable generation connect at distribution voltage level, mostly by power electronic devices. The resulting power flow can be in the opposite direction as to which the power system was designed for. Power electronic equipment also introduces nonlinear interaction to the power system.

Modern power systems normally consist of large interconnected networks with power exchanged between networks. Advanced monitoring functions are needed for reliable operation and control.

Power system blackouts resulting from inter-area instability have to be avoided. Modern economies require a predictable and reliable source of electricity [1].

1.3 The Smart Grid

The term Smart Grid has often been used in recent years to describe the vision for the power system of the future. The Smart Grid is defined as [2]:

> *"The Smart Grid encompasses the integration of power, communications, and information technologies for an improved electric power infrastructure that serves loads while providing for an ongoing evolution of end-use applications."*

The Smart Grid is an attempt to define a vision to address the difficulties and challenges found in the modern power system.

Technology from various fields is needed to realise the envisioned Smart Grid. Among these are Advanced Measurement Infrastructure (AMI) that enable improved monitoring functions.

1.4 Context and Motivation of Research

This research evaluates the innovative use of AMI that can find application in the Smart Grid architecture. A PMU is no longer necessarily the only source of synchronized data in a power system. GPS time-stamping (for example) is widely accessible and in combination with hardware capable of accurate voltage and current measurement, synchrophasor data can be generated by instruments all over the power system. It is no longer the domain of specialized application in transmission systems only.

The hardware in use has found application in the field of Power Quality (PQ). Firmware was developed to primarily enable Class A IEC 61000-4-30 PQ measurements, but secondarily, it simultaneously records voltage and current synchrophasors as all recordings are time-stamped within the requirements of the synchrophasor standard, the IEEE C37.118.1-2011.

Any similar advanced metering equipment could become a source of synchrophasor data. It is therefore expected that the availability of synchrophasor data will be widespread, allowing new innovation in power system operation and control.

Synchrophasor data from this instrument is evaluated for small signal stability monitoring with the view to enable widespread dissemination of power system dynamic behaviour. Small signal stability monitoring functions are generally exclusively available through expensive Wide Area Monitoring Systems (WAMS) software and specialised measurement instrumentation.

Operational value of small signal stability monitoring depends on the accuracy of results, but also on the capability of a monitoring method to produce outputs in real-time. Both of these aspects are addressed in the testing of the monitoring methods.

The methods are tested and verified with simulated data. A case study of a Southern African transmission line is used to validate the potential of these methods when based on field data.

1.5 Conclusion

Unique opportunities exist to face new challenges in the modern power system. Innovation to improve the control and operation of the power system has emerged to support Smart Grid concepts.

This research addresses how AMI can enable some of the Smart Grid visions. The benefits of existing monitoring systems can be extended if based on versatile instrumentation.

Chapter 2

Power System Oscillation and Monitoring

... where the theoretical background to the research will be established.

2.1 Introduction

In this chapter the theoretical background to various topics are discussed on which following chapters are based. Several concepts are introduced. Different focuses in power system stability are covered and rotor angle stability is elaborated on according to the focus of this research. The mathematical representation of a power system response to small perturbations (small signal stability) is presented.

The rest of this chapter focuses on methods of monitoring small signal stability, monitoring systems in practical use and the relevant instrumentation needed to realise such systems.

2.2 Power System Stability

Power system stability is defined as the ability of the power system to remain in equilibrium under normal operating conditions or return to equilibrium after it has been subjected to a disturbance.

Disturbances can be small or large. Small disturbances in the form of random load switching is continually present in the power system. The system must remain in equilibrium under these conditions to match the generation to the changing load. The system must further be able to remain stable after a larger disturbances like a major system fault or generator trip.

The broader problem of power system stability can be divided into subsections. This is necessary as power system stability is a very broad topic, influenced by a number of factors and manifesting instability in different forms. Different tools are needed to investigate different aspects of the power system stability problem. Power system stability can be divided as shown in Figure 2.1 [3].

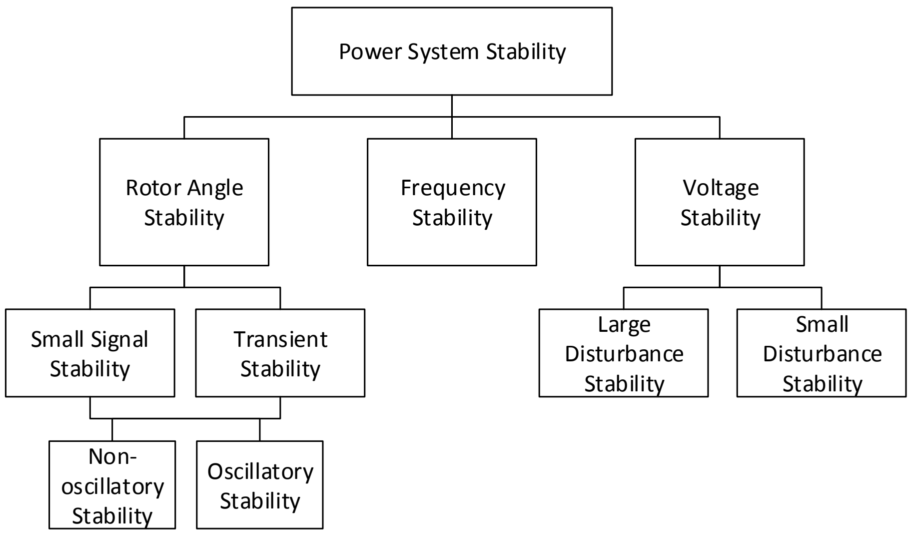

Figure 2.1: Classification of power system stability.

This research is concerned with aspects of rotor angle stability. Rotor angle stability will be discussed in detail in the following sections, while frequency stability and voltage stability will not be discussed.

2.3 Rotor Angle Stability

Rotor angle stability refers to the ability of the power system to stay in synchronism under normal and disturbance conditions. Synchronism is influenced by the ability of the power system to maintain equilibrium between electromagnetic and mechanical torques operating on the synchronous machine [4]. The field of rotor angle stability thus involves the study of electromechanical oscillations found in the power system.

2.3.1 Power-Angle Relationship of a Synchronous Machine

It is necessary to understand the non-linear relationship between power and angular position of a synchronous machine.

Consider two synchronous machines connected via a transmission line as shown in Figure 2.2. Machine A is operated as a generator and machine B as a motor. The transmission line has reactance X_L and negligible resistance and capacitance. Both machines are modelled as a voltage source and an effective reactance. Figure 2.3 presents the described model for the two-machine system.

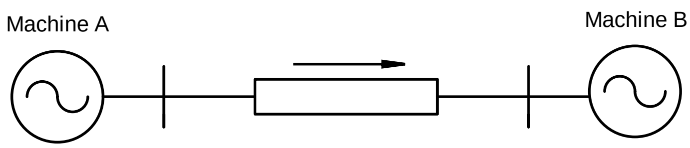

Figure 2.2: Two-machine system single line diagram.

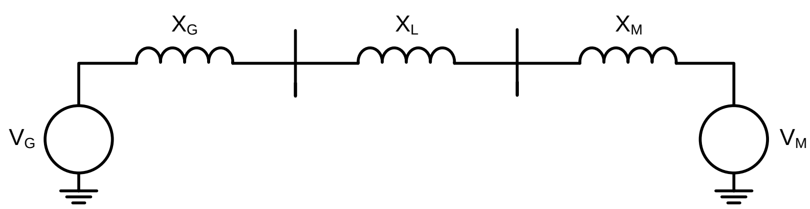

Figure 2.3: Two-machine system model.

Angular separation of the synchronous machine rotors are the mechanism by which power is transferred from the generator to the motor. Power transfer is determined by:

$$P = \frac{V_G V_M}{X_T} sin\delta \tag{2.1}$$

where

- V_G and V_M are the voltages of the generator and motor
- X_T is the total reactance given by $X_T = X_G + X_M + X_L$
- δ is the angular separation of the synchronous machine rotors

The power transferred is directly proportional to the sine of the angular separation, as seen from Equation (2.1). This relationship is depicted in Figure 2.4.

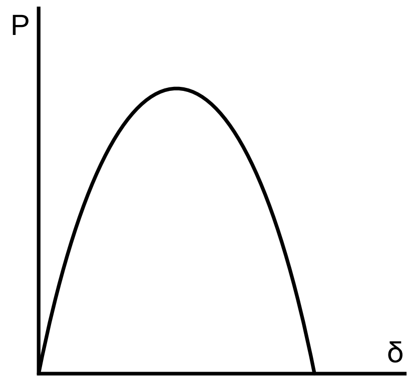

Figure 2.4: Power-angle relationship.

When the angular separation is 0°, no power is transferred. Power transfer increases with an increasing angular separation, until angular separation reaches 90° (for the simplistic system in Figure 2.2). Angular separation beyond 90° causes a decrease in power transfer.

This simplistic two-machine model is useful in describing the power-angle relationship, however many assumptions are made and the model is highly simplistic.

In a practical multi-machine system, angular separation similarly affects power transfer as in the two-machine case. The complex interaction of multiple points of generation and load result in limiting values for angular separation that is not as easily determined as in the simplistic two-machine case (90°) [4].

2.3.2 Rotor Angle Stability and Synchronism

Synchronism between machines is maintained by means of forces that act to counter the affect of any other influencing forces aiming to change the behaviour of the machine with respect to other machines in the system.

When the system is in a steady state the mechanical input power and the electromagnetic output power are balanced and the speed of the machine remains constant. When a disturbance occurs, the equilibrium between input and output powers are disturbed. The machine will accelerate or decelerate due to the imbalance of forces acting on it.

If a machine is accelerating with respect to the rest of the system, its rotor position will advance ahead of the rest of the system. According to the power-angle relationship described in section 2.3.1, the increased angular separation will increase the power generated by the machine. The larger load on the machine counteracts the accelerating force in an effort to regain equilibrium.

Synchronism will depend on whether the increased load on the accelerating machine provides sufficient torque to decelerate the machine before the limiting value for angular separation is reached. Angular separation beyond the limiting value will cause a decrease in electromagnetic torque, further increasing the angular separation due to growing unbalanced forces on the machine. For such a case, the machine loses synchronism and instability can result [4, 5].

Change in torque on a machine following a disturbance is divided into synchronising torque and damping torque. Both components are necessary to maintain synchronism. Insufficient synchronising torque leads to non-oscillatory instability, while insufficient damping torque causes oscillatory instability.

Transient Stability

Transient stability refers to the ability of the power system to maintain synchronism after a large disturbance like a generator trip or short circuit. Rotor angle swings and associated power transfers are expected to be large.

It can be expected that a large disturbance will alter the structure of the power system so that different system conditions will define steady state operation after the transient event.

Transient rotor instability mainly occur in the form of non-oscillatory instability. Synchronising torque following a large disturbance is insufficient to maintain synchronism after the first large excursion of rotor angle.

Instability may also occur as a result of superposition of oscillatory modes excited during the transient event, leading to instability after the first large excursion [3, 5]. Changes in the structure of the power system after the transient event can cause lowered oscillation damping, exciting oscillatory modes that can cause instability.

Small-Signal Stability

Small signal stability refers to the ability of the power system to maintain synchronism after being subjected to a small disturbance. A disturbance is regarded as small if the response of the power system can be modelled by linearising the non-linear power system equations around a given operating condition [3].

Small signal instability is mainly due to oscillatory instability. Small disturbances excite oscillatory modes in the system. When insufficient damping torque is available, instability results.

Random load switching that is always present in the power system is an example of a small disturbance that can excite oscillatory modes [6–8]. Random load switching can be modelled as stochastic white noise inputs. When the only excitation to oscillatory modes is low amplitude random variations which can be modelled as white noise inputs, the power system is said to be in an ambient condition.

Oscillations in the power system (also referred to as Low Frequency Oscillations (LFOs)) differ and can be classified according to which parts of the system are contributing towards the oscillation.

Local modes of oscillation occur when one machine oscillates against the rest of the power system. This type of oscillation is described as local because the behaviour is localised and all controls necessary to control the oscillation are normally in one central location like a single power plant. Local area modes exist in the 1 - 2 Hz range [9].

Inter-area oscillations present a bigger concern to power system stability. Machines in one area oscillating against machines in a different area form an inter-area oscillation. Inter-area oscillations are found in the 0.1 - 1 Hz range [9].

This type of oscillation is caused when different groups of closely coupled machines are connected via tie-lines with significant impedance (weak tie-lines). Large power transfers through the power system can further reduce damping of inter-area modes. Inter-area oscillations can become a big concern in large interconnected power systems as the conditions described above are likely to be found.

The dynamics influencing inter-area oscillations are much more complex than that of local area oscillations. The dynamics of the entire system determine the characteristics of an inter-area mode. This makes inter-area oscillations much harder to control, as no single control is solely responsible for the behaviour, rather all controls influencing the dynamics of the system.

The large geographical scale over which inter-area oscillations occur pose further difficulties in monitoring this phenomenon, unlike local area modes where oscillating machines and controls are situated in a localised area.

2.4 Small Signal Stability Analysis by State Space Model

To investigate small-signal stability the power system is described by a set of state equations, linearised around an operating point. Several textbooks are available describing the state space representation of a dynamic system [4, 10]. The notation used in [4] is adopted for this research.

2.4.1 State-Space Model

A set of n first-order non-linear ordinary differential equations can be used to describe the dynamic behaviour of the system:

$$\dot{x}_i = f_i(x_1, x_2, ..., x_n; u_1, u_2, ..., u_r; t) \qquad i = 1, 2, ..., n \tag{2.2}$$

This set of equations can be expressed in matrix notation by defining

$$\overline{x} = \begin{bmatrix} x_1 \\ x_2 \\ \vdots \\ x_n \end{bmatrix} \qquad \overline{u} = \begin{bmatrix} u_1 \\ u_2 \\ \vdots \\ u_r \end{bmatrix} \qquad \overline{f} = \begin{bmatrix} f_1 \\ f_2 \\ \vdots \\ f_n \end{bmatrix}$$

The vector $\overline{x}$ contains the n state variables x_i and is called the state vector. The vector $\overline{u}$ contains the r inputs to the system. If the state variables are not explicit functions of time, the system can be expressed as:

$$\dot{\overline{x}} = \overline{f}(\overline{x}, \overline{u}) \tag{2.3}$$

The output of the system can be expressed as

$$\overline{y} = \overline{g}(\overline{x}, \overline{u}) \tag{2.4}$$

where

$$\overline{y} = \begin{bmatrix} y_1 \\ y_2 \\ \vdots \\ y_m \end{bmatrix} \qquad \overline{g} = \begin{bmatrix} g_1 \\ g_2 \\ \vdots \\ g_n \end{bmatrix}$$

The vector $\overline{y}$ contains the m outputs while $\overline{g}$ contains the non-linear functions relating the state vector $\overline{x}$ and the inputs $\overline{u}$ to the outputs $\overline{y}$.

2.4.2 Linearisation of State-Space Model

Small signal stability analysis is concerned with the behaviour of the power system around a certain operating point. To this end, Equation (2.3) and (2.4) are linearised around an operating point. Let the operating point of interest be defined by $\overline{x}_0$ and $\overline{u}_0$. Small perturbations around this operating point can be defined in the state and input vectors as:

$$\overline{x} = \overline{x}_0 + \Delta\overline{x} \qquad \overline{u} = \overline{u}_0 + \Delta\overline{u} \tag{2.5}$$

The Δ operator implies a small perturbation. Equation (2.5) is now substituted into Equation (2.3) and (2.4), yielding:

$$\begin{aligned} \dot{\overline{x}} &= \dot{\overline{x}}_0 + \Delta\dot{\overline{x}} \\ &= \overline{f}[\overline{x}_0 + \Delta\overline{x}, \overline{u}_0 + \Delta\overline{u}] \end{aligned} \tag{2.6}$$

$$\begin{aligned} \overline{y} &= \overline{y}_0 + \Delta\overline{y} \\ &= \overline{g}[\overline{x}_0 + \Delta\overline{x}, \overline{u}_0 + \Delta\overline{u}] \end{aligned} \tag{2.7}$$

By applying Taylor series expansion and simplification the linearised state space equations are found:

$$\Delta\dot{\overline{x}} = A\Delta\overline{x} + B\Delta\overline{u} \tag{2.8}$$

$$\Delta\overline{y} = C\Delta\overline{x} + D\Delta\overline{u} \tag{2.9}$$

where

$\Delta\overline{x}$ is the state vector
$\Delta\overline{y}$ is the output vector
$\Delta\overline{u}$ is the input vector
A is the state matrix
B is the input matrix
C is the output matrix
D is the feedforward matrix

2.4.3 Eigenvalues

The stability of the state space system can now be determined. This is done by inspecting the eigenvalues of the state matrix A. The eigenvalues λ_i are the non-trivial solutions ($\overline{\phi} \neq 0$) of:

$$A\overline{\phi} = \lambda\overline{\phi} \tag{2.10}$$

where $\overline{\phi}$ is a $n \times 1$ vector. Eigenvalues are calculated by finding the n solutions of

$$\det(A - \lambda I) = 0 \tag{2.11}$$

The eigenvalues λ_i for $i = 1, ..., n$ are found. If A is a real matrix, the eigenvalues have the form $\lambda_i = \sigma_i + j\omega_i$. The time domain response of a mode corresponding to the eigenvalue λ_i is described by $e^{\lambda_i t}$. Eigenvalues determine stability. The time domain response of a mode is observed to determine whether it is stable or not.

A real eigenvalue indicates a non-oscillatory mode. Negative real eigenvalues represent a stable mode due to an exponential decay of the mode amplitude in its time domain response. Positive real eigenvalues represent unstable modes, identified by an exponentially increasing time domain response.

Complex eigenvalues will occur in conjugate pairs, indicating an oscillatory mode. The time domain response of a mode with a complex eigenvalue has an oscillatory behaviour (according to Euler's law). Similar to real eigenvalues, the real part of the eigenvalue determines if the mode is stable or not (real part produces exponential growth or decay of the mode as a function of time). For a complex eigenvalue, the frequency of oscillation is given by

$$f = \frac{\omega}{2\pi} \tag{2.12}$$

and the damping ratio is given by

$$\zeta = \frac{-\sigma}{\sqrt{\sigma^2 + \omega^2}} \tag{2.13}$$

2.4.4 Eigenvectors

All eigenvalues found will satisfy Equation (2.10), thus

$$A\overline{\phi}_i = \lambda_i \overline{\phi}_i \qquad\qquad i = 1, ...n \tag{2.14}$$

for the eigenvalue λ_i. The vector $\overline{\phi}_i$ is called the right-eigenvector and has the form

$$\overline{\phi}_i = \begin{bmatrix} \phi_{1i} \\ \phi_{2i} \\ \vdots \\ \phi_{ni} \end{bmatrix}$$

The left-eigenvector $\overline{\psi}_i$ for eigenvalue λ_i is given by

$$\overline{\psi}_i A = \lambda \overline{\psi}_i \qquad\qquad i = 1, ...n \tag{2.15}$$

where

$$\overline{\psi}_i = \begin{bmatrix} \psi_{1i} & \psi_{2i} & \dots & \psi_{ni} \end{bmatrix}$$

Modal matrices containing all right and left eigenvectors are formed:

$$\Phi = \begin{bmatrix} \overline{\phi}_1 & \overline{\phi}_2 & \dots & \overline{\phi}_n \end{bmatrix} \tag{2.16}$$

$$\Psi = \begin{bmatrix} \overline{\psi}_1^T & \overline{\psi}_2^T & \dots & \overline{\psi}_n^T \end{bmatrix}^T \tag{2.17}$$

For normalised eigenvectors, it holds that

$$\Psi\Phi = I \qquad\qquad \text{or} \qquad\qquad \Psi = \Phi^{-1} \tag{2.18}$$

To better understand the behaviour of a system, it is necessary to eliminate cross-coupling between state variables. The rate of change of the state variables are linear combinations of all the state variables according to Equation (2.8). A new set of state variables contained in the vector $\overline{z}$ is needed and defined by

$$\Delta\overline{x} = \Phi\overline{z} \tag{2.19}$$

Through the transform in Equation (2.19) the state space system in Equations (2.8) and (2.9) can be decoupled so that each state variable in $\overline{z}$ is associated with only one mode. The decoupled state space system is given by

$$\dot{\overline{z}} = \Lambda\overline{z} + B'\Delta\overline{u} \tag{2.20}$$

$$\Delta\overline{y} = C'\Delta\overline{z} + D\Delta\overline{u} \tag{2.21}$$

where Λ is a diagonal matrix containing all the eigenvalues in the diagonal and

$$B' = \Phi^{-1}B \tag{2.22}$$

$$C' = C\Phi \tag{2.23}$$

From Equation (2.19) we can see that the right-eigenvector Φ provides mode shape. For each mode, the response of a particular state variable can be examined. The response of the state variable x_k for the ith mode is given by ϕ_{ki} in $\overline{\phi}_i$. Mode shape is normally a complex number. The magnitude of ϕ_{ki} indicates the intensity with which x_k participates in the oscillation of the ith mode. The angle of ϕ_{ki} indicates the phasing of the oscillation in x_k for the ith mode [11, 12].

Right-eigenvector values are traditionally normalised to provide a consistent method for reporting these values. The normalised solution remains valid as $k\overline{\phi}_i$ is also a valid solution for Equation (2.14) [12].

2.5 Oscillation Monitoring Methods

Monitoring of power system oscillations are necessary for reliable operation of a power system. Oscillations in power systems limit power transfer capability and can cause power system instability and breakup as described in section 2.3.2. Several methods for power system oscillation monitoring have been developed.

Different approaches to electromechanical oscillation monitoring are available. Methods can be divided into groups according to the approaches taken, the fundamental mathematical foundation of the calculations and the conditions under which they are designed to work.

2.5.1 State Space Representation Methods

One approach to modal identification is to solve the set of linear equations describing the response of the power system after being subjected to a small disturbance. Eigenanalysis can be applied to gain complete knowledge of the system modes and mode shapes. For a given operating condition the power system response can be completely described by solving the state space model.

The state space model and eigenanalysis were presented in section 2.4 [8]. The dynamics driving the response of the power system can be found using this fundamental approach.

This approach holds several disadvantages for practical use. Complete knowledge of the system state matrix is needed. The system state matrix is likely to be based on models of the power system, thus it inherently includes any inaccuracies in the system models.

Eigenanalysis can easily be performed for small systems to find all the modes in the system. As the system increases in size, calculation of all modes become impractical due to restraints in computational power [8]. Typically, only a few modes are computed for a large system. Practical interconnected systems become too large to fully analyse using this approach. As a result, these methods are better suited towards offline system studies than online, real-time monitoring. System structure and operating point is time-varying and can not be included in the system model in real time [13].

2.5.2 Measurement Based Methods

Methods designed to use time-domain data provides an alternative for the modal analysis of power systems. These methods are designed to extract modal information from recorded or simulated time-domain signals. These methods do not require any knowledge regarding the structure of the power system. Measurement based methods can benefit various studies, e.g. stability monitoring, model validation and control design.

Measurement based methods also have limitations. Data availability and accuracy will influence the quality of the result. Solving the state space model can provide complete insight into the system modes, whereas only modes observable in the time-domain data can be identified. Not all system modes will be observable in every recorded parameter [8]. Well-damped modes will not be easily observable and can compromise the quality of the result. Measurement based methods are also prone to the effects of noisy recorded signals which can further compromise the result.

It is important to understand the advantages and limitations inherent in any method, in order to choose a method suitable for the problem. Measurement based methods will be further categorised according to the data they are suited to operate on. The condition and response of the power system determine which category of methods is best suited to analyse the data.

The list of methods is not at all exhaustive. Many more methods and variations are available. The aim is to summarise the most well known methods according to unifying criteria and discussing advantages and disadvantages to the use of the methods.

Linear Ringdown Methods

Ringdown methods are suited to perform modal identification on data measured after the power system experienced a transient event. The first developed methods of measurement based modal identification were ringdown methods. Ringdown methods assume that the transient response of the power system may be described by a set of linear equations [8].

Probably the most well known method based on published literature is the Prony method [14, 15]. Since the method has been introduced in [14], many variations and adaptations of the method have been developed and tested [16–23].

The Prony method describes measured datasets by decomposing it into linear sums of decaying sinusoids [23]. The decaying sinusoids are represented as complex exponential terms.

The Prony method is also referred to as a polynomial method in that it involves finding the roots of the characteristic polynomial in the z-domain. Two steps are required to complete the Prony method. The coefficients of the polynomial are first found and then processed to find the roots of the polynomial [24].

The Prony method is efficient and accurate when applied to equally spaced transient data, but can be extremely influenced by noise in the measured data [24].

The Eigensystem Realisation Algorithm (ERA) employs singular value decomposition (SVD) of a Hankel matrix to find the system matrices and determine system size. The eigenvalues of the system matrix provides the poles of the polynomial in the z-domain describing the linear response of the system [8, 25]. This algorithm is also employed in other fields of study, especially aerospace research. This method attracted interest within the power system community as it is easy to implement, it is a multivariate method and can identify closely spaced modes [26]. Examples of implementation, testing and use can be found in [13, 17, 27].

The Matrix Pencil (MP) method was first used in the field of communication theory for pole estimation from electromagnetic transient response of antennas [24,28]. This method has the advantage of being robust to noise in the recorded signal. In contrast to the Prony method, the Matrix Pencil method finds the poles of the z-domain polynomial in a single step by solving a generalised eigenvalue problem [8]. The method is computationally more efficient and displays better statistical characteristics than the Prony method [24].

Linear Ambient Methods

Ambient methods are specifically developed to use ambient measured data for modal analysis (refer to section 2.3.2 for the definition of a power system in an ambient condition) [7, 8, 29].

These methods are designed to be able to perform modal analysis when very low levels of oscillatory excitation are available. Unless a transient event occurs, the power system is in an ambient condition. It is expected that the power system is mostly in an ambient condition as transient events should not be a regular occurrence. For this reason, most ambient methods can also provide accurate answers in the case of a transient event when significant excitation to oscillatory modes is available. It has been found that modal accuracy of ambient methods improve when a ringdown is present in the data [30].

Ambient methods can be classified in various ways according to the underlying assumptions made and the method of processing the data.

Parametric methods assume that a model with a known form can be fitted to the data. The modal characteristics of the data can then be found from the parameters of the model.

Non-parametric methods in contrast extract all modal information from the signal itself. Parametric methods require assumptions be made regarding the content of the signal in order to fit a model. If these assumptions are made correct and a parametric method succeeds in fitting a model that closely approximates the data, a more accurate representation of the modal content can generally be found in comparison to using a non-parametric method [31]. Non-parametric methods are useful when little is known about the signal to be analysed.

Methods can also be classified as a *block processing* method or *recursive method.* Block processing methods base the results on a window of data. For each successive result, the window is moved forward in time and the calculation repeated on the new data inside the window.

Recursive methods update the result for each new sample of data. Current results are a combination of old results and results from the newest sample. Instead of employing a fixed window, a forgetting factor is used to determine how many previous results are considered when updating the result with the newest values.

Some methods perform calculations in the *time-domain*, while others perform all calculations in the *frequency domain*, providing an additional classification criterion. The first work in this field employed a frequency domain method [32].

Numerous methods based on the Yule-Walker (YW) equations are available in the literature. These parametric methods aim to fit an autoregressive (AR) or autoregressive moving average (ARMA) model to measured data. Variations of the method include the YW method fitting and AR model [29, 33], the modified Yule-Walker (MYW) method fitting an ARMA model [34, 35], the YW method with spectral analysis which performs some calculations in the frequency domain [33], and methods developed to use multiple signals as input [36, 37].

The Regularised Robust Recursive Least Squares method (R3LS) is a recursive method aiming to fit an autoregressive moving average exogenous (ARMAX) model [38]. In [39] a least mean squares (LMS) approach is used. The Numerical Algorithm for Subspace State Space System Identification (N4SID) was used in [40] and a frequency domain method called Frequency Domain Decomposition in [41].

In [42–44] a method using Independent Component Analysis (ICA) and the Random Decrement (RD) technique is presented and tested. Mode frequencies are estimated by decomposing a signal into its frequency components by using ICA. Mode damping is estimated by the RD technique. The RD technique was first developed by NASA to serve as an early identifier of structural failure in the space shuttles [45–47].

The mentioned methods provide estimations of the frequency and damping of oscillatory modes. Mode shape must also be found to fully characterise the oscillation. Mode shape can be calculated by spectral analysis of the measured signal as was done in [11] or by using a method to estimate the transfer function generating the signal [12].

Nonlinear and Non-Stationary Methods

The methods in this section could also be classified under different headings, however they are presented here as they fundamentally differ from the other methods in that they are not developed on the assumption of a system behaving linearly. These methods are capable of processing signals with non-linear and non-stationary characteristics.

The behaviour of the power system is non-linear and is a challenge for modelling methods aimed at linear systems. Time-dependent control strategies and non-linear dynamics introduce non-stationary behaviour. Linear modal estimation methods are not suited to process such signals [8].

The development of non-linear and non-stationary methods is some of the more recent work done in modal estimation. A number of these methods focus on analysing data from transient events. Transient behaviour of the power system is predominantly governed by non-linear and non-stationary processes and dynamics, more so than in the ambient condition. A smaller number of methods are available that are suited to perform modal estimation from ambient data.

A number of methods and variations are based on the theory of the Hilbert-Huang Transform (HHT) [48–53]. The HHT decomposes a non-linear and non-stationary signal into nearly orthogonal basis functions and instantaneous attributes. The time localisation of the instantaneous attributes is useful for characterising time-changing phenomena in a signal [8].

Wavelet based methods are also suited to process non-linear and non-stationary signals. These methods transform a time-domain signal into the time-frequency wavelet domain. Conventional Fourier analysis can give insight into the frequency content of a signal, but information concerning the time-localisation of a frequency component is not easily found.

In wavelet theory, a wavelet function is chosen to decompose the signal. Wavelets are better suited to time-frequency localisation as they are limited in time and frequency content. This enables characterisation of the frequency content of a signal at a specific point in time [54].

Wavelet methods suited to process ringdown data can be found in [55–59]. Wavelet methods suited to ambient conditions are found in [7, 44, 60–63].

2.6 Experiences and Practical Use of Monitoring Systems

Many of the methods discussed have been implemented in practical systems to monitor power system stability. These methods are implemented along with other functionalities typically found in WAMS.

WAMS are a tool used by system operators to monitor wide-area characteristics and overall system security of the power system. Practical results and experiences from the use of these systems from a number of countries and system operators are available in the literature [11, 64–73].

Alongside small signal stability monitoring, a number of further monitoring functions are normally implemented in WAMS. WAMS systems can aid in studying system dynamics, doing offline validation of system models, wide-area disturbance recording and state estimation.

2.6.1 Experiences with WAMS

WAMS systems use measurements from Phasor Measurement Units (PMUs) as input. The high measurement rate, accurate timestamps and availability of angle data are some fo the significant advantages PMUs have over traditional SCADA systems [64]. PMUs have the potential to fulfil many roles in system monitoring normally done by different specialised devices [6, 64].

WAMS systems based on PMU measurements are challenged by the large volumes of data produced by PMUs, posing limitations in storage, transmission and processing of the data [64]. PMUs must be very reliable as they become an integral part of monitoring power system dynamics. Furthermore, it must be ensured that results from WAMS systems are presented in a manner that enables timely operator reaction to developing conditions. Studies have shown that information presented in the form of a contour map displayed in geographical context provides intuitive insight into developing system conditions [64, 67].

2.6.2 Experiences in Small Signal Stability Monitoring

System operator experience pertaining specifically to the use of small signal stability functions in WAMS are very valuable. It was found that it is easy to determine modal characteristics after a large disturbance has occurred, but very challenging to do so when excitation to the modes is small, as is the case in the ambient condition. This is especially true in the case of damping estimation.

This phenomenon can intuitively be understood as a well-damped mode will be less prominent in the measured data. Unstable modes will be easy to identify because of higher excitation [74].

This is not a concern to practical application since well-damped modes do not present a risk to system security [70]. Unstable modes, which can be estimated accurately, are the important concern for network operation.

Frequency of the mode can be calculated with better accuracy than the damping ratio in all cases. Damping ratio result can have significant variances, especially for a well-damped mode.

The accuracy of the methods is further influenced by the choice of parameters, made during implementation. Incorrect choice may lead to inaccurate results.

It was found that angular separation can be a good choice as input signal for small signal stability monitoring. Modal observability of this signal is high. This is a further motivation for the use of PMUs for WAMS measurement equipment. Angular separation can only be derived from synchrophasor measurements [74].

2.7 Synchrophasor Measurements

All discussed measurement based methods need accurate coherent data as input. Measurements must be taken at regularly spaced time intervals with accurate timestamps referenced to UTC. This is especially important for methods using more than one signal (possibly from different measurement devices) as input. Synchrophasor measurements compliant to the C37.118.1-2011 standard are ideally suited.

Synchrophasor measurements provide a way to directly compare different sets of measurements. Measurements are accurately time-stamped and referenced to UTC by GPS for example.

Consider the waveform described by

$$x(t) = X_m\ cos(\omega t + \phi) \tag{2.24}$$

Equation (2.24) can also be written as a phasor at frequency ω:

$$\begin{aligned} \boldsymbol{X} &= (X_m/\sqrt{2})\ e^{j\phi} \\ &= (X_m/\sqrt{2})\ (cos\phi + j\ sin\phi) \end{aligned} \tag{2.25}$$

where $(X_m/\sqrt{2})$ is the rms of the signal and ϕ is the phase angle.

Equation (2.25) is the synchrophasor representation of the waveform in Equation (2.24), where ϕ is defined as the instantaneous phase angle measured relative to a cosine signal at nominal system frequency and synchronised to UTC time [75]. Figure 2.5 illustrates how ϕ is measured.

Quantities such as magnitude and frequency are never a fixed value in a practical power system. It is thus necessary to expand the synchrophasor definition accordingly.

$X_m(t)$ is the magnitude defined as a function of time. By considering that frequency will also be a function of time, $f(t)$, the difference between system frequency and nominal frequency is defined by

$$g(t) = f(t) - f_0 \tag{2.26}$$

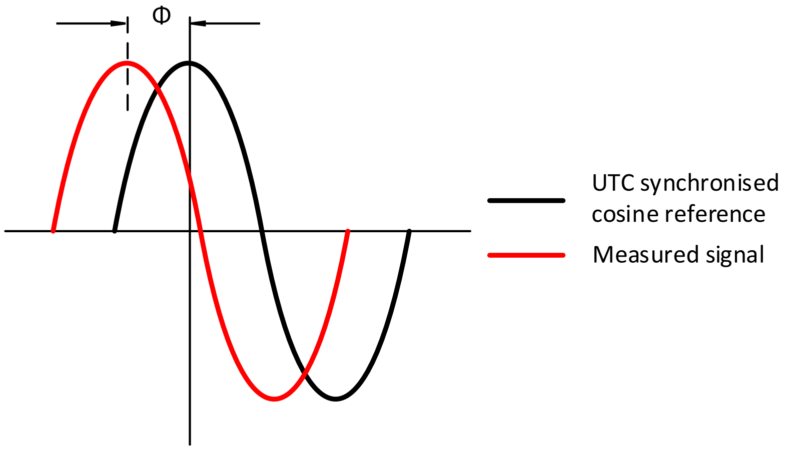

Figure 2.5: Measurement of synchrophasor phase angle ϕ for a signal at nominal system frequency.

Equation (2.24) is now expressed as:

$$\begin{aligned} x(t) &= X_m(t)\ cos(2\pi \int f dt + \phi) \\ &= X_m(t)\ cos(2\pi \int (f_0 + g(t))dt + \phi) \\ &= X_m(t)\ cos(2\pi f_0 + 2\pi \int g dt + \phi) \end{aligned} \tag{2.27}$$

The synchrophasor representation of Equation (2.27) becomes:

$$\boldsymbol{X} = (X_m(t)/\sqrt{2})\ e^{(2\pi \int g dt + \phi)} \tag{2.28}$$

Subsequent angle measurements will differ by $2\pi \int g dt$ radians, where $g(t)$ is the offset from nominal system frequency integrated over the time between measurements. Figure 2.6 illustrates this case where a signal with off-nominal frequency is measured at regular intervals synchronised to UTC time.

Synchrophasor measurements rely on a highly accurate time source to time stamp measurements and determine phase angle. An instrument measuring synchrophasor data is called a PMU and could be equipped with GPS to provide a reliable and accurate time source.

Because all synchrophasors are measured to a common reference and accompanied by a highly accurate time stamp, measurements from different PMUs are directly comparable.

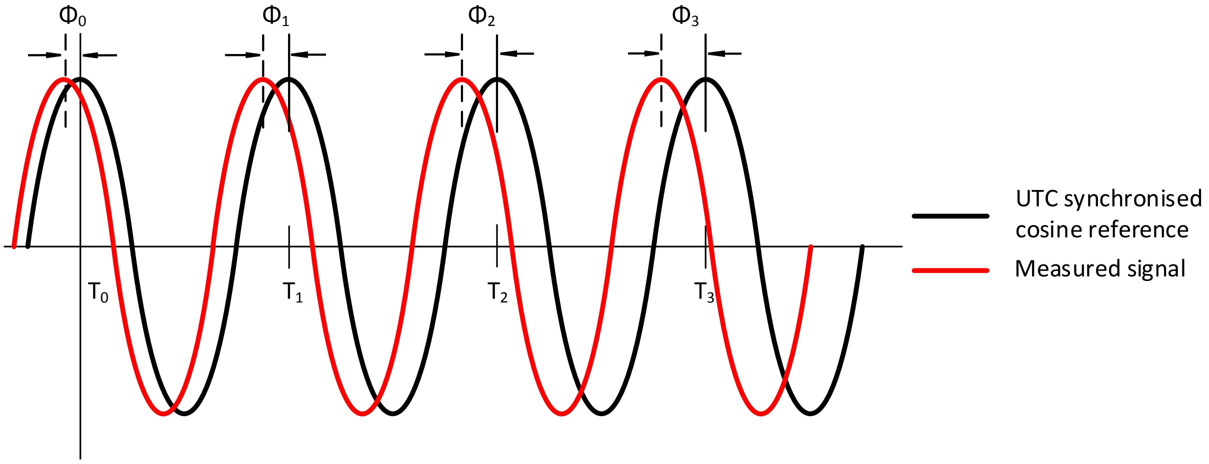

Figure 2.6: Measurement of synchrophasor phase angle ϕ for a signal at off-nominal frequency.

Furthermore, the availability of rms and angle measurements make a variety of advanced applications possible. Synchrophasor applications include [76, 77]:

- Small signal stability monitoring
- Voltage stability monitoring
- Power system control
- State estimation
- Transmission line monitoring
- Line parameter calculation
- Protection
- Model validation

2.8 WAMS Instrumentation

As explained in section 2.6, WAMS and small signal monitoring algorithms make use of data from PMUs. Synchrophasor measurement accuracy for PMUs are defined in the

IEEE C37.118.1-2011 standards document [75]. It specifies that a PMU must measure with sufficient accuracy to produce a total vector error (TVE), frequency error (FE), and rate of change of frequency error (RFE) below certain limits.

These specifications dictate a need for high accuracy in measurements and a highly accurate time source for time stamping and angle measurements. In addition to the hardware needed for accurate voltage and current measurement, a GPS can serve as the time source.

The C37.118.1-2011 does not explicitly define values for compliance on accuracy for each measured parameter, rather it is contained in the definitions for TVE, RFE and FE.

The accuracy of PQ instruments is defined in the IEC 61000-4-30 standards document. Compliance values for accuracy of each measured parameter is explicitly defined. Instruments complying to Class A accuracy is required to have time uncertainty of less than 20 ms for a 50 Hz system and 16.7 ms for a 60 Hz system. It is suggested that some time synchronisation procedure be used to achieve the required time uncertainty, such as a GPS receiver.

Time uncertainty much better than the IEC 61000-4-30 Class A specification can be achieved if a PQ instrument is equipped with GPS. It enables time and measurement accuracy that complies with specifications for TVE, FE and RFE as set in the C37.118.1-2011.

Advances in instrumentation make it possible to merge functions of previously separate instruments into one. PMU functionality according to C37.118.1 specification can be implemented in parallel with IEC 61000-4-30 Class A PQ measurement requirements on a single instrument.

PQ instruments can now record synchrophasor data with minimal extra sophistication, whilst also providing PQ data (with high accuracy in time stamping) that can enhance power system monitoring. A similar suggestion to merge different WAMS functionalities into one instrument is made in [64].

WAMS were solely the domain of specialised devices like PMUs. Enabling PQ instruments to also record synchrophasor data presents the opportunity to deploy powerful features of WAMS to more role players in network control and operation. Opportunities exist to implement WAMS functions through synchrophasor enabled PQ instruments.

A larger number of PQ instruments are expected to be installed in the network than PMUs, including instruments on distribution voltage level. PMU data from various locations in the network can facilitate better management of the network. PMU functionality at distribution voltage level can be used to address specific issues and challenges faced in distribution networks that are not a concern in transmission networks. This was not possible before due to limited (or no) availability of synchrophasor data at these locations in the network.

2.9 Conclusion

This chapter presents topics that create context for the chapters to follow. Power system stability was introduced, with some detail on rotor angle stability.

This research focusses on small signal stability monitoring. The application of small signal stability in monitoring rotor angle stability was presented. Theoretical concepts of small signal stability analysis was analysed and methods to monitor small signal stability.

An overview of experiences reported in the literature on small signal stability monitoring have been discussed. Synchrophasor data and instrumentation requirements were addressed. Access to synchrophasor data without specialized PMUs and WAMS have been proposed to be possible by modern power quality instrumentation being able to record voltage and current phasors accurately enough and with sufficient certainty in time stamping to comply with the requirements of the IEEE C37.118.1.

Chapter 3

Methodology for Low Frequency Oscillation Monitoring

... where specific methods chosen to perform real-time modal identification from ambient measured data is presented.

3.1 Introduction

In this chapter two methods are chosen to perform modal identification in a power system. The methods are chosen based on their applicability to the conditions of intended use. Methods are needed that can perform modal identification under the following conditions:

- Perform modal identification from recorded data.
- Use ambient measured data.
- Be suitable for real-time implementation.

The specification to process recorded data dictates a method from section 2.5.2 must be used. Further, ringdown methods are not suitable due to the need to process ambient data.

Only linear ambient methods and nonlinear/non-stationary methods are considered for use. Whether a method is suitable for real-time implementation depends on the time needed to perform the calculation and the ability to reflect sudden changes in the result shortly after it occurred.

For instance, the window length of a block processing method will determine its response to changing system conditions. A large window length will include in the calculation much of the system state prior to the change.

Similarly, recursive methods with a long forgetting factor will base current results on many results before the change, obscuring the change. One method is chosen from each category. This enables comparison and cross-validation of results based on similar datasets.

All methods presented in this section are implemented from first principles using the Matlab™ environment.

3.2 Linear Ambient Method

Methods for modal identification from ambient data have been a focus in the field of small signal stability for a number of years, resulting in different methods developed. Few extensive comparisons of the available methods exist.

Comparisons of some more successful methods in the field can be found in [30, 33]. It is reported that the Yule-Walker (YW) based methods can provide an accurate estimation of modal parameters. The YW method is well established and easy to implement. The extended modified Yule-Walker method (MYW) was chosen to implement in this research based on the claims made in the literature.

This method aims to fit an autoregressive moving average (ARMA) model to recorded data. The data is modelled by a transfer function with both poles and zeros. This type of model has the advantage that it can model sharp peaks and deep nulls in the frequency response [31].

This method assumes that the system is excited by an input that can be approximated as white noise. The white noise is assumed to be relatively stationary over the block of data used per calculation [35]. Random load changes in the power system constitute the assumed white noise.

3.2.1 Frequency and Damping Calculation

A measured dataset $y(t)$ described by an ARMA model is given by [31]:

$$y(t) = \frac{B(z)}{A(z)}e(t) \tag{3.1}$$

where
z^{-1} is the unit delay operator such that $(z^{-k}y(t) = y(t-k))$
$e(t)$ is white noise with variance of σ^2

$A(z)$ and $B(z)$ represent polynomials in z of the form:

$$A(z) = 1 + a_1z^{-1} + a_2z^{-2} + ... + a_nz^{-n} \tag{3.2}$$

$$B(z) = b_0 + b_1z^{-1} + b_2z^{-2} + ... + b_mz^{-m} \tag{3.3}$$

Equations (3.2) and (3.3) can be written in the frequency domain using the substitution $z = e^{j\omega}$:

$$A(\omega) = 1 + a_1e^{-j\omega} + a_2e^{-j2\omega} + ... + a_ne^{-jn\omega} \tag{3.4}$$

$$B(\omega) = b_0 + b_1e^{-j\omega} + b_2e^{-j2\omega} + ... + b_me^{-jm\omega} \tag{3.5}$$

The ARMA model has an order of (n, m) and can be described by the difference equation [35]:

$$y(t) + a_1y(t-1) + ... + a_ny(t-n) = b_0e(t) + b_1e(t-1) + ... + b_me(t-m) \tag{3.6}$$

where a_i for $i = 1, ..., n$ are the coefficients of $A(z)$ and b_j for $j = 0, ..., m$ are the coefficients of $B(z)$. The summated form of Equation (3.6) is given by

$$y(t) + \sum_{i=1}^{n} a_i y(t-i) = \sum_{j=0}^{m} b_j e(t-j) \tag{3.7}$$

The MYW method uses the relationship between the autocorrelation function of the input data and the a_i coefficients to find the mode information. The autocorrelation function is defined as:

$$r(k) = E\{y(t)y(t-k)\} \tag{3.8}$$

Multiplying both sides of Equation (3.6) with $y(t-k)$ and taking the expected value gives [35]:

$$r(k) + \sum_{i=1}^{n} a_i r(k-i) = \sum_{j=0}^{m} b_j E\{e(t-j)y(t-k)\} \tag{3.9}$$

When considering that the output of the system has to be uncorrelated with future white noise inputs, Equation (3.9) reduces to [31]:

$$r(k) + \sum_{i=1}^{n} a_i r(k-i) = 0 \qquad\qquad \text{for } k > m \tag{3.10}$$

Writing (3.10) in matrix form for $k = m+1, m+2, \ldots, m+M$ results in what is known as the modified Yule-Walker (MYW) equations:

$$R\,\overline{a} = -\overline{r} \tag{3.11}$$

In Equation (3.11):

$$R = \begin{bmatrix} r(m) & r(m-1) & \cdots & r(m+1-n) \\ r(m+1) & r(m) & \cdots & r(m+2-n) \\ \vdots & & & \\ r(m+M-1) & \cdots & & r(m+M-n) \end{bmatrix}$$

and

$$\overline{a} = \begin{bmatrix} a_1 \\ a_2 \\ \vdots \\ a_n \end{bmatrix} \qquad \overline{r} = \begin{bmatrix} r(m+1) \\ r(m+2) \\ \vdots \\ r(m+M) \end{bmatrix}$$

Since the true values for $r(k)$ is unknown, values are estimated [31]:

$$\widehat{r}(k) = \frac{1}{N} \sum_{t=k+1}^{N} y(t)y(t-k) \tag{3.12}$$

Equation (3.11) can now be solved to find a_i for $i = 1, ..., n$. In solving Equation (3.11) a value for M must be chosen. If M is chosen so that $M < n$, then there are fewer equations than unknowns and the solution is underdetermined. No unique solution for a_i can be found.

Choosing $M = n$ produces a unique solution for a_i. By choosing $M > n$, an overdetermined solution for a_i is found that can be solved as a least-squares problem [35].

It was found that an overdetermined solution can provide increased accuracy [34]. For the overdetermined case, the higher lag elements of the autocorrelation sequence are included when the R matrix is formed. The higher lag elements of the autocorrelation sequence contain information of narrowband frequency content. In the overdetermined solution, these higher lag coefficients are included in the calculation, improving the estimation accuracy [31, 34].

The z-domain roots of Equation (3.2) can be determined once a_i are known. The s-domain roots are found by

$$s_i = \frac{\ln(z_i)}{T} \tag{3.13}$$

where T is the sampling period and z_i the z-domain roots of $A(z)$. With the s_i roots known, the mode frequency and damping ratio can be calculated by using Equation (2.12) and (2.13).

The MYW method can be extended to take multiple signals as inputs. Construct Equation

(3.11) for each input signal $j = 1, ..., n_0$ and concatenate into one matrix problem to result in the extended MYW equations [33]:

$$\begin{bmatrix} R_1 \\ R_2 \\ \vdots \\ R_{n_0} \end{bmatrix} \overline{a} = - \begin{bmatrix} \overline{r}_1 \\ \overline{r}_2 \\ \vdots \\ \overline{r}_{n_0} \end{bmatrix} \tag{3.14}$$

3.2.2 Mode Selection

Mode selection is the process of determining which identified modes are dominant modes. The number of modes identified will be determined by the order of the ARMA model used.

Practical power systems will have a very high order, in terms of the complete model, however very few dominant modes will be contained in the recorded signal, typically six or less [33].

A high-order ARMA model will usually be chosen to improve the estimation, resulting in more modes being identified than there are dominant modes. Extra modes identified can be attributed to numerical artefacts and weak modes that are not of interest. A process is needed to determine which modes are dominant.

This can be achieved by considering the observability of a mode. Observability of a mode is evaluated by inspecting the energy in its autocorrelation sequence. This can not be directly determined and a pseudo energy must be estimated for this purpose. The autocorrelation form of the ARMA model is given in Equation (3.10). Taking the z-transform of Equation (3.10) yields

$$r_j(k) = \sum_{i=1}^{n} B_{ji} z_i^{k-m-1} \qquad \text{for } k > m \tag{3.15}$$

where B_{ji} is the residue of the z-domain root z_i for signal j. Equation (3.15) can be solved as a matrix problem:

$$\overline{r}_j = Z\overline{B}_j \tag{3.16}$$

where

$$Z = \begin{bmatrix} z_1^0 & z_2^0 & \cdots & z_n^0 \\ z_1^1 & z_2^1 & \cdots & z_n^1 \\ \vdots & & & \\ z_1^{M-1} & z_2^{M-1} & \cdots & z_n^{M-1} \end{bmatrix}$$

and

$$\overline{B}_j = \begin{bmatrix} B_{j1} \\ B_{j2} \\ \vdots \\ B_{jn} \end{bmatrix} \qquad \overline{r}_j = \begin{bmatrix} r_j(m+1) \\ r_j(m+2) \\ \vdots \\ r_j(m+M) \end{bmatrix}$$

The pseudo energy of mode i is estimated by

$$E_i = \sum_{j=1}^{n_0} \left(B_{ji}^* B_{ji} \sum_{q=0}^{M-1} \left[\left(z_i^q\right)^* \left(z_i^q\right) \right] \right) \tag{3.17}$$

3.2.3 Modified Yule-Walker ARMA Spectral Estimator

In the previous sections, the process of finding the ARMA mode frequency and damping is described. Mode frequency and damping is found by determining the a_i coefficients of the ARMA model. From the a_i coefficients, only the auto regressive (AR) part of the ARMA model is known. The moving average (MA) part of the model must also be found to describe the spectral content of the signal it is fitted to.

The power spectral density (PSD) of a rational function is generally described by [31]:

$$\xi(\omega) = \frac{\sum_{k=-m}^{m} \gamma_k e^{-i\omega k}}{\sum_{k=-n}^{n} \rho_k e^{-i\omega k}} \tag{3.18}$$

Equation (3.18) can be factored to have the form

$$\xi(\omega) = \left| \frac{B(\omega)}{A(\omega)} \right|^2 \sigma^2 \tag{3.19}$$

Equation (3.19) describes the PSD of the ARMA model in Equation (3.1).

An AR model is formed when $m = 0$ for the model in Equation (3.1). AR models are also referred to as all-pole models as their transfer function contains only poles. AR models are suitable to model narrowband signals as zeros in the A-polynomial in Equation (3.19).

If $n = 0$ in Equation (3.1), an MA model is formed. The all-zero structure of an MA model make it suitable to model signals containing broad peaks and deep nulls with zeros in the B-polynomial in Equation (3.19).

The ARMA model used is a combination of AR and MA models. It is capable of modelling sharp peaks and deep nulls in the frequency spectrum.

To investigate the spectral content of the signal, the MA part of the ARMA model must be found. Following the discussion of the MA model above, the PSD of the MA model is

$$\sigma^2 \left|B(\omega)\right|^2 = \sum_{k=-m}^{m} \gamma_k e^{-i\omega k} \tag{3.20}$$

where γ_k represents the covariance sequence of the MA part that needs to be estimated, and is given by [31]

$$\gamma_k = E\{[B(z)e(t)][B(z)e(t-k)]^*\} \tag{3.21}$$

Note from Equation (3.1) that

$$A(z)y(t) = B(z)e(t) \tag{3.22}$$

Substituting Equation (3.22) into Equation (3.21) gives

$$\begin{aligned}\gamma_k &= E\{[A(z)y(t)][A(z)y(t-k)]^*\} \\ &= \sum_{j=0}^{n}\sum_{p=0}^{n} a_j a_p^* E\{y(t-j)y^*(t-k-p)\} \\ &= \sum_{j=0}^{n}\sum_{p=0}^{n} a_j a_p^* r(k+p-j)\end{aligned} \tag{3.23}$$

for $k = 0, ..., m$. The MA covariance sequence γ_k can now be estimated using previously estimated values for a_i and $r(k)$:

$$\widehat{\gamma}_k = \begin{cases} \sum_{j=0}^{n} \sum_{p=0}^{n} \widehat{a}_j \ \widehat{a}_p^* \ \widehat{r}(k+p-j), & k = 0, ..., m \\ \widehat{\gamma}_{-k}^*, & k = -1, ..., -m \end{cases} \tag{3.24}$$

The complete signal spectrum can now be found by:

$$\widehat{\xi}(\omega) = \frac{\sum_{k=-m}^{m} \widehat{\gamma}_k e^{-i\omega k}}{\left|\widehat{A}(\omega)\right|^2} \tag{3.25}$$

Equation (3.25) is known as the modified Yule-Walker ARMA spectral estimator.

3.2.4 Mode Shape

The mode shape must be calculated for each identified mode. First it is necessary to recall Equation (2.19) and (2.20). For the mode given by eigenvalue λ_i the following holds:

$$\Delta\overline{x}(t) = \sum_{i=1}^{n} z_i(t)\overline{\phi}_i \tag{3.26}$$

$$\dot{z}_i(t) = \lambda_i z_i(t) + \overline{\psi}_i B \Delta\overline{u}(t) \tag{3.27}$$

A spectral method for estimating mode shape is used [11]. A relationship can be derived between the power-spectral density (PSD) and cross-spectral density (CSD) functions of the recorded signal and the eigenvectors of the system [11, 78]. The CSD and PSD functions are defined as follows:

$$S_{kl}(\omega) = \lim_{T\to\infty} \frac{1}{T} E\{Y_k^*(\omega)Y_l(\omega)\} \tag{3.28}$$

$$S_{kk}(\omega) = \lim_{T\to\infty} \frac{1}{T} E\{Y_k^*(\omega)Y_k(\omega)\} \tag{3.29}$$

where $S_{kl}(\omega)$ is the CSD function of $y_k(t)$ and $y_l(t)$, $Y_k(\omega)$ represents the Fourier transform of $y_k(t)$ and $Y_l(\omega)$ represents the Fourier transform of $y_l(t)$. Similarly, $S_{kk}(\omega)$ is the PSD function of $y_k(t)$.

Let $y_k(t) = \Delta x_k(t)$ and $y_l(t) = \Delta x_l(t)$. Substituting Equation (3.26) into (3.28) gives

$$S_{kl}(\omega) = \lim_{T\to\infty} \frac{1}{T} E\left\{ \left(\sum_{r=1}^{n} Z_r(\omega)\phi_{rk} \right)^* \left(\sum_{p=1}^{n} Z_p(\omega)\phi_{pl} \right) \right\} \tag{3.30}$$

The Fourier transformation of Equation (3.26) and (3.27) results in

$$Z_i(\omega) = \frac{\overline{\psi}_i B\overline{U}(\omega)}{j\omega - \lambda_i} \tag{3.31}$$

where $\overline{U}(\omega)$ is the Fourier transform of $\overline{u}(t)$. Substitution of Equation (3.31) into (3.30) yields:

$$S_{kl}(\omega) = \lim_{T\to\infty} \frac{1}{T} E\left\{ \left(\sum_{r=1}^{n} \frac{\overline{\psi}_r B\overline{U}(\omega)}{j\omega - \lambda_r} \phi_{rk} \right)^* \left(\sum_{p=1}^{n} \frac{\overline{\psi}_p B\overline{U}(\omega)}{j\omega - \lambda_p} \phi_{pl} \right) \right\} \tag{3.32}$$

Recall that $\lambda_i = \sigma_i + j\omega_i$ and for a practical power system with lightly damped modes $\omega_i \gg \sigma_i$. When $\omega = \omega_i$, the magnitude of Equation (3.31) is very large. The summation in Equation (3.32) is dominated by the term when $\omega = \omega_i$. For this reason, Equation (3.32) can be approximated by

$$\begin{aligned} S_{kl}(\omega_i) &\cong \lim_{T\to\infty} \frac{1}{T} E\{(Z_i(\omega_i)\phi_{ik})^*(Z_i(\omega_i)\phi_{il})\} \\ &\cong \phi_{ik}^*\phi_{il}\left[\lim_{T\to\infty} \frac{1}{T} E\left\{|Z_i(\omega_i)|^2\right\}\right] \end{aligned} \tag{3.33}$$

The random nature of the input $\overline{u}$ to the system produces a real number for the converged limit term in Equation (3.33) (does not contain angle value). The angle of the CSD value can be estimated as

$$\angle S_{kl}(\omega_i) \cong \angle\phi_{il} - \angle\phi_{ik} \tag{3.34}$$

A similar formulation for the PSD can be found by letting $k = l$ in Equation (3.33):

$$S_{kk}(\omega_i) \cong |\phi_{ik}|^2 \left[\lim_{T\to\infty} \frac{1}{T} E\left\{|Z_i(\omega_i)|^2\right\}\right] \tag{3.35}$$

It is observed that the PSD examined at ω_i provides $|\phi_{ik}|^2$ scaled by the real numbered result of the converged limit term in Equation (3.35). If the oscillation frequency ω_i is known, mode shape can be derived from the PSD and CSD functions. The PSD examined at ω_i is a measure of the observability of the mode at each measured location. The phasing of the mode is provided by the angle of the CSD examined at ω_i.

3.3 Non-linear/Non-Stationary Method

Two approaches to non-linear/non-stationary methods were introduced in Section 2.5.2. Methods are available that are based on the HHT transform as well as methods based on the wavelet transform.

The HHT family of methods focuses on analysis of ringdown data. Practical identification of modal characteristic by using the HHT method can be complex.

The HHT approach uses Empirical Mode Decomposition (EMD) to decompose a signal into a series of amplitude and frequency modulated components, Intrinsic Mode Functions (IMF) [50]. The EMD method suffers from mode mixing, especially when closely spaced modes are present in the data. Modes are referred to as closely spaced when their mode frequencies are within an octave [51]. This method fails to decompose closely spaced modes into separate IMFs. It can also produce end effects which are associated with the computation of the Hilbert transform [50].

A wavelet based method was chosen as the alternative approach to the small signal stability analysis in the research reported in this dissertation. Only wavelet methods suited to ambient data processing are considered. Two methods capable of ambient wavelet based modal estimation were discussed in section 2.5.2.

A method based on the continuous wavelet transform (CWT) and random decrement (RD) technique is presented and tested in [44,60–62]. An alternative wavelet method using the CWT and orthogonal wavelet base functions is presented in [7]. Both of these two methods are shown to produce accurate results from the tests conducted with simulated and practical data.

The effect of window length with regards to practicality for real-time monitoring has to be considered. Both wavelet methods of interest are block processing methods. A trade-off exists between accuracy of the result and response of the estimation to changing system conditions. The result from a smaller window length will react faster to modal changes in the signal as the calculation is based on only the most recent data.

A longer window length will improve accuracy as more data is available from which to estimate modal characteristics. These two properties come at the expense of each other. The aim is to identify a method that can produce the most accurate result with the smallest possible window length.

All tests in the literature conducted on the CWT and RD based method used window lengths of 5 min to 20 min. The development of the CWT method using orthogonal wavelet bases was motivated by the need to find a method capable of accurate results with short window lengths. Window lengths as short as 1 min is reported to provide accurate results [7]. The CWT method with orthogonal wavelet bases was chosen to implement in this research.

3.3.1 Wavelet Theory

In wavelet theory a signal is decomposed using a wavelet function. A mother wavelet describes the wavelet function used to decompose the signal. The mother wavelet $\varphi(t)$ is defined such that it has zero mean and is normalised [79]:

$$\int_{-\infty}^{+\infty} \varphi(t) = 0 \tag{3.36}$$

$$\| \varphi(t) \| = 1 \tag{3.37}$$

The mother wavelet is centred around $t = 0$. Different wavelets of the same form, called daughter wavelets are formed when the mother wavelet is scaled by s and translated by u [79]. Daughter wavelets are given by

$$\varphi_{u,s}(t) = \frac{1}{\sqrt{s}}\, \varphi\left(\frac{t-u}{s}\right) \tag{3.38}$$

A signal can be transformed to the wavelet domain by applying the CWT [79]:

$$\begin{aligned} Wf(u,s) &= < f(t), \varphi_{u,s} > && (3.39) \\ &= \int_{-\infty}^{+\infty} f(t)\, \varphi^{*}\left(\frac{t-u}{s}\right) dt && (3.40) \end{aligned}$$

The CWT transforms a time domain signal into the time-frequency wavelet domain. The signal can be transformed back to the time domain via the inverse of the CWT:

$$f(t) = \frac{1}{C_\Phi} \int_0^\infty \int_{-\infty}^{+\infty} Wf(u,s)\ \varphi\left(\frac{t-u}{s}\right) du\ \frac{ds}{s^2} \tag{3.41}$$

where C_Φ is defined by the admissibility condition

$$C_\Phi = \int_0^\infty \frac{|\Phi(\omega)|^2}{\omega} d\omega < \infty \tag{3.42}$$

$\Phi(\omega)$ is the Fourier transform of the mother wavelet $\varphi(t)$.

3.3.2 Wavelet Monitoring Method

The wavelet method presented in [7] proposes a linear transformation to extract decaying oscillatory signals. The inverse CWT is used for this transformation:

$$F(t) = \frac{1}{C_\Phi} \int_0^\infty C(s) \frac{1}{\sqrt{s}} W\left(\frac{t}{u}\right) \frac{ds}{s^2} \qquad \text{for } t \geq 0 \tag{3.43}$$

The function $W_s(t)$ is the daughter wavelet function used as the base in the inverse transform. $W_s(t)$ is defined as

$$W_s(t) = \frac{1}{\sqrt{s}} W\left(\frac{t}{s}\right) \tag{3.44}$$

and it has the following properties:

1. $W_s(t) \in L^2(\boldsymbol{R})$
2. $W_s(t)$ are decaying oscillatory functions with different frequencies and damping ratios.
3. $W_s(t)$ is an orthogonal function such that: $\int_{-\infty}^{+\infty} W_{s1}(t)W_{s2}(t)dt = 0$ for $s1 \neq s2$.
4. $W_s(t)$ is zero-mean: $\int_{-\infty}^{+\infty} W_s(t)dt = 0$ for $s = 1, ..., M$
5. $W_s(t)$ is normalised: $\parallel W_s(t) \parallel = 1$

The Morlet wavelet is chosen as it has all the properties listed above. The term $C(s)$ in Equation (3.43) needs to be determined. $C(s)$ can be determined as:

$$C(s) = \int_{-\infty}^{+\infty} f(t)\frac{1}{\sqrt{s}}W^*\left(\frac{t}{s}\right)dt \tag{3.45}$$

It is assumed that the measured signal $f(t)$ has some noise in the measurement. The estimation of $C(s)$ can be improved by calculating it as the average values of the PSD of the different translated wavelets:

$$\widehat{C}(s) = \frac{1}{T}\int_0^T [C(s,u)C^*(s,u)]du \tag{3.46}$$

$C(s,u)$ is simply the CWT transform of the signal $f(t)$:

$$C(s,u) = \int_{-\infty}^{+\infty} f(t)\frac{1}{\sqrt{s}}W^*\left(\frac{t-u}{s}\right)dt \tag{3.47}$$

Multiple input signals can be used to improve the estimation accuracy of $\widehat{C}(s)$. Expressed for discrete computer implementation, Equation (3.47) and (3.43) is written as:

$$C_i(s,u) = \sum_{n=0}^{N} f_i(n)\frac{1}{\sqrt{s}}\ W^*\left(\frac{(n-u)/f_s}{s}\right) \tag{3.48}$$

$$F(t) = \frac{1}{C_\Phi}\ \sum_{s=0}^{S}\widehat{\widehat{C}}(s)\ \frac{1}{\sqrt{s}}\ W^*\left(\frac{t-u}{s}\right) \tag{3.49}$$

where N is the number of data points, S is the number of scales, U is the number of translations and f_s is the sampling frequency of the signal. Suppose there are L input signals. The coefficients of the CWT of each signal found in Equation (3.48) is formed into a matrix for each scale s, producing an $L \times U$ matrix:

$$P(s) = \begin{bmatrix} C_1(s,u) \\ C_2(s,u) \\ \vdots \\ C_L(s,u) \end{bmatrix} \tag{3.50}$$

The PSD of this matrix is calculated as

$$P_{xy}(s) = \frac{1}{U}P(s)P^*(s) \tag{3.51}$$

where $P^*(s)$ is the transpose complex conjugate of $P(s)$. $\widehat{C}(s)$ is given by any norm of the PSD matrix. The norm can be found by performing singular value decomposition (SVD) of the PSD matrix. Through SVD the decomposed PSD matrix is found:

$$\begin{aligned} P_{xy} &= [u_1(s), ..., u_L(s)] \begin{bmatrix} \sigma_1(s) & & \\ & \ddots & \\ & & \sigma_L(s) \end{bmatrix} \begin{bmatrix} v_1(s)^H \\ \vdots \\ v_1(s)^H \end{bmatrix} \\ &= U(s)\Sigma(s)V(s)^H \end{aligned} \tag{3.52}$$

According to its properties, P_{xy} after SVD can be written as:

$$P_{xy} = \sigma_1(s)u_1(s)u_1(s)^H + \ ... \ + \sigma_L(s)u_L(s)u_L(s)^H \tag{3.53}$$

From Equation (3.53), $\widehat{C}(s) = \sigma_1(s)$ and $u_1(s)$ indicates how each signal contributed towards the decomposition of P_{xy} for singular value $\sigma_1(s)$. $u_1(s)$ thus contains information regarding the mode shape of the system.

For increased robustness against noise in the measured signal, $\widehat{C}(s)$ is averaged over multiple analysis windows. For T consecutive analysis windows we have T values for $\widehat{C}(s)$. $\widehat{C}(s)$ is averaged as:

$$\widehat{\widehat{C}}(s) = \frac{1}{T}\sum_{i=1}^{T} \widehat{C}_i(s) \tag{3.54}$$

The system impulse response in the time domain can be found by performing the inverse CWT in Equation (3.49) with the estimated $\widehat{\widehat{C}}(s)$. All modal information extracted by the wavelet transform is contained in the time domain reconstruction of the system impulse response. Modal characteristics can now be extracted with any of the available ringdown methods. Prony analysis was used for this purpose.

3.3.3 Prony Analysis

A decaying oscillatory signal with n modes can be modelled with the following equation [8]:

$$y(t) = \sum_{i=1}^{n} A_i e^{\sigma_i t} cos(\omega_i t + \theta_i) \tag{3.55}$$

For a signal where N samples are recorded at regular intervals the discrete form of Equation (3.55) can be written as [14]:

$$y(k) = \sum_{i=1}^{n} R_i z_i^k \tag{3.56}$$

where

$$z_i = e^{\lambda \Delta t} \tag{3.57}$$

The z_i terms are the roots of the polynomial equation describing the response of the system:

$$z^n - (a_1 z^{n-1} + a_2 z^{n-2} + ... + a_n z^0) \tag{3.58}$$

It can be shown that the coefficients a_i can be found via the matrix equation shown [14]:

$$\begin{bmatrix} y(n-1) & y(n-2) & \dots & y(0) \\ y(n) & y(n-1) & \dots & y(1) \\ \vdots & & & \\ y(N-2) & y(N-3) & \dots & y(N-n-1) \end{bmatrix} \begin{bmatrix} a_1 \\ a_2 \\ \vdots \\ a_n \end{bmatrix} = \begin{bmatrix} y(n) \\ y(n+1) \\ \vdots \\ y(N-1) \end{bmatrix} \tag{3.59}$$

The roots of the polynomial in Equation (3.58) can now be found to identify the modes present in the signal, similar to the method described in Section 3.2.1.

With the roots of the polynomial from Equation (3.58) known, Equation (3.56) can be expanded into matrix form and solved for the residues R_i [17].

$$\begin{bmatrix} y(0) \\ y(1) \\ \vdots \\ y(N-1) \end{bmatrix} = \begin{bmatrix} z_1^0 & z_2^0 & \dots & z_n^0 \\ z_1^1 & z_2^1 & \dots & z_n^1 \\ \vdots & & & \\ z_1^{N-1} & z_2^{N-1} & \dots & z_n^{N-1} \end{bmatrix} \begin{bmatrix} R_1 \\ R_2 \\ \vdots \\ R_n \end{bmatrix} \tag{3.60}$$

3.3.4 Choice of Parameters in Method

Choices regarding parameters associated with the method must be made during implementation. Choice of these parameters can influence the accuracy of the method. Parameters must be chosen according to the proposed application.

Mother Wavelet

A wavelet must be chosen for use in the CWT and inverse CWT. The complex Morlet wavelet satisfies all the criteria as set in Section 3.3.2 and is well suited to the application of oscillation monitoring [7]. The Morlet wavelet in the time and frequency domain is given by:

$$W_{Morlet}(t) = \pi^{-1/4} e^{j\omega_0 t} e^{-t^2/2} \tag{3.61}$$

$$w_{Morlet}(\omega) = \pi^{-1/4} e^{-(\omega-\omega_0)^2/2} \tag{3.62}$$

where ω_0 is the central frequency.

Central Frequency

The central frequency used for the daughter wavelets must be chosen. The choice of central frequency influences the range of frequencies and damping ratios that can be identified.

The process followed to choose the central frequency for this method can be found in [7]. The central frequency is chosen according to the proposed application of the method, experience with using the method and trail and error testing performed by the authors of [7]. The discussion in [7] concludes the choice by selecting the central frequency as:

$$\omega_0 = 90\pi$$

It is chosen in this research to use the same parameters for the method as the authors in [7], because the parameters have already been selected with the goal of power system oscillation monitoring in mind.

Scales

It is necessary to choose scales for use in the CWT. The choice of scales determine the frequency band that will be investigated by the wavelet method.

It is convenient to choose the scales equal to fractional powers of two [80]:

$$s_j = s_0 2^{j\delta_j} \qquad\qquad j = 0, 1, ..., J \tag{3.63}$$

In order to investigate the modal content of the signal between 0.1 Hz and 2 Hz, the parameters pertaining to scale selection is chosen as follows in [7]:

$$s_0 = 22.5 \qquad\qquad \delta_j = 0.02 \qquad\qquad J = 217$$

Wavelet Translations and Averaging Windows

The number of translations used in the CWT of Equation (3.48) must be chosen. A larger number of translations increase processing time, without significant improvement in accuracy [7]. The number of wavelet translations is chosen $U = 2$ in this research.

Equation (3.54) describes the averaging of the wavelet coefficients over multiple analysis windows. The number of windows over which to perform averaging must be chosen. Averaging over a larger number of windows will provide a smoother response in the results, but may reduce the visibility of rapid changes. The wavelet coefficients were averaged using $T = 5$ for the research in this dissertation.

3.4 Additional Considerations

Additional aspects relating to the measured data must be addressed prior to the application of any small signal stability analysis method. This includes preparing the data to be used and choosing suitable input signals. These issues are discussed here.

3.4.1 Input Signals

Successful modal identification from recorded data depends on the observability of the mode in the signal. Observability of a mode can be determined through investigating the state-space model. In the absence of a state-space model, performance of a method can be improved by selecting a signal or multiple signals that might capture the dynamics of interest.

An obvious choice of input signal could be active power as the mechanism for power system oscillations are the exchange of active power between different components. Active power relates directly to the phenomena of interest. The non-linear nature of the power system could hold disadvantages to using active power, especially when angular separation becomes large [81]. In the case of a three-phase system the positive sequence active power is used.

Angular separation can also be used as input signal. The dynamics of the system will be contained in the angle measurement. Angular separation is closely linked to active power transfer. Angular separation has the advantage of exhibiting less non-linear behaviour for large power transfers than active power [81]. PMUs make it possible to measure angular separation, which was not previously possible. The common measurement reference used by PMUs make it possible to record distributed parameters such as angular separation across a transmission system.

Frequency and angular separation share most properties. Frequency, similar to angular separation is well suited for oscillation monitoring. An added advantage is that jumps in angle and power are not observed in frequency measurement due to the integral relationship of frequency and angular separation [81].

Since both methods are capable of using multiple signals as input, a combination of the signals mentioned above can also be used.

3.4.2 Data Pre-processing

Data needs to be pre-processed for optimal performance of any oscillation monitoring method. Data preprocessing generally consists of the following steps:

1. Filtering

   Filtering is used to remove unwanted effects such as noise from signals measured by PMUs. It also prevents aliasing when a signal is downsampled.

2. Downsampling

   Data from PMUs are typically recorded in the range of tens of samples per second. Down sampling can reduce the computational time as fewer data points need to be processed. A sample rate of approximately 5 samples per second has been found to produce the most accurate results for oscillation monitoring methods [33].

3. De-trending

   De-trending is used to remove trends from signals that do not carry any information regarding the dynamics of the system [82]. In the case where ambient small signal stability is the focus, small deviations in recorded parameters around the operating set point are of interest. De-trending aims to remove all signal components that do not form part of the small, rapid changes recorded in the data. The shift introduced by the set point is removed while the small deviations are retained.

4. Normalising different data inputs

   Both methods presented can use multiple recorded parameters as input. The deviations in recorded signals are expected to have different scales. Deviations in frequency or angular separation are expected to be in the order of single or double digits (single digits in the case of frequency, single or double digits in the case of angular separation). Deviations in active power are expected to be in the order of megawatts (deviations of order thousands).

   These signals cannot be used as is for the multiple input scenario. The active power input will dominate the calculation and obscure the dynamics captured by the other recorded signals. It is necessary to normalise the data. Deviations captured in each signal must be of the same order.

   Standard deviation is used to characterise the deviations in each data input. All datasets are then scaled to have the same standard deviation.

3.4.3 Missing Data

All oscillation monitoring methods rely on data recorded at regular intervals. Both methods presented in this dissertation use multiple recorded signals as input. These signals can originate from different PMUs.

It is necessary to adopt a strategy in the case of missing data from a PMU. If the missing data is relatively minor, interpolation can be used to reconstruct the missing data. Alternatively, for small amounts of missing data the available data can be concatenated to remove the missing segment. This approach is successful when the duration of the missing data accounts for a small portion of the analysis window [8]. If a large amount of data is missing, concatenation and interpolation may no longer be effective and other methods must be used.

In this research it was assumed that any data that might be missing accounts for a small enough portion of the analysis window that concatenation can be applied effectively.

3.5 Conclusion

This chapter presented two different methods to monitor LFOs in real-time from ambient measured data.

The mathematical background of each method was discussed in detail. Each method characterises LFOs in terms of frequency, damping ratio and mode shape.

Additional work is needed besides implementation of the mathematical operations for each method. This includes choosing input signals, pre-processing data before a method is applied and also developing strategies in the case of missing data.

The methods presented in this chapter will be tested to simulated and field data in the next chapters.

Chapter 4

Verification of Methods

... where the performance of both methods presented in Chapter 3 is verified by testing on simulated data.

4.1 Introduction

This chapter reports on evaluation of the ARMA and wavelet methods, using simulated power system data in order to verify the perceived performance when used for small signal analysis.

With the performance, restrictions and requirements of each method understood, it can be prepared for application on field data as validation of the results obtained by simulation in this chapter.

4.2 Kundur Two-Area Test System

The Kundur two-area test system is simulated to produce test data [4]. Fig. 4.1 presents this simplified power system.

It consists of 4 synchronous machines connected by two coherent areas. Area 1 consists of machine M1 and M2 and Area 2 contains machines M3 and M4. The two areas are connected via long transmission lines between bus 3 and 13. Each machine is equipped with a Power System Stabiliser (PSS).

This Kundur two-area test system is frequently used for small-signal stability analysis because of its relative simplicity, whilst still being complex enough to study the fundamental nature of power system oscillations.

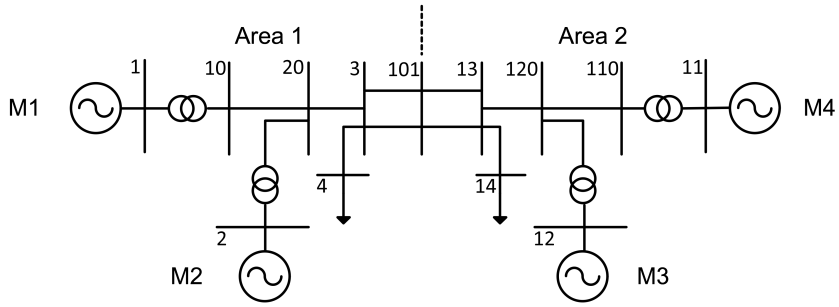

Figure 4.1: Kundur 4-machine, 2-area test system.

The system is simulated using the PST toolbox in the Matlab™ environment [83]. Each simulation of the system is performed for one hour of simulated time. 100 samples per second are recorded.

4.3 Window Length

The effect of window length is examined first. Literature indicates that the accuracy of ambient methods tend to decrease with a decrease in window length. This is especially true for the damping ratio result [61].

Window length affects the response of this method to changing conditions. An algorithm with a shorter window length will react faster to system changes than one with a longer window length. A trade-off exists between acceptable accuracy and fast reaction to system change.

A consequence of window length for practical use is in the case of lost communication with a PMU. Window length determines the time that needs to elapse after communication has been restored. Only after this time, equal to the window length, the algorithm can produce an answer.

Each method is alternatively applied to an hour of simulated data from the Kundur test system. Different window lengths are used ranging from 1-min to 20-min in 1-min increments.

Having direct control over the parameters of the test system allows for a state-space investigation of its behaviour through eigenanalysis functions available in the PST toolbox. The theoretical frequency, damping ratio and mode shape of a mode in the system is found in this way. An inter-area mode is present in the system. The characteristics of the inter-area mode are listed in Table 4.1.

Table 4.1: Inter-area mode in Kundur system.

Eigenvalues		Frequency (Hz)	Damping (%)
Real	Imaginary		
-0.1475	$\pm$ 3.5641	0.5672	4.13

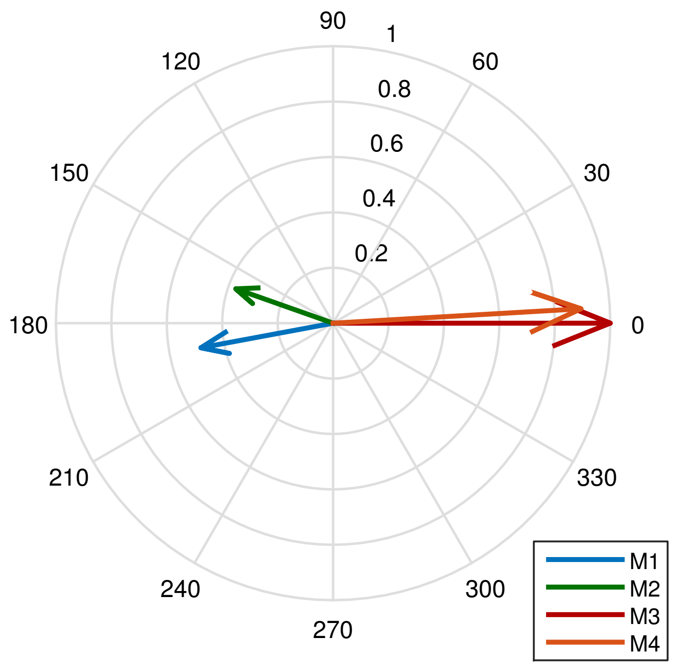

Figure 4.2: Mode shape for Kundur system.

4.3.1 Window Length: Impact on Frequency Result

The sensitivity of frequency result to window length is evaluated. To evaluated the impact of window length, frequency trends using a 2-min, 5-min and 10-min window is plotted on the same axes. Results from the two methods are presented simultaneously to enable comparison.

Figure 4.3 and Figure 4.4 presents the frequency trends for different window lengths for the ARMA and wavelet method respectively.

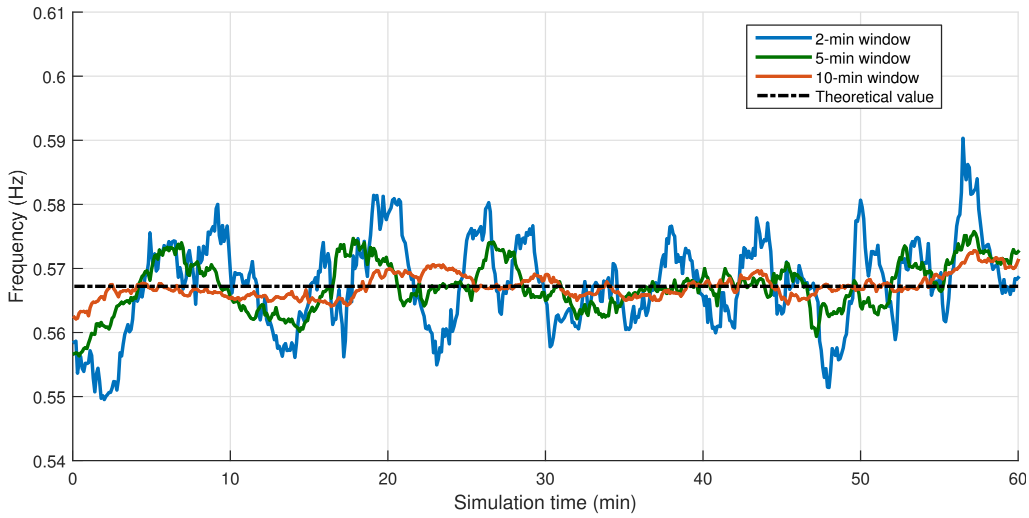

Figure 4.3: ARMA frequency trends for different window lengths.

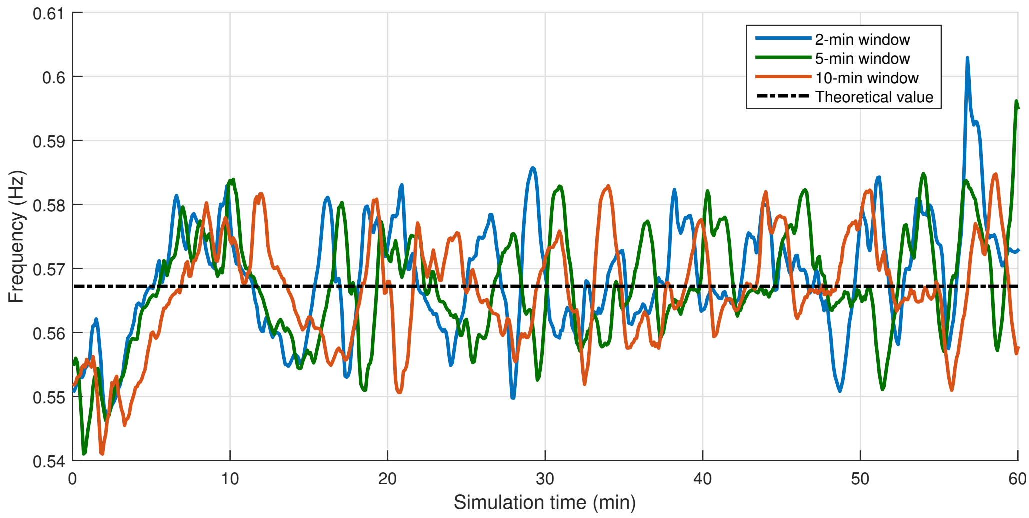

Figure 4.4: Wavelet frequency trends for different window lengths.

It is clear that both methods are capable of calculating frequency of the inter-area oscillation. Trended results approximate the theoretical value for frequency. Observe the scale on the y-axis. Frequency result is very accurate with deviations in results limited to the second decimal.

Visual inspection of the ARMA trends shows an improvement in accuracy as the window length is increased. Results from the 10-min window length show significantly less variance than the results from the 2-min window length.

Very little difference in behaviour for the wavelet method is noted as window length is increased. Variance in results remains largely unchanged. The wavelet method produces smoother results than the ARMA method. Successive results for the wavelet method do not differ significantly, in contrast to the ARMA method. Different window lengths produce similar trends, however a time shift is observed. This highlights the consequence of using a large window length for any ambient method.

Using a larger window length in an ambient method generally increases result accuracy, as more data is available for the calculation. This implies that for a large window length, the current result is based on a block containing a large amount of old data. This will reduce the rate of response of the method to changing system conditions. For a small window length, the result is based on only the most recent data, possibly at the expense of accuracy. A trade-off thus exists between accuracy and rate of response to changing system conditions. This effect is further discussed when the ability of the method to track changing system conditions is investigated.

For each set of results using a different window length, the mean and standard deviations of the results are calculated. Figure 4.5 and Figure 4.6 show frequency mean and standard deviation as a function of window length. The mean of each set of results are indicated as a solid line, with standard deviation indicated by error bars.

The improvement in accuracy for the ARMA method versus window length is apparent from Figure 4.5. Frequency mean converges to the theoretical value, while standard deviation of the results decrease with an increase in window length.

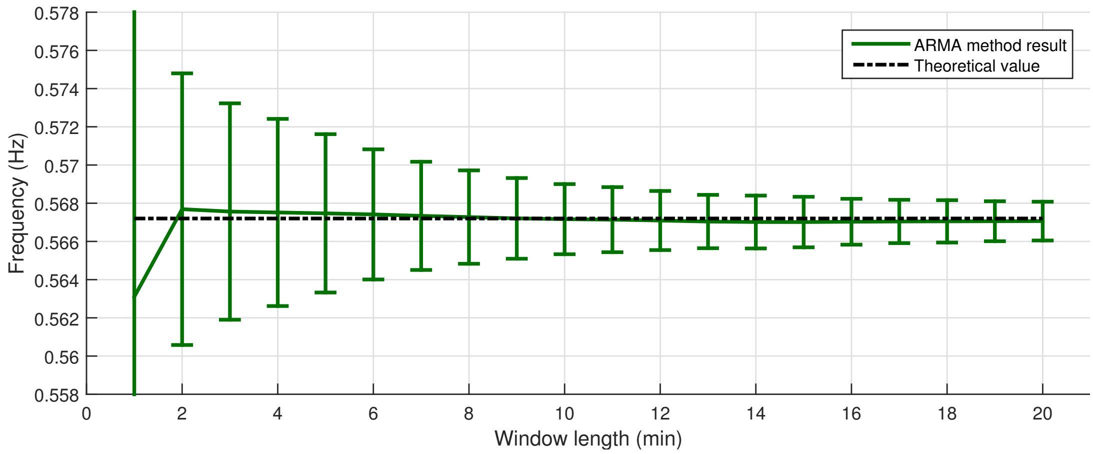

Figure 4.5: ARMA frequency mean and standard deviation as function of window length.

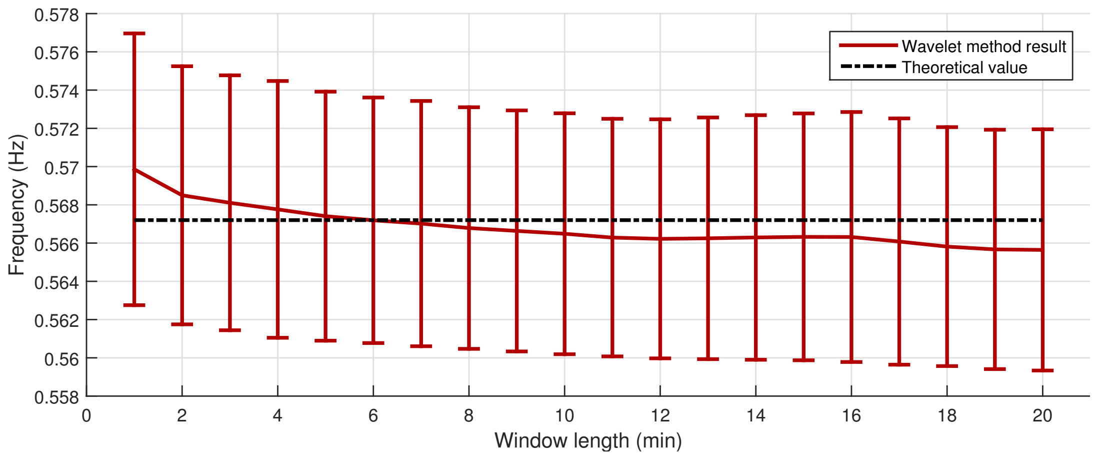

Figure 4.6: Wavelet frequency mean and standard deviation as function of window length.

Wavelet method results are less sensitive, with very little change in standard deviation. Frequency mean remains near to the theoretical value for all window lengths.

Observe that the y-axis of Figure 4.5 and 4.6 are the same. The y-axis for the results obtained by the ARMA method is intentionally restricted to be equal to that of the results obtained by the wavelet method (standard deviation for ARMA results at 1-min fall outside plotted area). This is done to enable visual comparison of the behaviour of the two methods. Similar frequency mean and standard deviations are found when using a 2-min window length.

4.3.2 Window Length: Impact on Damping Result

The influence of window length on damping ratio result is evaluated using the same approach as for frequency result. Trended results from both methods are shown using a 2-min, 5-min and 10-min window length. Figure 4.7 presents the ARMA results and Figure 4.8 the wavelet results.

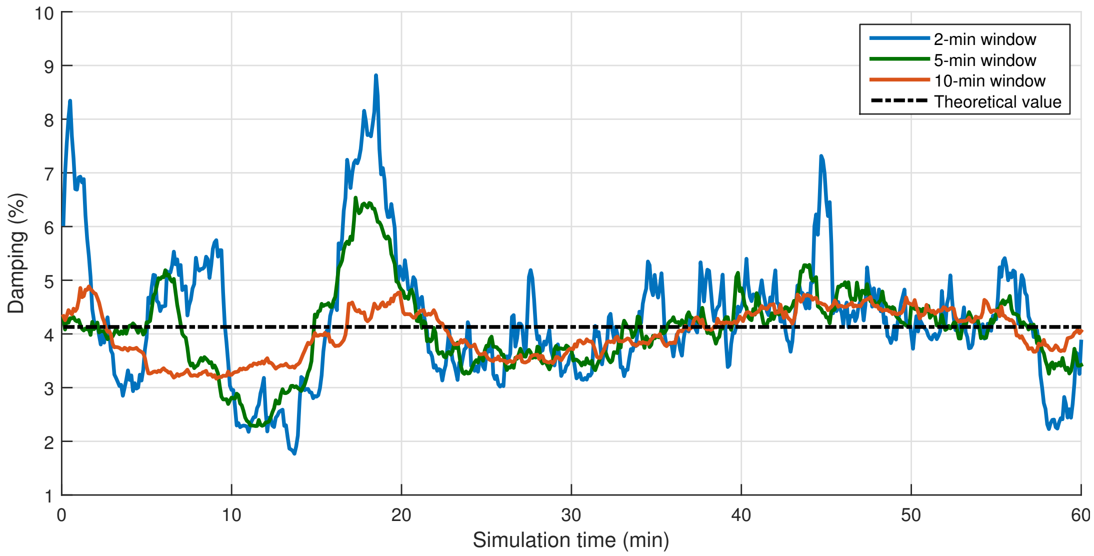

Figure 4.7: ARMA damping trends for different window lengths.

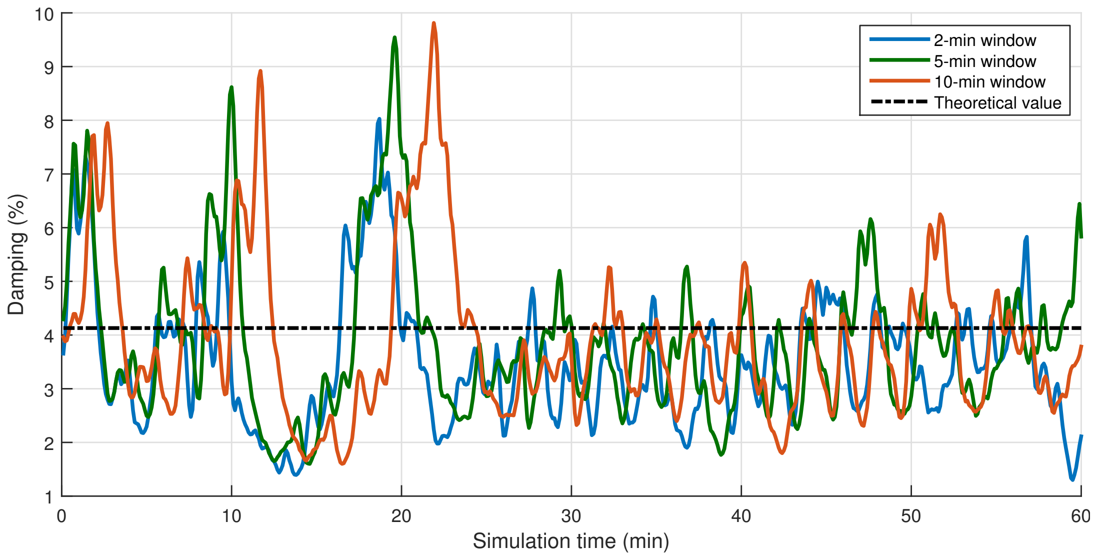

Figure 4.8: Wavelet damping trends for different window lengths.

Both methods produce a damping ratio result centred around the theoretical value. Observe the y-axis scale. Results for damping ratio is not as accurate as for frequency.

Damping ratio result obtained by the ARMA method displays a similar behaviour as the results for frequency when changing window lengths. Damping ratio variance decreases with an increase in window length.

The wavelet method displays relatively large variance in damping ratio results, showing an increase in variance for increasing window length (10-min results have larger variance than 2-min results). Influence of window length is once again observed in the time shift of the trends.

Figure 4.9 and 4.10 presents the mean and standard deviations versus window length.

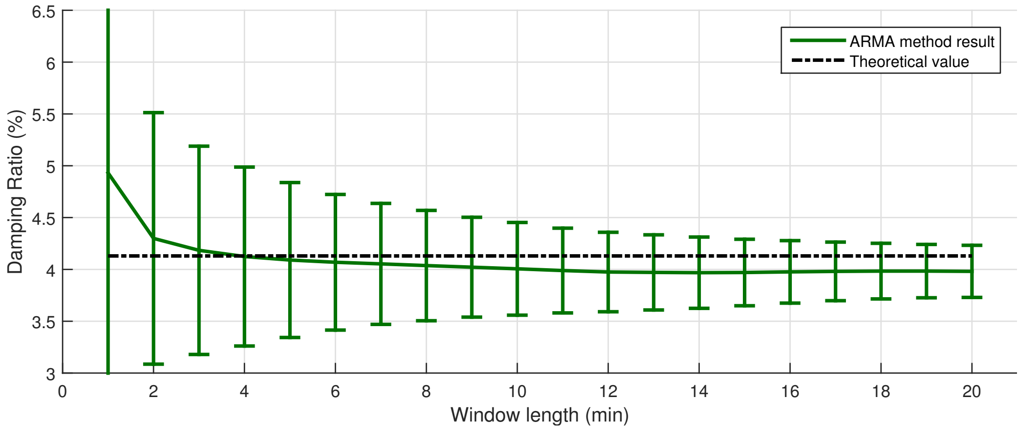

Figure 4.9: ARMA damping mean and standard deviation as function of window length.

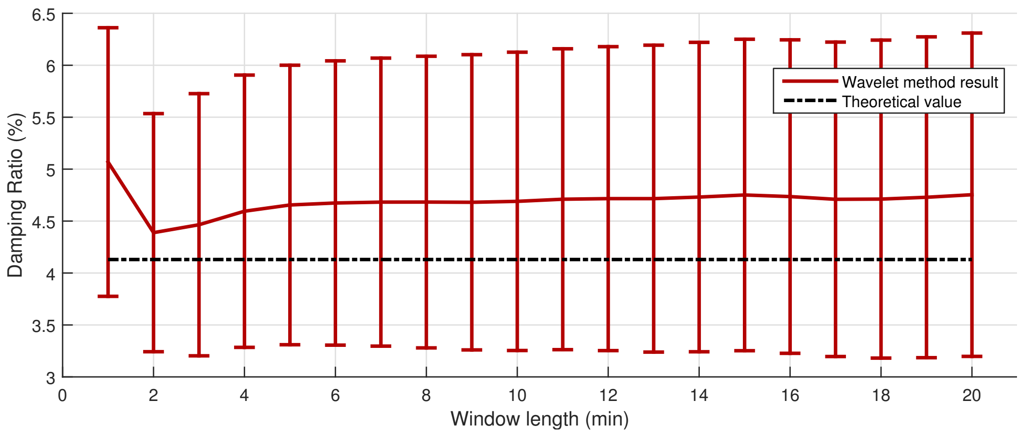

Figure 4.10: Wavelet damping mean and standard deviation as function of window length.

Similar to the results for frequency, damping ratio standard deviation decreases and the mean value stabilises with increasing window length for the ARMA method. Being a time domain method, it is expected that a change in window length could have a larger effect on the ARMA method, rather than the wavelet method where all calculations are performed in the wavelet domain.

The wavelet method displays an increase in standard deviation for larger window lengths. A slight positive bias is noticed for the damping ratio results obtained by the wavelet method. It is the largest at a 1-min window length. The authors of [7] found unacceptably high biases when a window length shorter than 1-min is used.

Note again that the y-axis values for the ARMA results on damping ratio (Figure 4.9) are restricted to enable visual comparison of the methods.

By comparing the results for frequency and damping between the two methods, it is observed that results with a similar mean accuracy and standard deviation are found when a 2-min window length is used. For all tests that follow a 2-min window length will be used for both methods as comparative results are then expected.

4.3.3 Window Length: Impact on Signal Spectrum

The frequency content of signals can aid the understanding of developing system conditions, especially if tracked over time. Increasing energy in a frequency component can be a visually intuitive indication of unstable modes. To this end, the spectral content of the signals used are investigated over time.

This is achieved via the modified Yule-Walker spectral estimator for the ARMA method, discussed in section 3.2.3. For the wavelet method, energy in the signal spectrum can be identified by simply inspecting the CWT coefficients over time. For both methods, ridges in the frequency spectrum indicate energy identified in the specific frequency component.

The spectral content of the signal is investigated using a 2-min, 5-min and 10-min window length for each method. Figure 4.11 presents the ARMA spectral estimation for different window lengths and Figure 4.12 presents the CWT coefficients of the wavelet method.

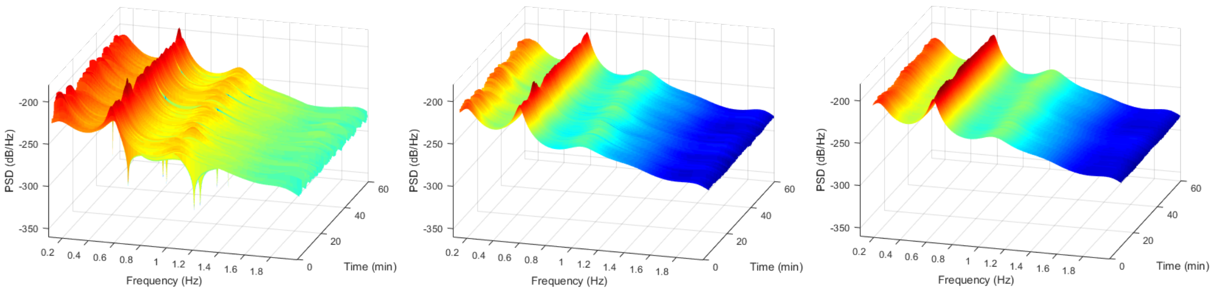

(a) 2-min window length **(b)** 5-min window length **(c)** 10-min window length

Figure 4.11: ARMA spectral estimate for different window lengths.

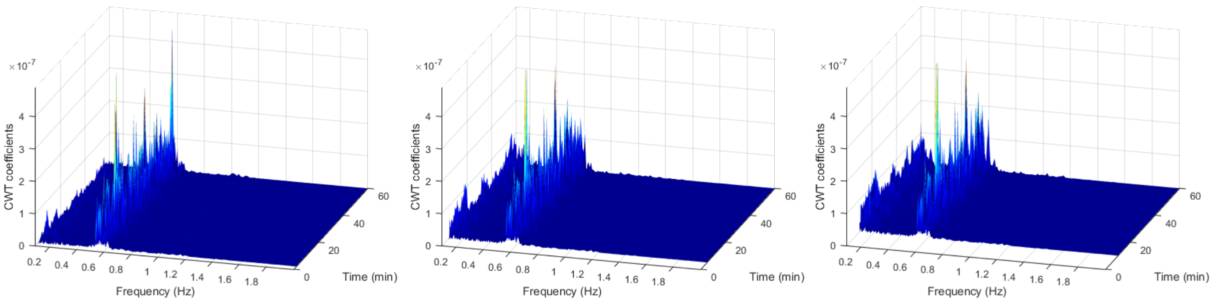

(a) 2-min window length **(b)** 5-min window length **(c)** 10-min window length

Figure 4.12: Wavelet method CWT coefficients for different window lengths.

In both figures, the presence of energy near the 0.5 Hz component is significant and expected. Energy is identified in this frequency component throughout the duration of the simulation.

Very little change is observed in the spectral content for different window lengths for both methods. The only appreciable difference is observed in the ARMA spectral estimation at 2-min window length (see Figure 4.11a). Deep nulls are modelled in the frequency spectrum for some results. This is observed as downward vertical spikes in the spectrum. However, this does not impact negatively on the ability to identify energy near the 0.5 Hz component. No significant difference is observed in the wavelet CWT coefficients (Figure 4.12).

4.3.4 Window Length: Impact on Mode Shape

The influence of window size on the result for mode shape is evaluated. Mode shape is calculated in addition to every frequency and damping value. Mode shape results are based on a 2-min, 5-min and 10-min window length. The results for frequency and damping are used to select five points where the calculated parameter differs the most from the theoretical value. Mode shape calculated at these instances are plotted on a single axis. If the mode shape results from these selected points (with the worst accuracy) can still indicate the presence of an inter-area mode, it is assumed that for any other instant the mode shape result should also be accurate.

Figure 4.13 presents the selected mode shape results from the ARMA method for different window lengths. The spread of the results for all window lengths are minimal and compare well to the theoretical values shown in Figure 4.2. Results from all window lengths clearly show a 180° phase shift between machines M1/M2 and M3/M4. The presence of an inter-area mode is thus clearly indicated with no significant effect of window length observed.

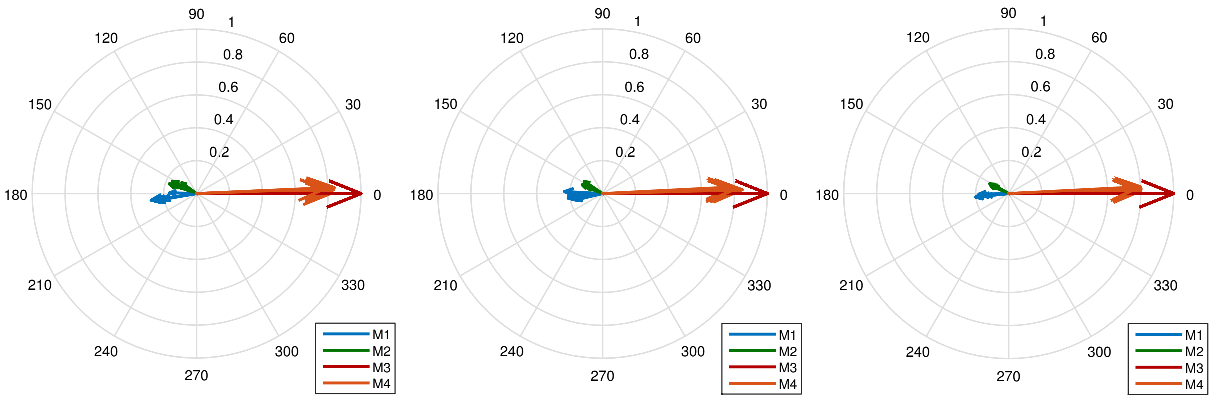

(a) 2-min window length **(b)** 5-min window length **(c)** 10-min window length

Figure 4.13: Spread of ARMA method mode shape results for different window lengths.

Figure 4.14 presents the selected mode shape results from the wavelet method for different window lengths. A larger, but consistent spread for mode shape values are observed. No significant correlation with window length change is noticed. Despite the larger spread of the values, an approximate 180° phase shift can still be discerned between machines M1/M2 and M3/M4, indicating the inter-area mode.

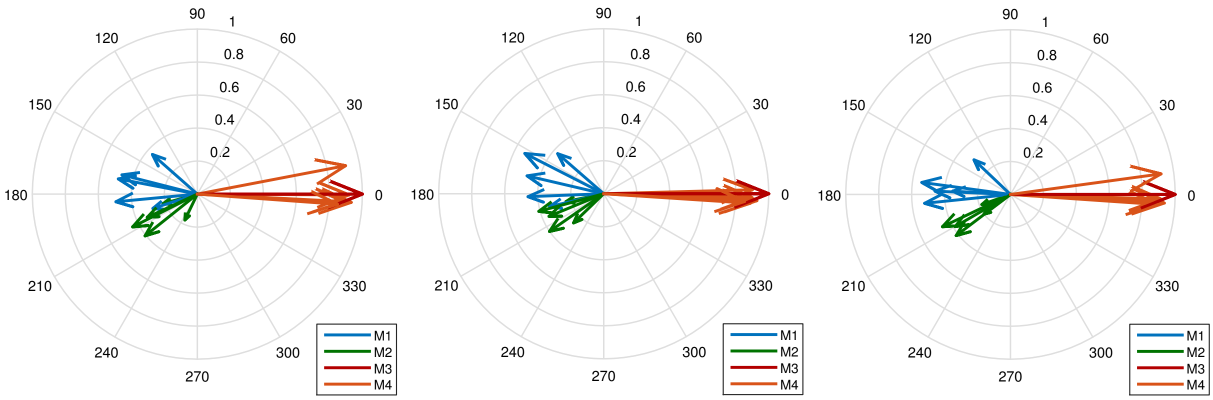

(a) 2-min window length **(b)** 5-min window length **(c)** 10-min window length

Figure 4.14: Spread of wavelet method mode shape results for different window lengths.

Both methods are able to provide accurate mode shape estimations. No significant change in mode shape behaviour is noticed for different window lengths. Both methods correctly identify the inter-area mode in the test system.

4.4 System Damping

The effect of system damping on the behaviour of each method is evaluated. The amount to which a system can damp a low frequency oscillation has a significant effect on the accuracy of any small signal monitoring method.

Three simulated cases of the Kundur system was prepared for this purpose. The damping in the system is manipulated by varying the number of Power System Stabilizers connected to the machines. The characteristics of the inter-area modes for each case is listed in Table 4.2.

Table 4.2: Simulated cases for system damping test.

Case	Number of PSSs	Frequency (Hz)	Damping (%)
1	2	0.5672	4.13
2	3	0.5598	9.67
3	4	0.5410	16.64

4.4.1 System Damping: Impact on Frequency and Damping Ratio Results

A 2-min window length is used for both methods to calculate the inter-area characteristics. The frequency results are used to indicate the effect of system damping on the methods.

The theoretical frequency for the 3 simulated cases is not identical, and thus direct comparison of the frequency results is not strictly possible. However, the comparison of frequency trends still illustrate the effect of system damping and it is chosen to plot the trends on a single axis.

The theoretical value for frequency indicated on Figure 4.15 and Figure 4.16 is taken as the average theoretical frequency of the 3 simulated cases. This compromise is deemed acceptable as the 3 theoretical frequency values differ only from the second decimal value onward.

Figure 4.15 and Figure 4.16 aim to illustrate the difference in performance brought about by changes in system damping, the theoretical value is only added as reference. Figure 4.15 presents the results from the ARMA method and Figure 4.16 presents the results from the wavelet method.

The effect of system damping is observed in Figure 4.15 and Figure 4.16. Reduced system damping produces more accurate results in both methods. Variance in the results is less for lower system damping. This result is confirmed in the literature and has also been discussed in section 2.6.2.

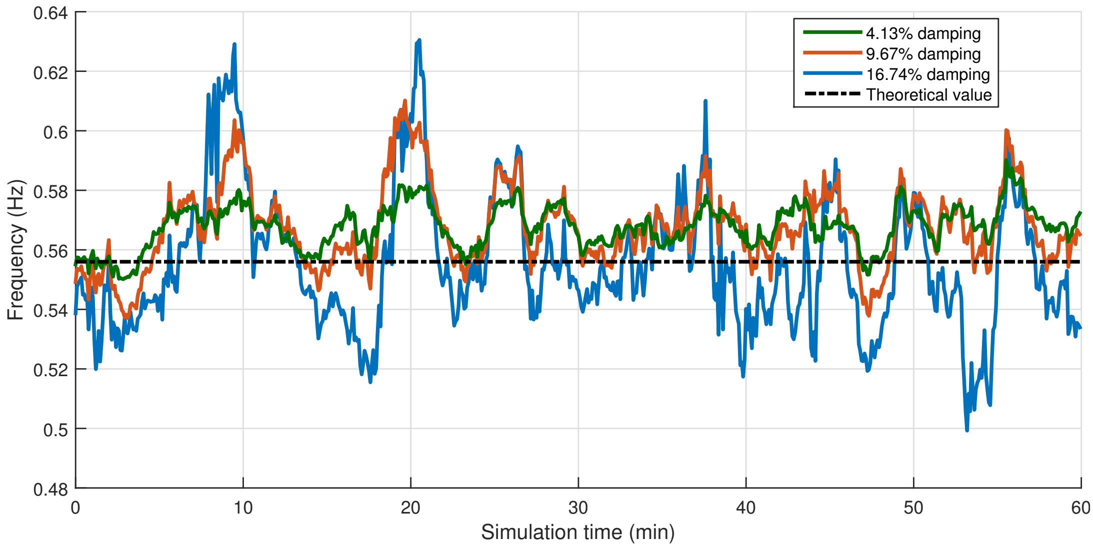

Figure 4.15: Frequency trend for ARMA method at different system damping levels.

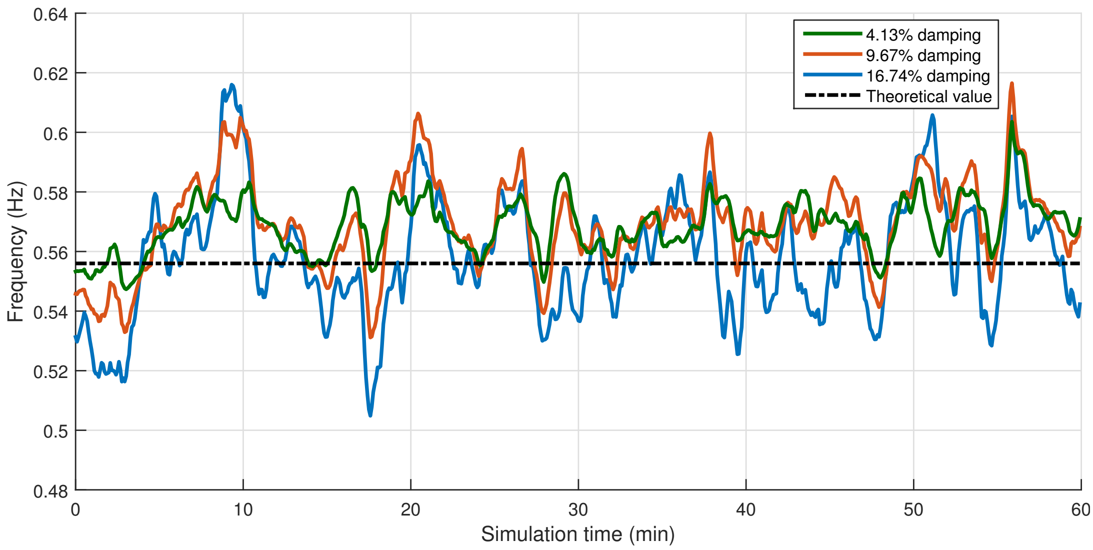

Figure 4.16: Frequency trend for wavelet method at different system damping levels.

Well-damped modes will be less prominent in recorded data as the oscillation decays very quickly due to a high damping ratio. Modes with low damping (less stable modes) do not decay as quickly and is easier to identify from field data.

Plotting the mean error and standard deviation for each set of frequency and damping ratio results as a function of system damping further evaluate the effect of system damping. Figure 4.17 presents the mean errors, while Figure 4.18 presents the standard deviation for frequency and damping ratio results.

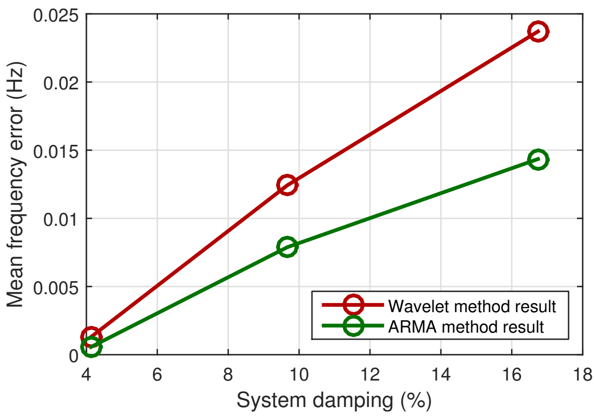

(a) Frequency result mean error vs system damping.

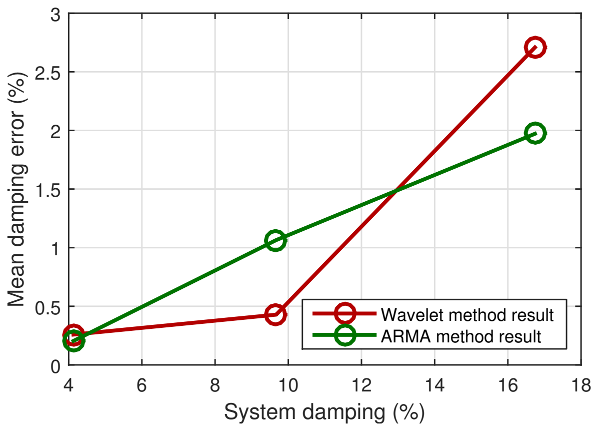

(b) Damping result mean error vs system damping.

Figure 4.17: Mean error in frequency and damping results as function of system damping.

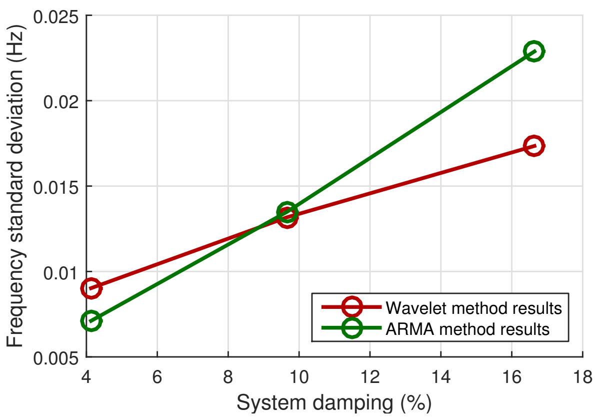

(a) Frequency result standard deviation vs system damping.

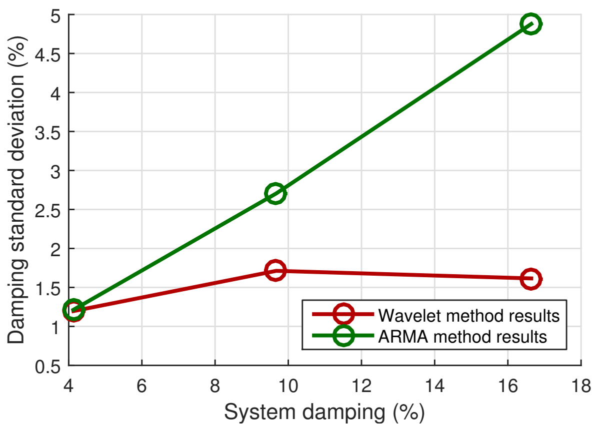

(b) Damping result standard deviation vs system damping.

Figure 4.18: Standard deviation in frequency and damping results as function of system damping.

Accuracy degrades with increasing system damping, observed as an increase in both mean errors and standard deviations for frequency and damping results. Accuracy decreases approximately linearly for both the ARMA and wavelet methods.

4.4.2 System Damping: Impact on Signal Spectrum

The influence of system damping on the spectral content of the signal is investigated. The ARMA spectral estimation and CWT coefficients are computed using a 2-min window length for the 3 simulated cases. Figure 4.19 presents the ARMA spectral estimate and Figure 4.20 presents the CWT coefficients for increasing damping from left to right.

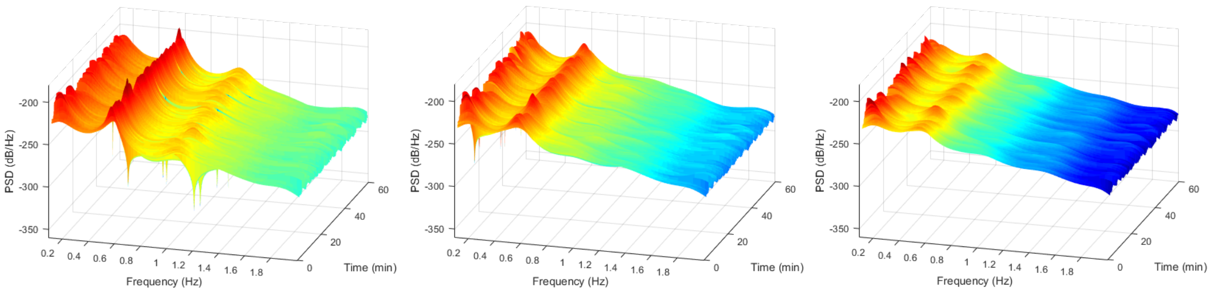

(a) 4.13% system damping **(b)** 9.67% system damping **(c)** 16.64% system damping

Figure 4.19: ARMA spectral estimate for different system damping levels.

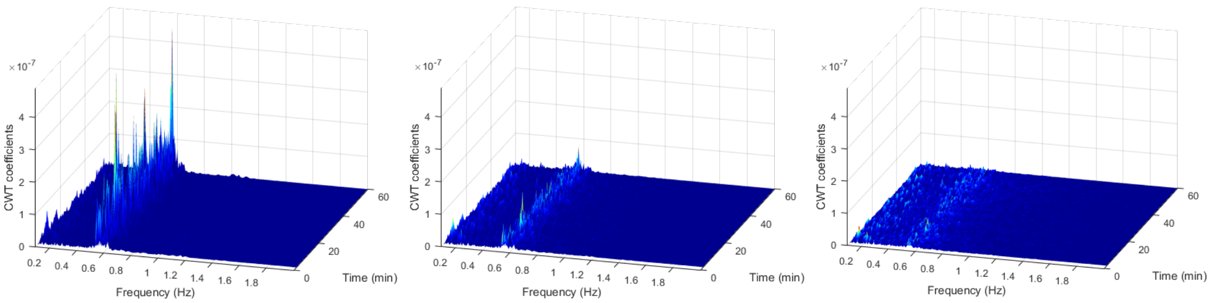

(a) 4.13% system damping **(b)** 9.67% system damping **(c)** 16.64% system damping

Figure 4.20: Wavelet method CWT coefficients for different system damping levels.

Both methods identify decreasing energy near the 0.5 Hz component as damping increases. The effect of increased system damping is clearly seen. The methods will have increasing difficulty in reliably identifying the inter-area mode characteristics when mode energy reduces.

A single spectral estimate for each method and each damping case is extracted at the start of the simulation to clearly show the behaviour described above. Figure 4.21 and Figure 4.22 presents the ARMA spectral estimate and CWT coefficients respectively.

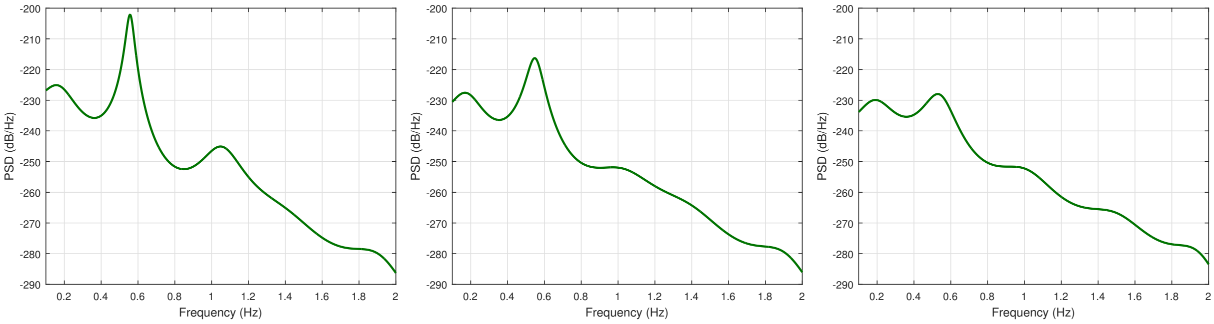

(a) 4.13% system damping **(b)** 9.67% system damping **(c)** 16.64% system damping

Figure 4.21: Single ARMA spectral estimate for different system damping levels.

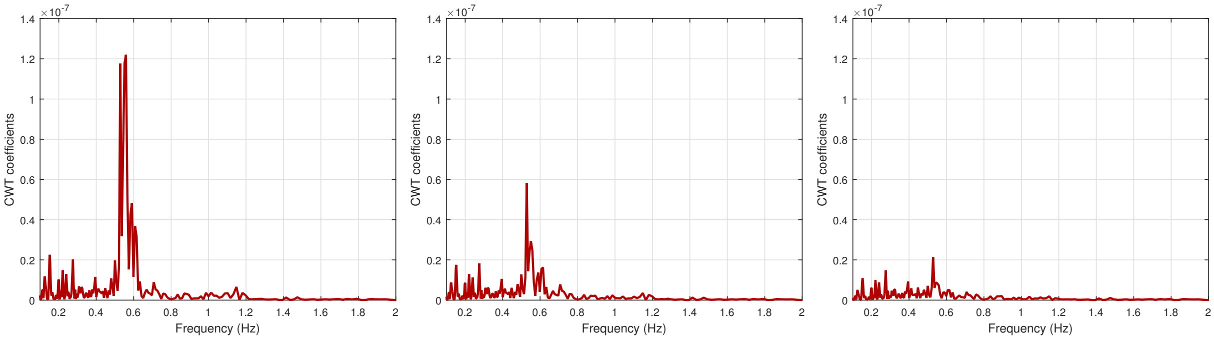

(a) 4.13% system damping **(b)** 9.67% system damping **(c)** 16.64% system damping

Figure 4.22: Single wavelet method CWT coefficients for different system damping levels.

Figure 4.21 and Figure 4.22 clearly indicate the decrease in inter-area mode energy as system damping increases.

4.4.3 System Damping: Impact on Mode Shape

The effect of system damping on mode shape accuracy is evaluated. A similar approach is adopted as in section 4.3.4. Five points are selected from each set of results, where the calculated value differs the most from the theoretical value. Mode shape at these points is plotted on a single axis. These points are assumed to be the most inaccurate, displaying the maximum spread of mode shape values to be expected for a given result set.

Figure 4.23 presents the ARMA mode shape results for changing system damping. Extremely little spread of mode shape values is observed when system damping is low (Figure

4.23a). Figure 4.23b shows increasing spread in mode shape results. The presence of an inter-area mode is still clear. The simulation case with the highest system damping produces significant spread in mode shape values (Figure 4.23c). The spread of values can hamper reliable identification of the inter-area mode shape.

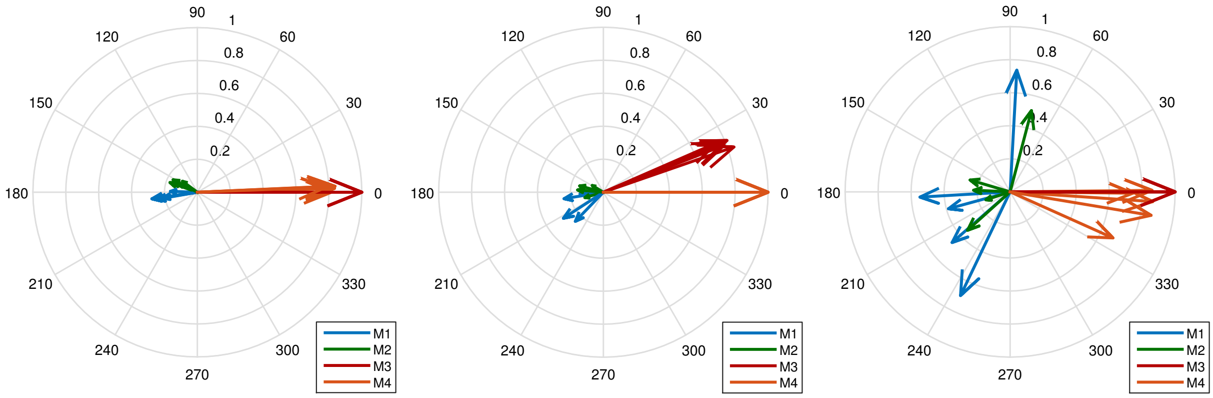

(a) 4.13% system damping **(b)** 9.67% system damping **(c)** 16.64% system damping

Figure 4.23: Spread of ARMA method mode shape results for different system damping levels.

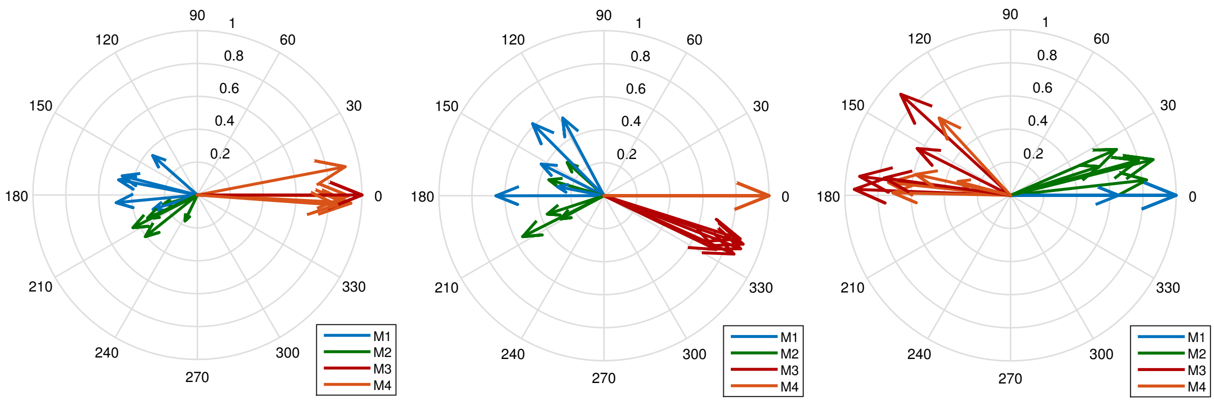

(a) 4.13% system damping **(b)** 9.67% system damping **(c)** 16.64% system damping

Figure 4.24: Spread of wavelet method mode shape results for different system damping levels.

Figure 4.24 presents the mode shape results for the wavelet method. The mode shape result show an increase in spread for increasing system damping. For the highest damping simulation (shown in Figure 4.24c) the largest spread of values are observed but the mode can still be reliably classified as an inter-area mode. The wavelet method performs better at mode shape calculation than the ARMA method for high system damping.

4.5 Simulink Model

A simple Simulink™ model was used for further testing of the two methods. It consists of a single pole pair transfer function with white noise as inputs. The modes present in the system are manipulated by the value of the poles of its transfer function. The Simulink™ model is presented in Figure 4.25.

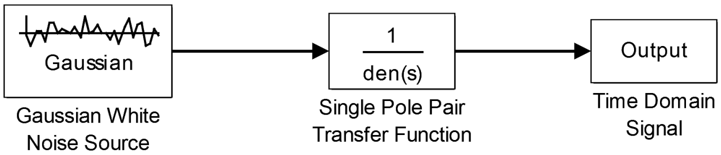

Figure 4.25: Simulink™ test system.

This model is used to investigate the ability of both methods to track changing system conditions in the next section.

4.6 Ability to Track Changes

The ability of both methods to track changes in mode characteristics are evaluated in this section. The Simulink™ model introduced in the previous section is used to produce simulation data containing a single inter-area mode with changing characteristics.

4.6.1 Tracking Slow Changes

The Simulink™ model in Figure 4.25 is configured to produce a single slow changing mode over the course of 45 minutes of simulation data. Characteristics of the mode are changed linearly over the period from 15 to 30 minutes in the simulation. The characteristics of the mode are listed in Table 4.3.

Figure 4.26 and Figure 4.27 presents the frequency and damping result respectively. Both methods are capable of tracking slow changing frequency and damping ratio.

Table 4.3: Characteristics of inter-area mode with slow changing behaviour.

Time (min)	Frequency (Hz)	Damping (%)
0 - 15	0.3	7
15 - 30	0.3 - 0.7	7 - 2
30 - 45	0.7	2

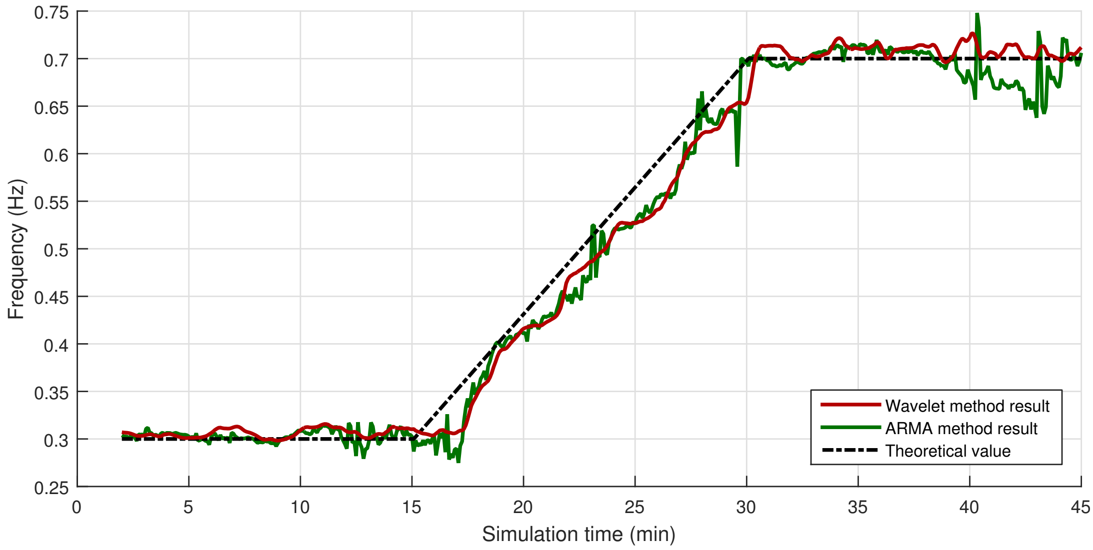

Figure 4.26: Slow changing frequency tracking performance

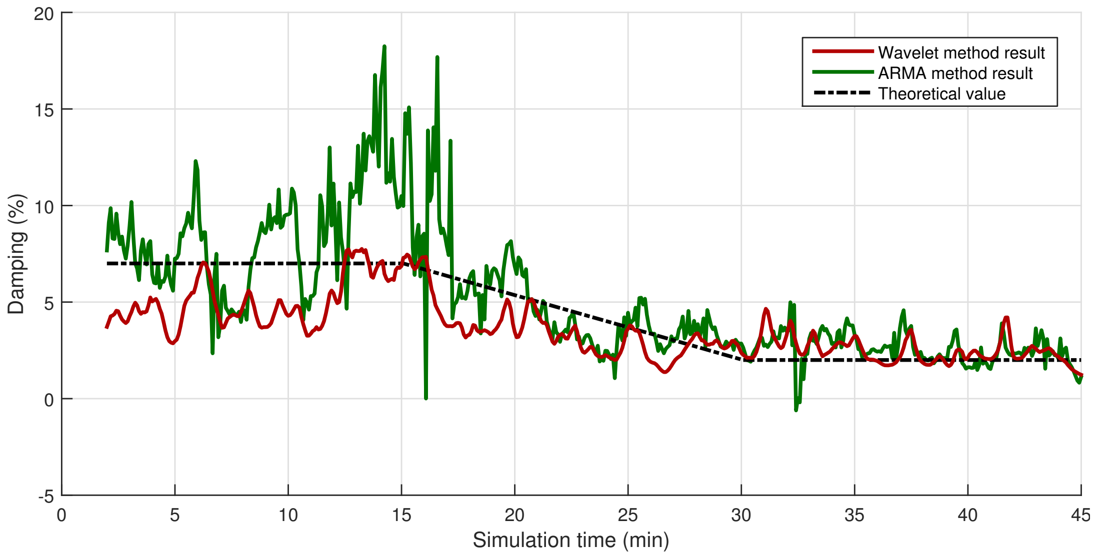

Figure 4.27: Slow changing damping tracking performance.

Frequency is tracked accurately by both methods. Damping estimation is less accurate, especially in the region where damping is high (0 to 15 minutes). A delay is observed between the calculated and theoretical values during the period of change (15 to 30 minutes). This delay is equal to the window length of 2-min used for each method. This result shows the influence of window length on the response of ambient methods. The trade-off between increased accuracy and method responsiveness is highlighted.

Figure 4.28 presents the spectral content of the signals for the ARMA and wavelet methods respectively. The three-dimensional plot is shown from above in order to see the ridges in the plot, indicating the presence of a frequency component. The colours in the bar on the right side of each plot indicate the relative size of features on the plot. The spectral estimate shows the changing frequency during the simulation.

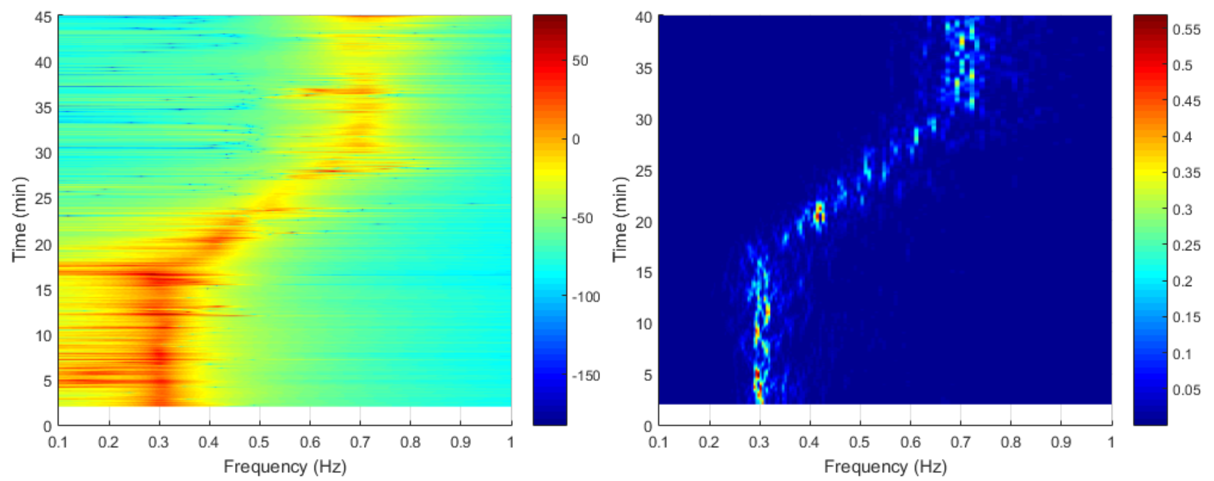

(a) ARMA method **(b)** Wavelet method

Figure 4.28: Spectral estimation for slow changing simulation.

4.6.2 Tracking Step Changes

The Simulink™ model in Figure 4.25 is configured to produce a step change in frequency and damping over the course of 40 minutes of simulation data. Mode characteristics make a step change at 20 minutes into the simulation. The characteristics of the mode are listed in Table 4.4.

Table 4.4: Characteristics of inter-area mode with step change behaviour.

Time (min)	Frequency (Hz)	Damping (%)
0 - 20	0.3	7
20 - 40	0.7	2

Figure 4.29 and 4.30 presents the frequency and damping results for both methods when a step change in mode characteristics is present. High system damping produces inaccurate results, similar to Figure 4.27. The delay in method response is clearly observed at the step change.

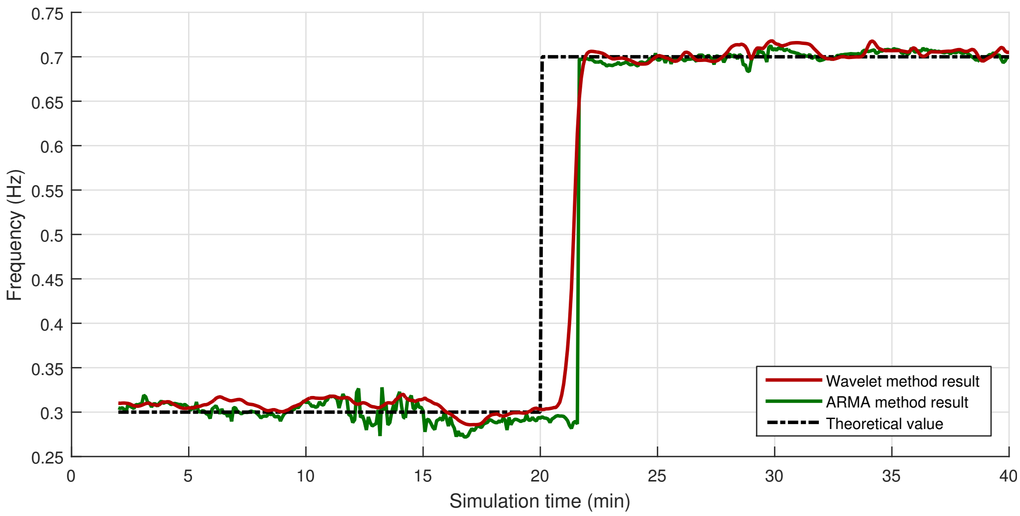

Figure 4.29: Step changing frequency tracking performance.

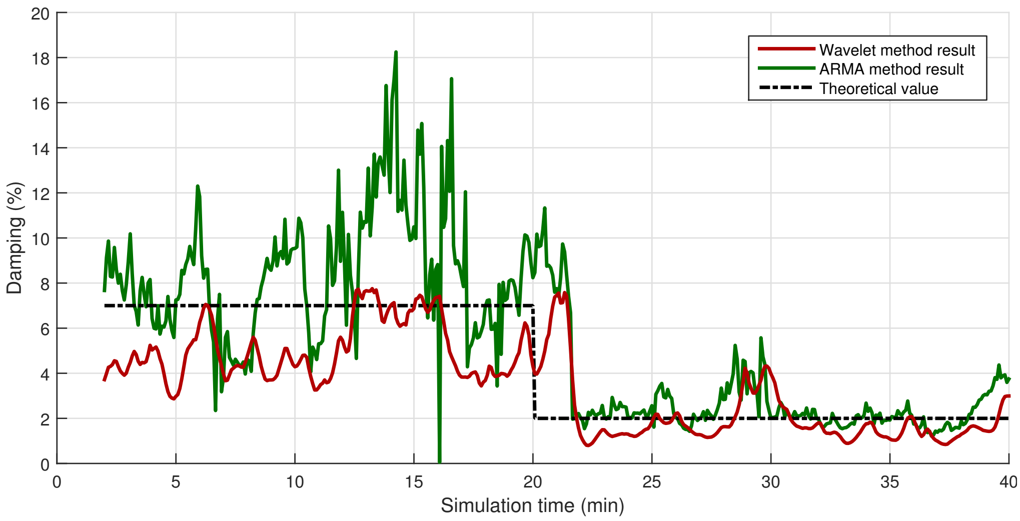

Figure 4.30: Step changing damping tracking performance.

Figure 4.31 presents the spectral content of the signal with the ARMA method on the left and wavelet method on the right. Again, the three-dimensional plot is shown from above, with the colours in the bar indicating size of the features on the plot. Observe the period just after 20 minutes has passed. An overlap of identified frequency components are observed. For the short time when the window contains data from before and after the step change, the presence of both frequency components is identified.

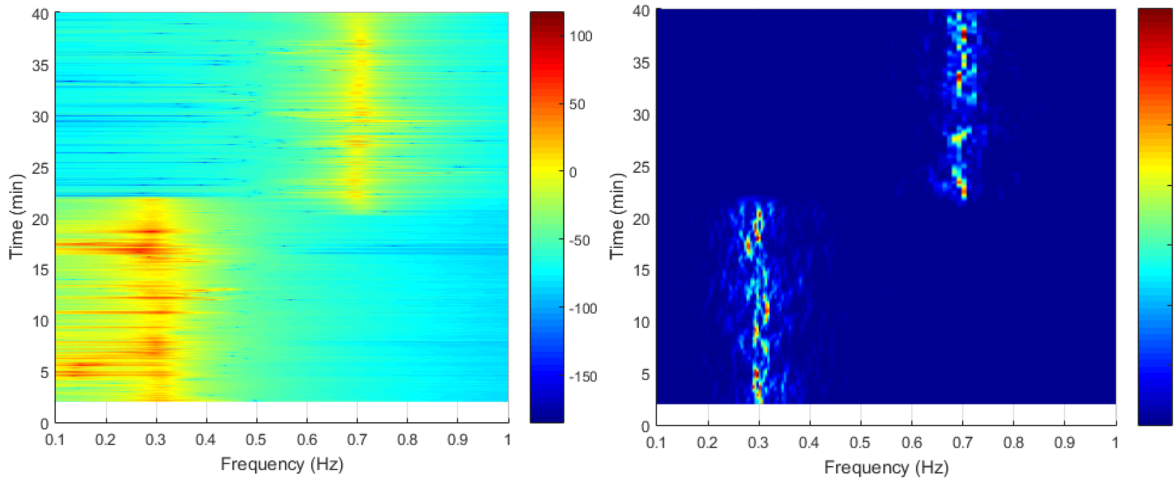

(a) ARMA method

(b) Wavelet method

Figure 4.31: Spectral estimation for step changing simulation.

4.7 Comments on Method Behaviour and Performance

Additional comments and experiences with the use of both methods are described to complement the test results presented in this chapter.

All tests conducted show a smoother response for the wavelet method than the ARMA method. ARMA method results do not display the smooth trends as for the wavelet method. The ARMA method produces small changes in consecutive results. Choice of the number of windows to consider for averaging $\widehat{C}(s)$ must be made during wavelet method implementation. This averaging process produces a smoothed response for the wavelet method. Choice of this parameter was discussed in section 3.3.4.

The process of mode selection was discussed in section 3.2.2. This process is necessary to identify dominant modes when using the ARMA method. No additional mode selection procedure is necessary for the wavelet method. The residues R_i from the Prony analysis in section 3.3.3 is used to determine dominant modes in the signal. The residues from the Prony analysis are able to reliably identify dominant modes, even at increased system damping levels. The mode selection process of the ARMA method did not consistently identify dominant modes in the signal when system damping increased. Extra filtering steps are needed to identify dominant modes and prevent mixing of modes in a single trend.

Both methods have calculation times sufficiently small enough to enable real-time implementation. Time needed to calculate results from a single 2-min window for the ARMA method is in the range of 0.04 seconds and 0.46 seconds for the wavelet method.

It should be feasible to update the calculation result at least every second, which should be sufficient for LFO monitoring applications. This calculation time is found on a standard desktop computer running Matlab™. No special effort was made to implement the method in a way to minimize calculation time. It is expected that calculation time could be significantly reduced by using more powerful hardware or an implementation of a method tailored for efficiency in processing time.

4.8 Conclusion

Accuracy of the 2 LFO monitoring methods was verified in this chapter. Both methods were applied to simulated datasets. It was shown that both methods are capable of characterising LFOs in real-time.

Performance of each method under various conditions was investigated. The effect of window length and system damping was shown. Increased window length improves ARMA method accuracy at the expense of rapid response. The wavelet method is affected much less by window length. Increased system damping degrades performance of both methods.

The capability of each method to track changing system conditions was illustrated. Behaviour of each method is highlighted in these tests, giving insight into the operation of each method and their applicability for practical use.

The next chapter contains a case study where each method is applied to field data recorded on a practical transmission line. Simulated testing has shown that the methods have sufficient accuracy to be applied to field data.

Chapter 5

Practical Validation of Methods

... where the potential of the oscillation monitoring methods is validated by application to recorded power system field data.

5.1 Introduction

This chapter presents results from the two oscillation monitoring methods when applied to field data. The effect of the measurement instrumentation on the methods is first investigated. This is done to confirm that the measurement instrumentation does not adversely affect the accuracy of the method results.

The two methods are then applied to data from a practical case study of a Southern African power system to validate the potential of these methods for practical real-time use. Insight into the behaviour of the studied power system is gained by performing three case studies on recorded field data.

5.2 Emulation of Small Signal Stability Parameters

In this section the instrumentation is included in an initial validation to verify accuracy of the data recording system and the performance of the analysis methods when subjected to recorded data (as opposed to data generated by simulation). This is achieved by emulating field data whilst retaining full control over the low frequency oscillation characteristics.

The measurement instrument used is a commercially available PQ instrument complying to IEC 61000-4-30 Class A edition 3 specifications. IEEE C37.118.1-2011 synchrophasor measurement functionality is implemented in parallel with PQ recordings. The reader is referred to section 2.8 for a discussion of the possibility to implement various measurement methodologies on a single instrument.

The Kundur system is used to prepare a 10 minute simulation with Simulink™. The inter-area mode in the system has the characteristics as detailed in Table 4.1. The simulation computed 1000 samples per second. Complex voltages from bus 20 and 120 is captured and reconstructed to a waveform. Figure 5.1 indicates the buses in question.

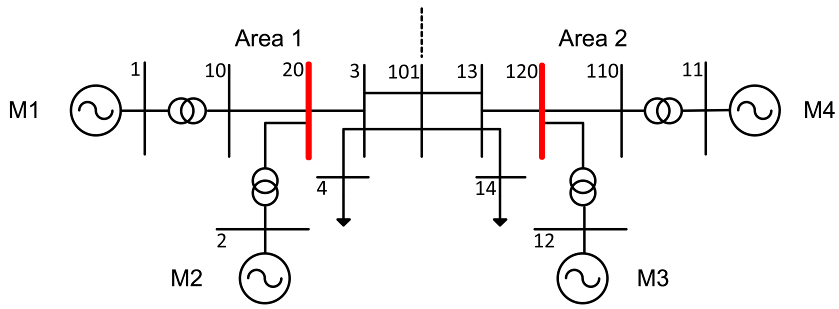

Figure 5.1: Selected buses from Kundur system.

The recording instrument was then connected to a waveform generator, a CMC256plus™. Voltage waveforms from bus 20 and 120 were generated at field conditions of 110 V (rms) by this instrument based on the computer simulation. The performance of the hardware that records the synchrophasor data can now be included in the performance investigation.

This recorded data were used in the analysis as it emulates recordings in a real power system. Data was extracted from the recording instrument and subjected to both small signal analysis methods. This process is described in Figure 5.2.

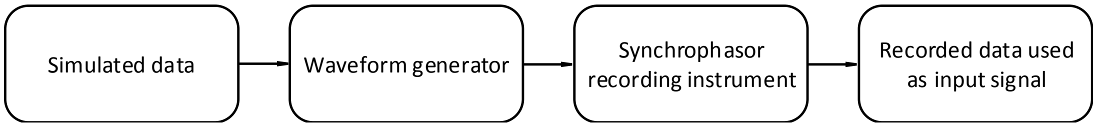

Figure 5.2: Practical setup for emulation test.

A comparison is done between results from the computer simulated data and the emulated field data. Figures 5.3 to 5.6 present the results for frequency and damping ratio of both methods for the simulated and emulated datasets.

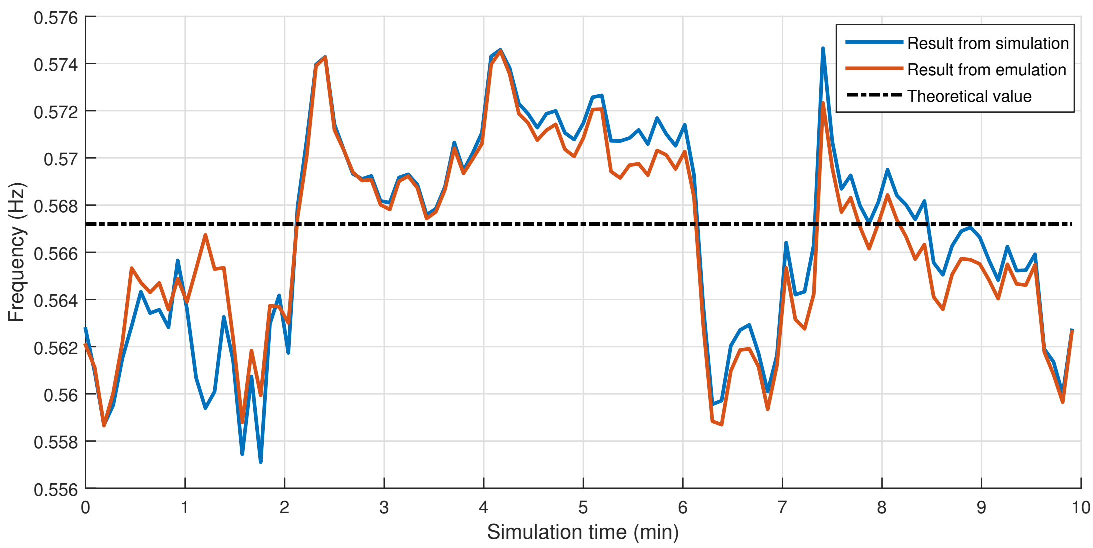

Figure 5.3: ARMA frequency results for simulated and emulated datasets.

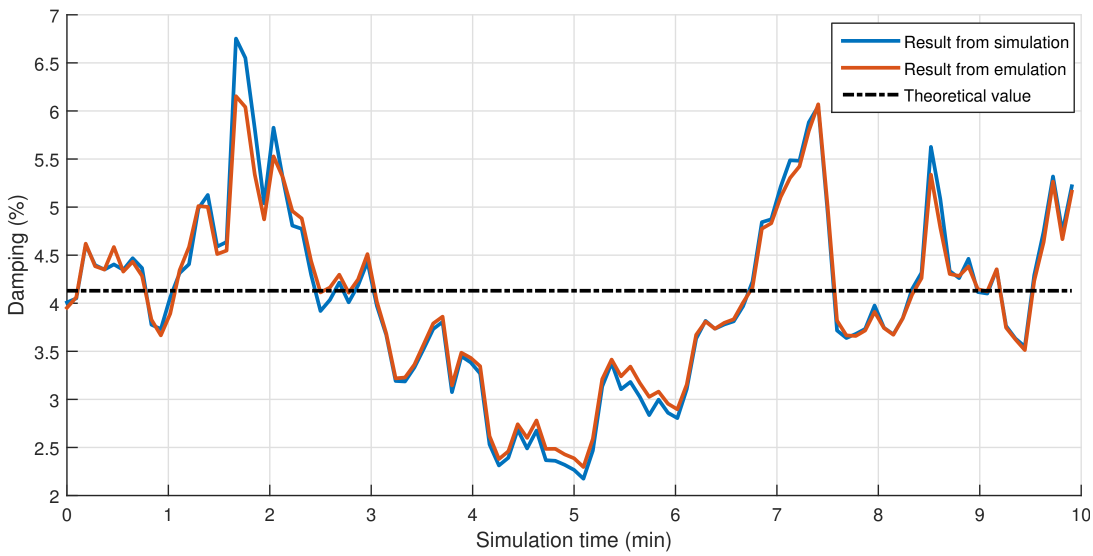

Figure 5.4: ARMA damping results for simulated and emulated datasets.

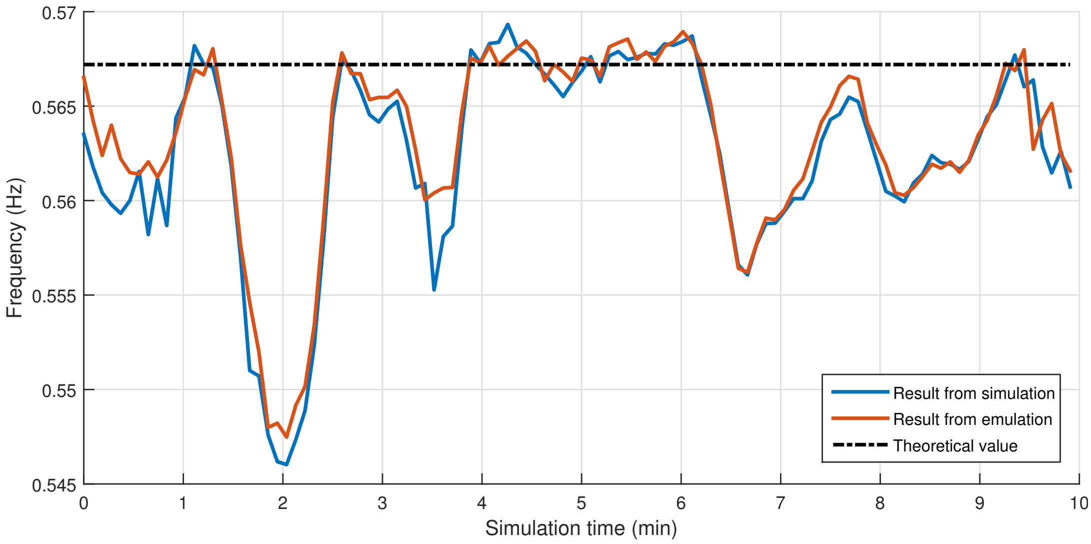

Figure 5.5: Wavelet frequency results for simulated and emulated datasets.

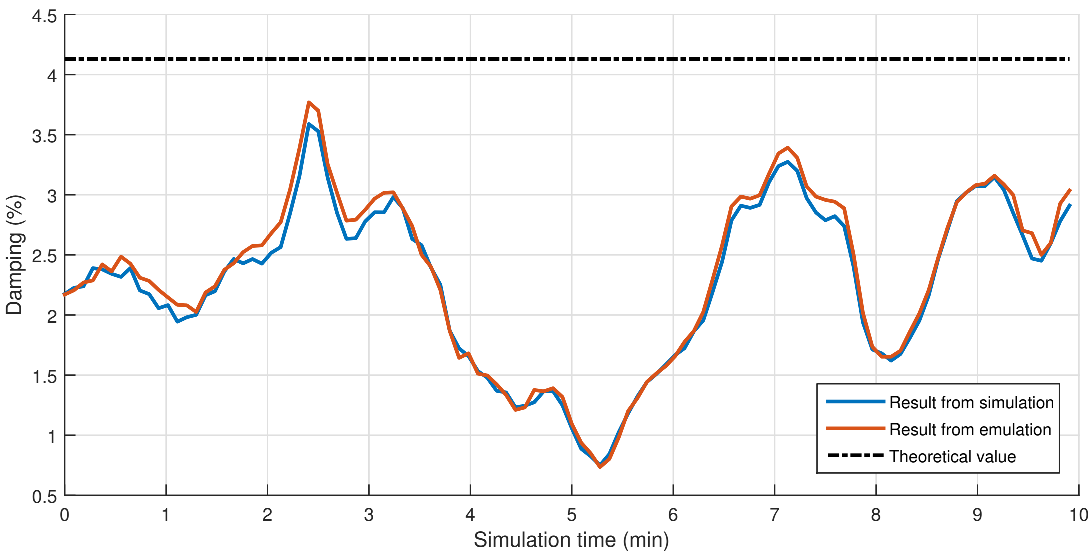

Figure 5.6: Wavelet damping results for simulated and emulated datasets.

The results obtained from simulated and emulated datasets are near identical. The wavelet method damping result displays a slight negative bias from the theoretical value, but this behaviour is observed for both the simulated and emulated datasets, confirming measurement accuracy.

This test indicates that the measurement instrumentation in use can record power system parameters accurate enough and does not introduce measurement noise to the extent that it adversely affects method accuracy.

5.3 Practical Case Study

Synchrophasor data was recorded on a 330 kV, 521 km transmission line. The transmission line connects a hydro-generation plant to a transmission switching substation, with no loading, injection or compensation in between.

Recall the discussion concerning versatile measurement instrumentation in WAMS from section 1.4 and 2.8. Synchrophasor field data for this practical case study was recorded using measurement instrumentation where synchrophasor measurement capability is implemented according to C37.118.1 specifications in parallel with PQ recordings of IEC 61000-4-30 Class A edition 3 specifications. The advantages of versatility in power system instrumentation is illustrated next by performing specialised WAMS functions from data recorded by low cost hardware.

5.4 Case Study: 1 February 2015

Synchrophasor data recorded on 1 February 2015 is used as the first field case study. Figure 5.7 presents the active power transfer recorded during this day. It is observed that the generation is reduced from approximately midnight to 07:00, and again from 21:00. This is a daily pattern of this hydro station in matching a national loading profile of the country in which the data was recorded.

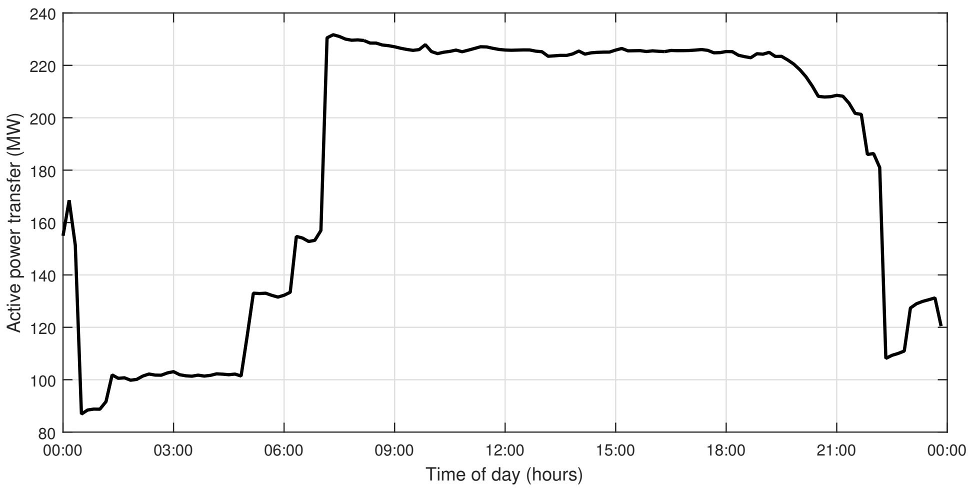

Figure 5.7: Active power generation at hydro-station. (1 February 2015)

5.4.1 Input Signal Selection

Input signals to the modal analysis methods must first be selected. Discussion regarding input signal selection was presented in section 3.4.1. The best signal to use as input will depend on the dynamics of the power system as it determines which signal will have the best observability of a mode.

The linear decoupling transform in Equation (2.19) from section 2.4.4 uncouples the state space model so that each mode is associated with one state variable only. Without knowledge of the system model, it is challenging selecting the best signal to use as input.

Both methods can use multiple signals as input. Results from using different input signals are compared. Three sets of results are based on a single parameter, consisting of either one or two signals. The 4$^{\text{th}}$ set of results is based on using a combination of all the possible input signals. Table 5.1 lists the input signals used to produce each result set in Figures 5.8 to 5.11.

Table 5.1: Input signals used for different result sets.

Result set	Colour code	Input signal used
1	Blue	- Hydro-station frequency - Switching substation frequency
2	Green	- Angular separation across transmission line
3	Orange	- Hydro-station active power - Switching substation active power
4	Red	- Hydro-station frequency - Switching substation frequency - Angular separation across transmission line - Hydro-station active power - Switching substation active power

Figure 5.8 and 5.9 present the frequency results for both methods, while Figure 5.10 and 5.11 present the damping results for both methods. Results using angular separation,

active power and a combination as input show similar results for both methods. Both methods identify a dominant mode between 0.4 - 0.5 Hz at 5 - 10 % damping during the period of high generation.

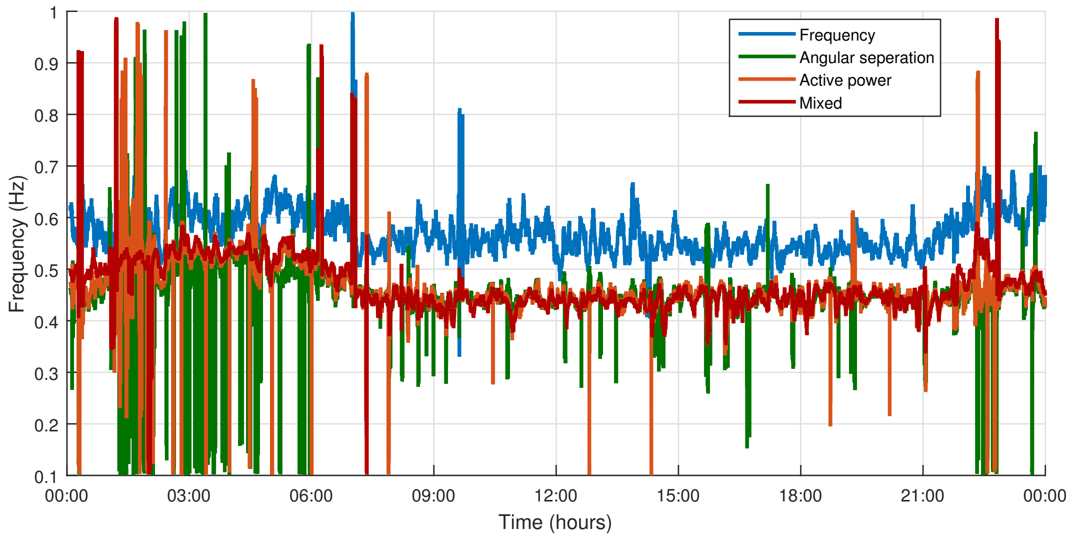

Figure 5.8: ARMA method frequency results for different input signals. (1 February 2015)

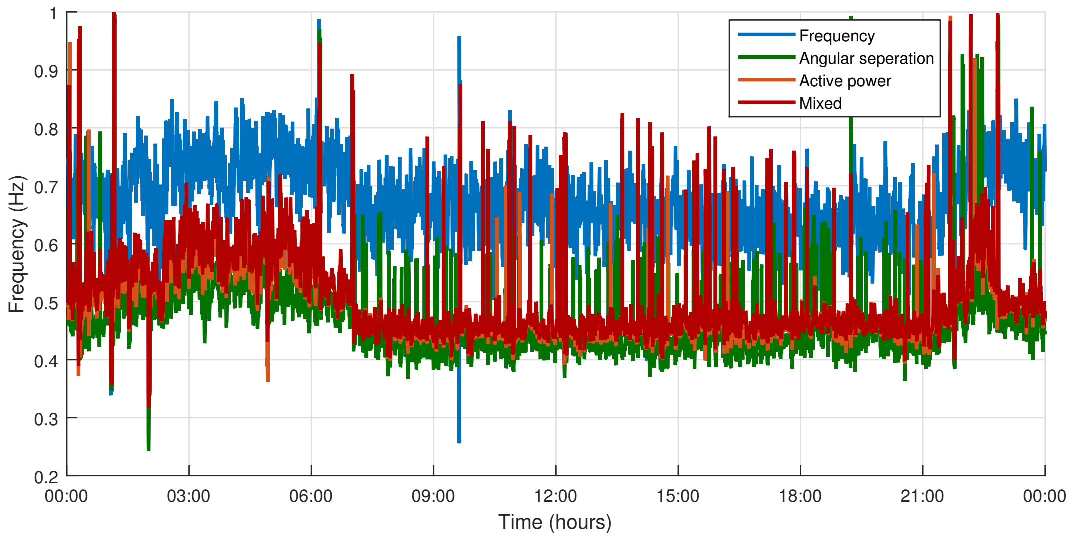

Figure 5.9: Wavelet method frequency results for different input signals. (1 February 2015)

A difference in damping result between the two methods are noticed. The wavelet method damping result is approximately 5 % during high generation whilst the ARMA method produces a damping estimate around 15 % for the same time. Very little is known regarding inter-area characteristics of this specific power system and the true damping value is unknown. Note also that the scale for damping result differs between Figures 5.10 and 5.11. ARMA and wavelet method damping results display similar variance.

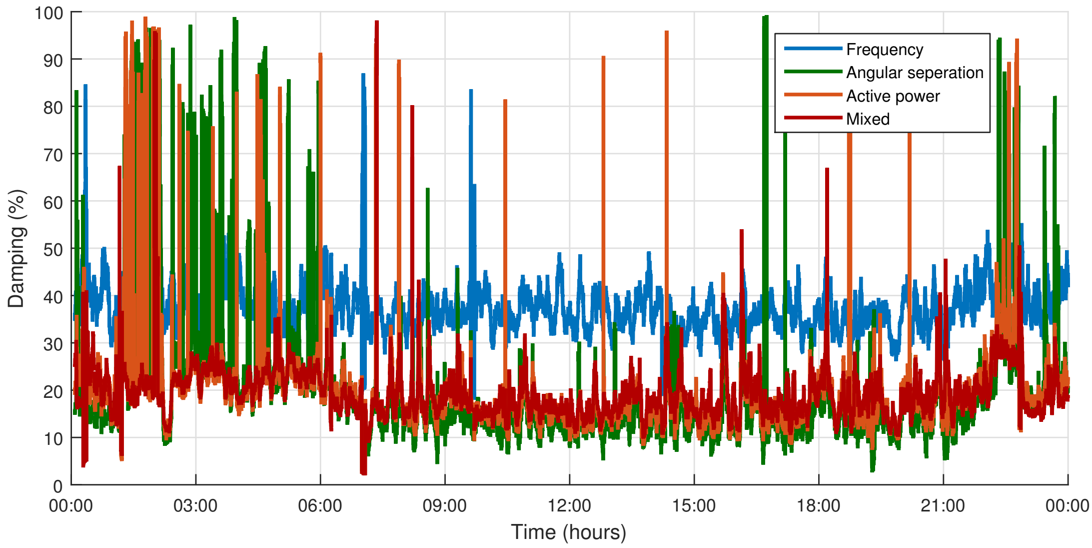

Figure 5.10: ARMA method damping results for different input signals. (1 February 2015)

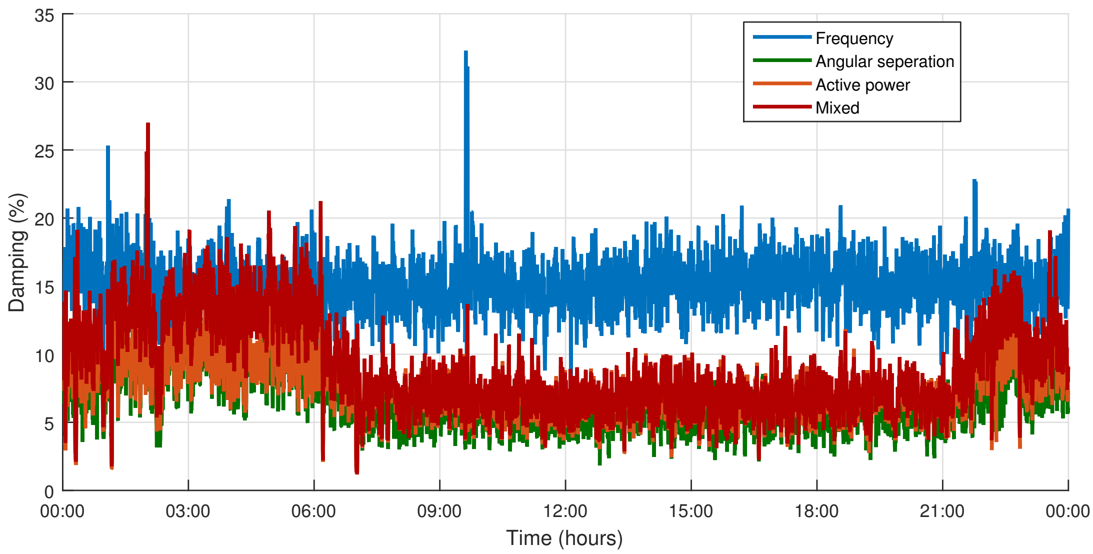

Figure 5.11: Wavelet method damping results for different input signals. (1 February 2015)

Results based on the frequency signal consistently produce higher estimates for frequency and damping than results based on the other input signals. Figure 5.12 shows the PSD of the frequency, active power and angular separation signals. The active power and angular separation signals contain energy at approximately 0.4 Hz. The frequency signal does not contain significant energy in this band. Observability of inter-area oscillations in the frequency signal is limited. This causes incorrect results based on the frequency signal.

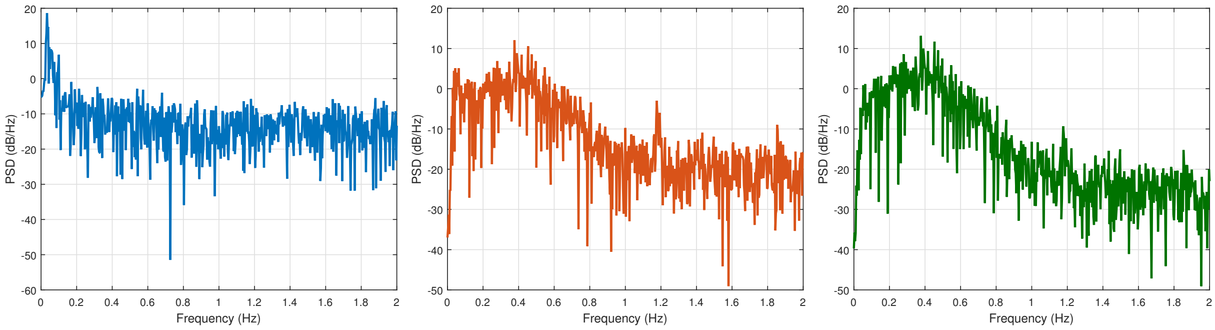

(a) Frequency signal **(b)** Active power signal **(c)** Angular separation signal

Figure 5.12: PSDs of various input signals.

It is a challenge selecting an input signal without prior knowledge of the observability of inter-area modes in each measured signal. By using multiple inputs, signals with good observability of a mode enable accurate results. Results from using a combination of input signals in Figure 5.8 to 5.11 validate that such an approach is feasible. The mixed input signal produces results similar to signals with high observability.

A 2-min window length is used when the wavelet method is applied to measured data, as previous tests on simulated data used this window length. A 5-min window of field data is used for the ARMA method.

Practical results from the ARMA method with a 2-min window varied so much that mode frequency and damping identification became unreliable. Specifically, the mode selection procedure (see section 3.2.2) fails to extract the inter-area mode from the modes identified by the method. Modes identified due to numerical artefacts or noise get selected as dominant modes, making monitoring of the true inter-area modes unreliable.

The periods of the greatest inaccuracy in the results coincide with periods of reduced generation at the hydro-station, presented in Figure 5.7. The reduced power transferred over the transmission line results in increased oscillation damping in the system. This is confirmed by the damping result shown in Figure 5.10 and 5.11. A higher damping ratio is obtained when generation is decreased. It was shown in section 4.4 that the accuracy of both methods degrade with higher oscillation damping, accounting for the reduced accuracy at high damping values.

5.4.2 Signal Spectral Content

The frequency content of the measured signals tracked over time can aid the understanding of developing conditions. Increasing energy in a frequency component can be a visually intuitive indication of unstable modes.

For the ARMA method, the ARMA spectral estimation is calculated for each window and displayed over time in a surface plot in Figure 5.13. For the wavelet method, the coefficients from the CWT are similarly plotted over time in Figure 5.14. It was found that viewing the spectral plot straight from the top provided the easiest way to observe sudden changes in the spectrum.

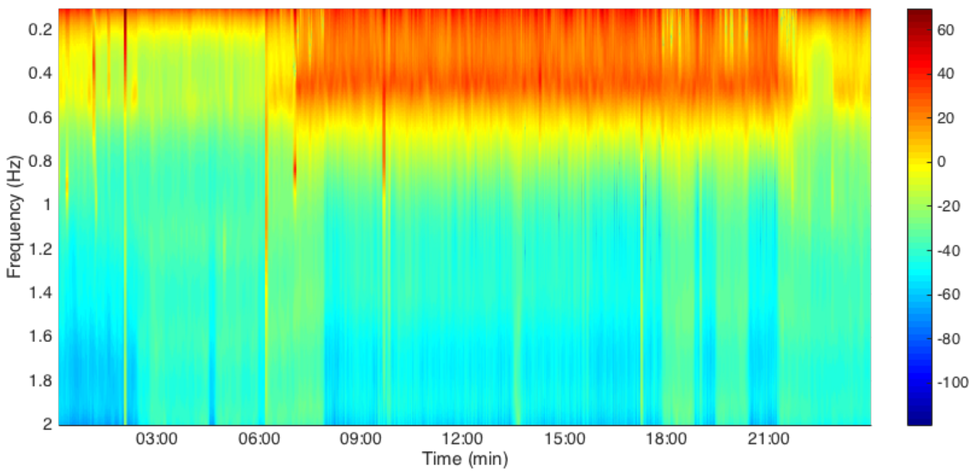

Figure 5.13: ARMA spectral estimation over time. (1 February 2015)

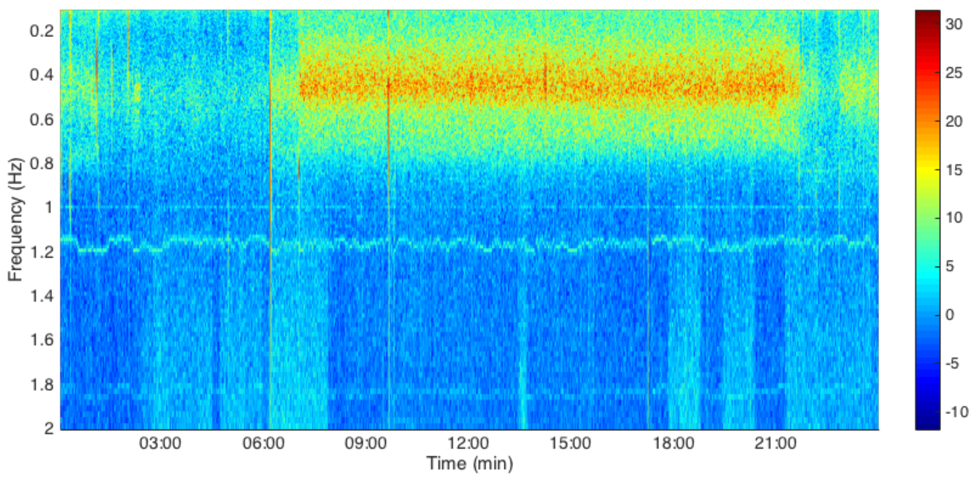

Figure 5.14: CWT coefficients over time. (1 February 2015)

Sudden changes can be obscured if the spectrum is viewed in three-dimensional orientation. Intensity of the spectrum is interpreted through the colours in the bar shown on the side of the plot.

The ARMA spectral estimation and the CWT coefficients show the absence of significant energy between 0.1 Hz and 2 Hz when hydro-generation is reduced (early morning). As soon as generation is increased, the inter-area mode is excited at 0.4 Hz. The inter-area mode remains excited when active power transfer is high.

Observe the sudden increase in energy over a wide range of frequencies between approximately 06:00 and 10:00. Both methods identify 3 instances with a sudden increase in spectral energy. This is observed as 3 prominent red vertical lines on Figure 5.13 and 5.14 between 06:00 and 10:00. The energy in these frequency components decay quickly.

The times of these events coincide with sudden increases in generation at the hydro-station (see Figure 5.7). Sudden increases in generation lead to a transient behaviour that decays fast.

5.4.3 Mode Shape

Mode shape for the power system is presented. The mode shape at 12:00 on 1 February refers.

The inter-area oscillation in the system is well excited at this time and the system is in a steady state condition. Figure 5.15 presents the mode shapes calculated by both methods.

The mode shape from both methods shows the switching substation oscillating in phase with the hydro-station. The smaller magnitude associated with the switching substation indicates that the oscillation is not as severe at this point.

With only 2 points of measurement available, it is not possible to determine which areas of the interconnected power system take part in the opposing side of the oscillation. System wide synchrophasor data is needed to determine this.

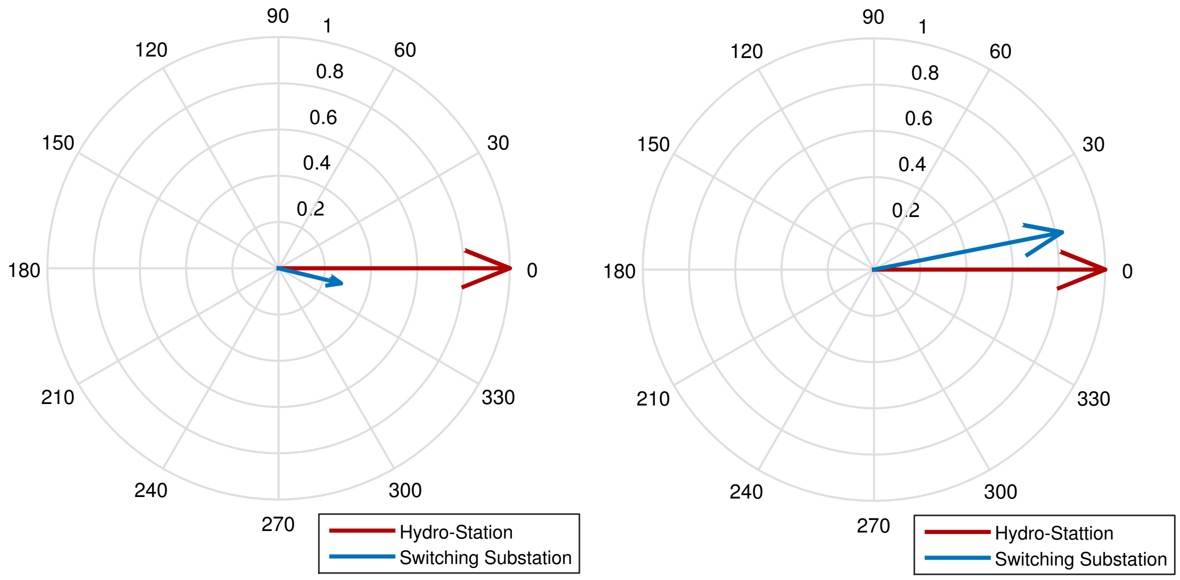

(a) ARMA method

(b) Wavelet method

Figure 5.15: Mode shape. (1 February 2015 12:00)

5.5 Case Study: 14 - 21 March 2015

Synchrophasor data recorded from 14 - 21 March 2015 is analysed to understand the performance of both methods over a longer period. Figure 5.16 presents the active power transfer recorded for this period. An operating pattern similar to data from 1 February is observed (see Figure 5.7).

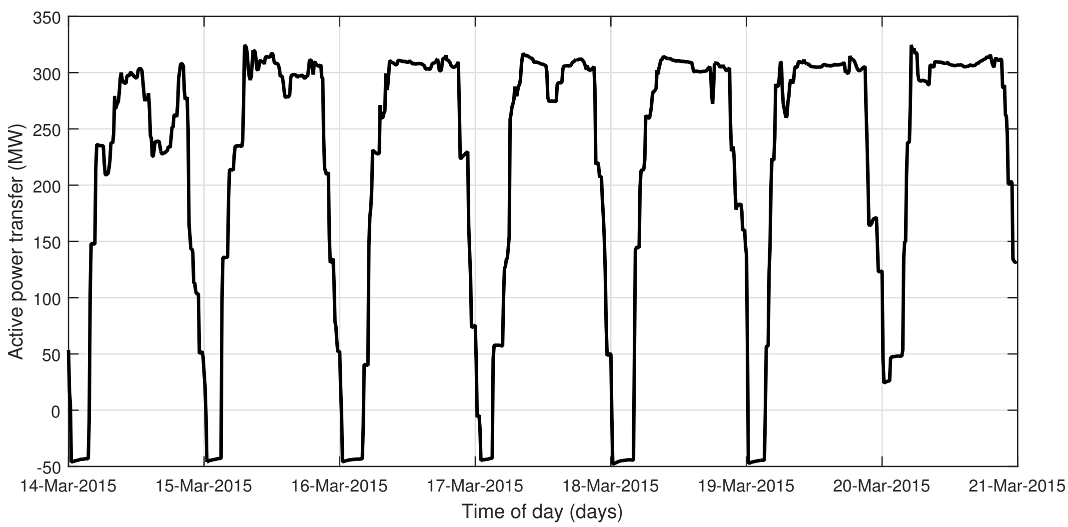

Figure 5.16: Active power generation at hydro-station. (14 - 21 March 2015)

Power transfer is reduced during the early hours of each day. Observe the reversed power flow during these hours. All generation at the hydro-station is stopped and the hydro-station becomes a consumer of electric energy during these hours.

5.5.1 Result Filtering

Experience of field data use from 1 February 2015 highlighted conditions when results from both methods become inaccurate. The inter-area mode in the system is not excited at low power transfer levels.

Figure 5.13 and 5.14 can be used to find the instances when the inter-area mode is sufficiently excited. Energy in the inter-area mode is observed from approximately 07:00. Correlating this time with the active power transfer in Figure 5.7, it is observed that the inter-area mode is only sufficiently excited for power transfers above roughly 200 MW.

Results found when power transfer is below 200 MW is not regarded as accurate and gets discarded. Only results at power transfers above 200 MW are considered.

5.5.2 Frequency and Damping Results

Mode frequency and damping is calculated for the period 14 - 21 March 2015. Results are based on using a combination of input signals, as discussed in section 5.4.1. A 5-min window length is used for the ARMA method and a 2-min window length for the wavelet method. Figure 5.17 and 5.18 presents the frequency result and Figure 5.19 and 5.20 the damping result for the ARMA and wavelet methods respectively.

Observe the gaps where results have been filtered out according to the discussion in the previous section. This approach removes much of the inaccurate values, improving the operational value of the results. Some inaccurate values still remain near the filtered periods.

An inter-area mode is identified in the 0.5 Hz range. Slightly different damping ratios

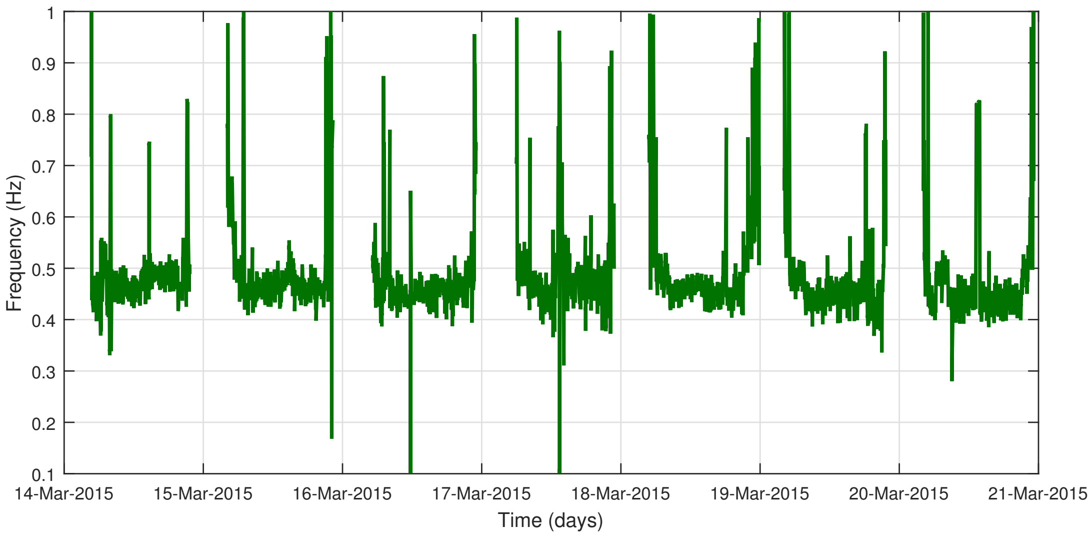

Figure 5.17: ARMA method frequency result. (14 - 21 March 2015)

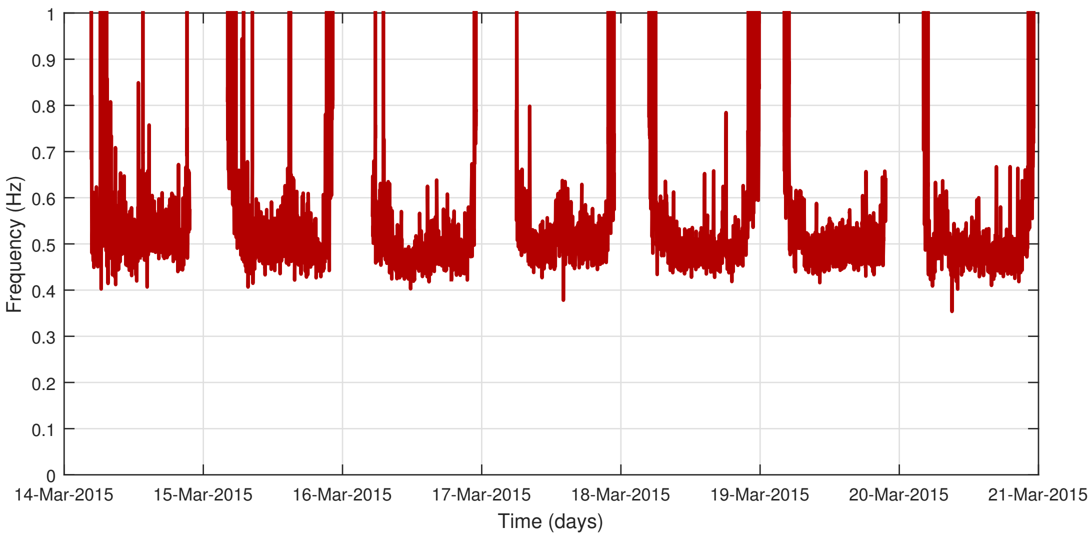

Figure 5.18: Wavelet method frequency result. (14 - 21 March 2015)

are identified by the two methods. The ARMA method damping result (approximately 10 - 20 %) is slightly higher than the wavelet result (approximately 5 - 10 %). The true damping of the system is unknown.

It is therefore not possible to comment on which result is indeed correct, however both results fall inside the range of values that are probable for a practical power system with lightly damped modes. The ARMA method has significantly larger spread of values than the wavelet method.

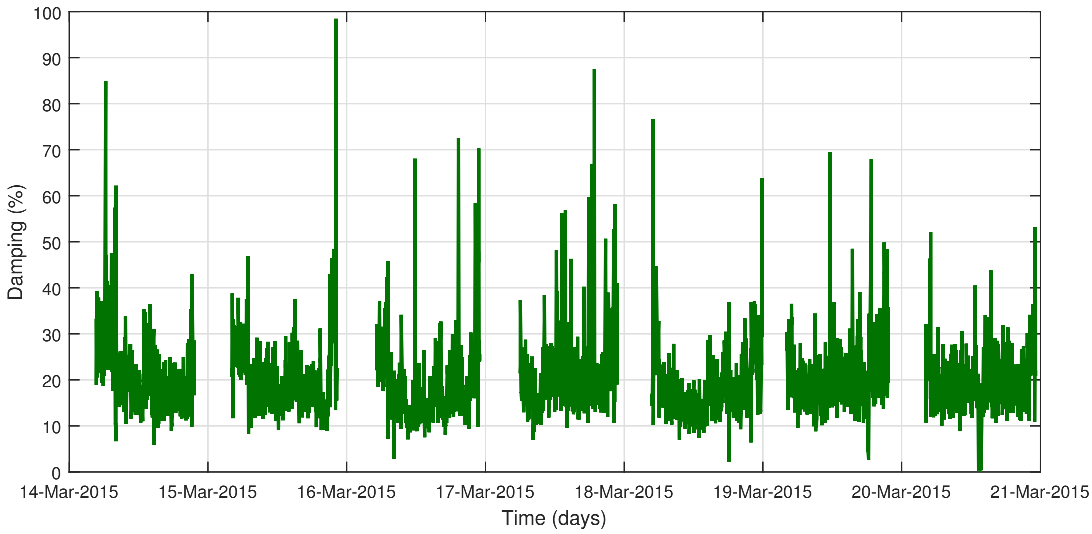

Figure 5.19: ARMA method damping result. (14 - 21 March 2015)

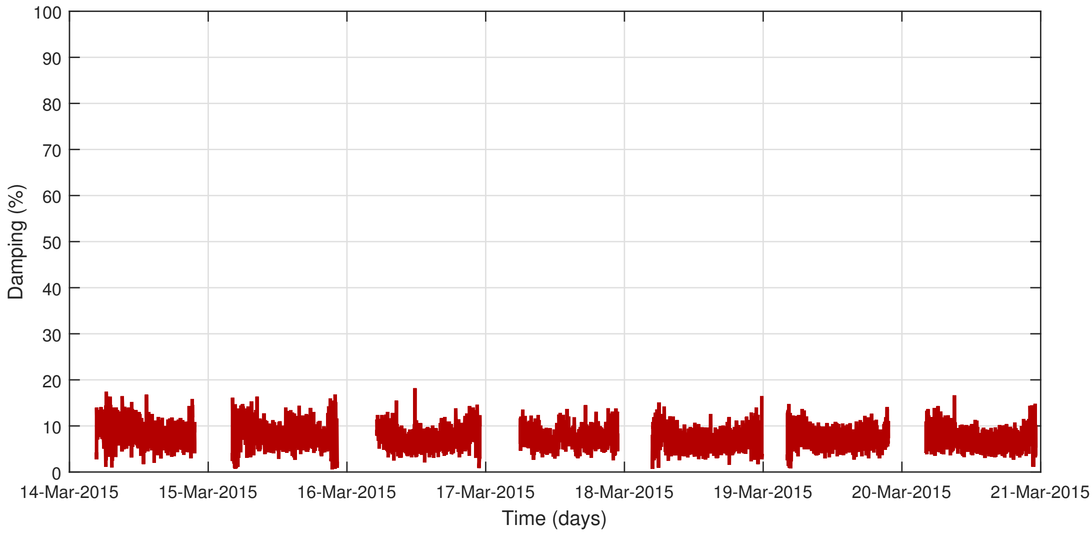

Figure 5.20: Wavelet method damping result. (14 - 21 March 2015)

5.6 Case Study: 15 March 2015

It is impractical to view detail behaviour of inter-area modes over the period of multiple days. Results from only 15 March 2015 will be treated as a detail case study of the data for the week 14 - 21 March 2015. Figure 5.21 presents the active power transfer for 15 March 2015.

Active power transfer follows a similar pattern than on 1 February 2015 and thus similar

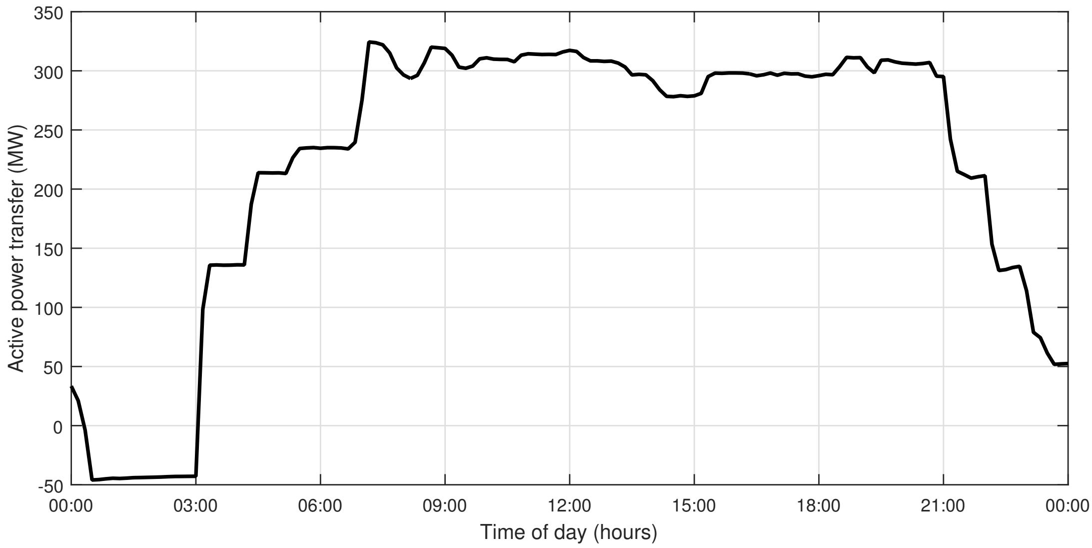

Figure 5.21: Active power generation at hydro-station. (15 March 2015)

results are expected. However, reversed power flow is recorded between 00:00 and 03:00 and also the peak power transfer is higher on 15 March 2015 (± 300 MW) than on 1 February 2015 (± 220 MW).

From previous results, it is expected that the inter-area mode will only be excited when power transfer increases. No inter-area mode is expected during reverse power flow conditions or low power transfer.

5.6.1 Frequency and Damping Result

Results of frequency and damping for only 15 March is presented to observe detail behaviour of the inter-area mode. Figure 5.22 and 5.23 presents the frequency result, while Figure 5.24 and 5.25 presents the damping result for the two methods respectively.

Frequency results are similar for the two methods. Inter-area mode frequency of 0.5 Hz is identified. The wavelet method again produces some inaccurate results, even after filtering results with low power transfer.

A difference in damping results is noted in Figure 5.24 and Figure 5.25. It is not clear which method provides the correct result.

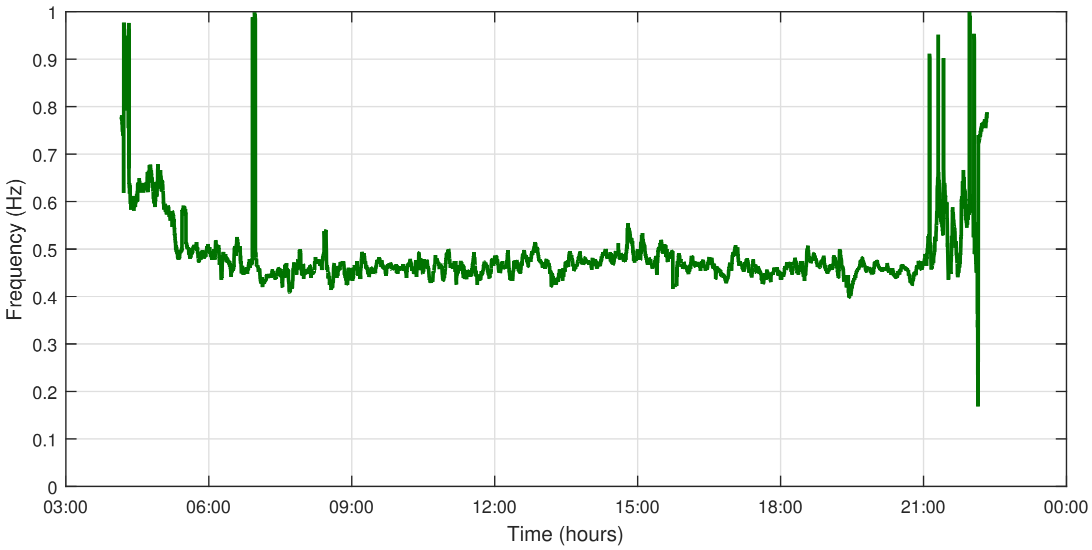

Figure 5.22: ARMA method frequency result. (15 March 2015)

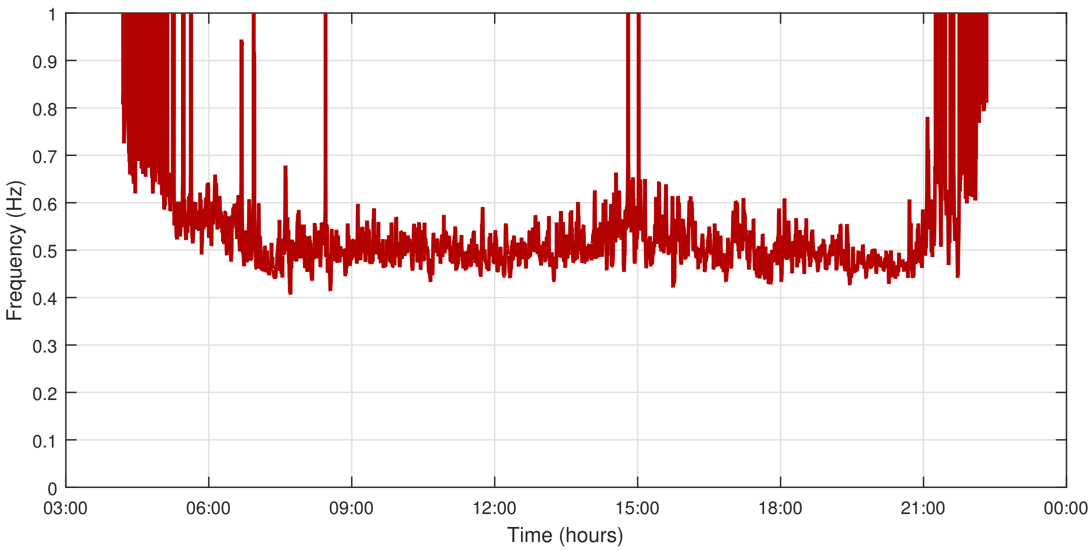

Figure 5.23: Wavelet method frequency result. (15 March 2015)

5.6.2 Signal Spectrum

The signal spectrum for 15 March 2015 is analysed. Figure 5.26 and 5.27 presents the ARMA and wavelet signal spectrum respectively.

As expected, the inter-area mode is excited only when significant power transfer is recorded. Correlating the spectrum plots with active power transfer in Figure 5.21 shows the inter-area mode is only excited when power transfer exceeds approximately 200 MW.

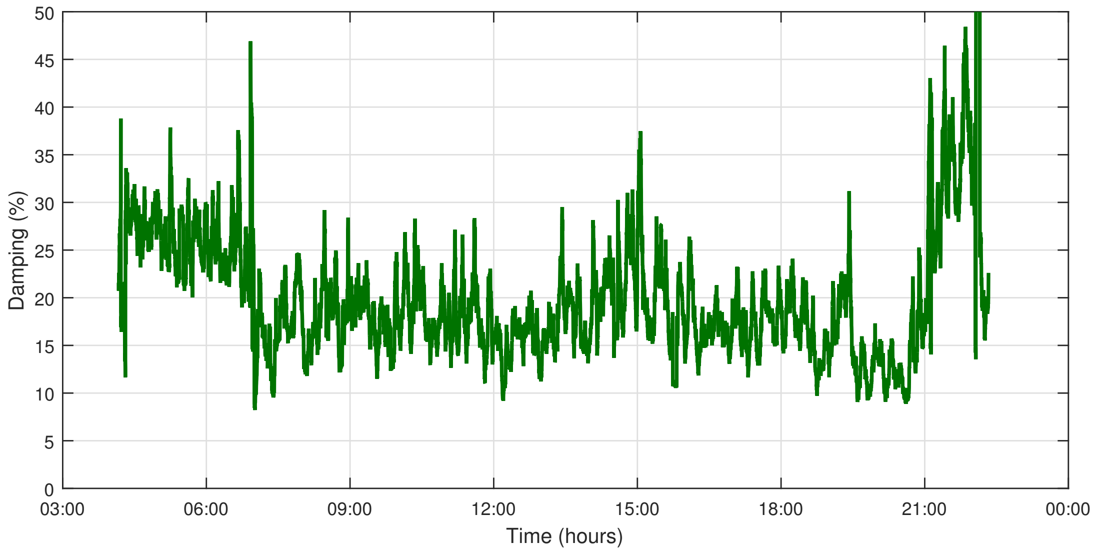

Figure 5.24: ARMA method damping result. (15 March 2015)

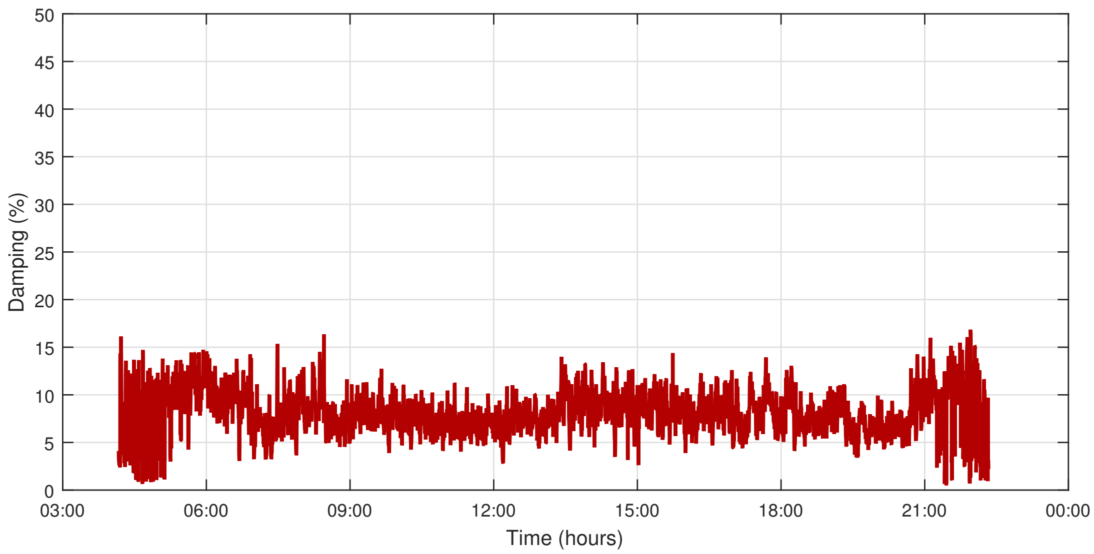

Figure 5.25: Wavelet method damping result. (15 March 2015)

Observe the period from 00:00 to 03:00 when power transfer is reversed. Power transfer is lowest during this time at 50 MW, not taking in to account the direction of power transfer.

During this time, the lowest energy in the signal spectrum is observed (indicated by the blue colour - see colour in the bar legend on the side of the plot). As soon as power flow becomes positive, an increase in energy is observed over the entire spectrum of interest. This is observed as a sudden change from the blue to greenish colour.

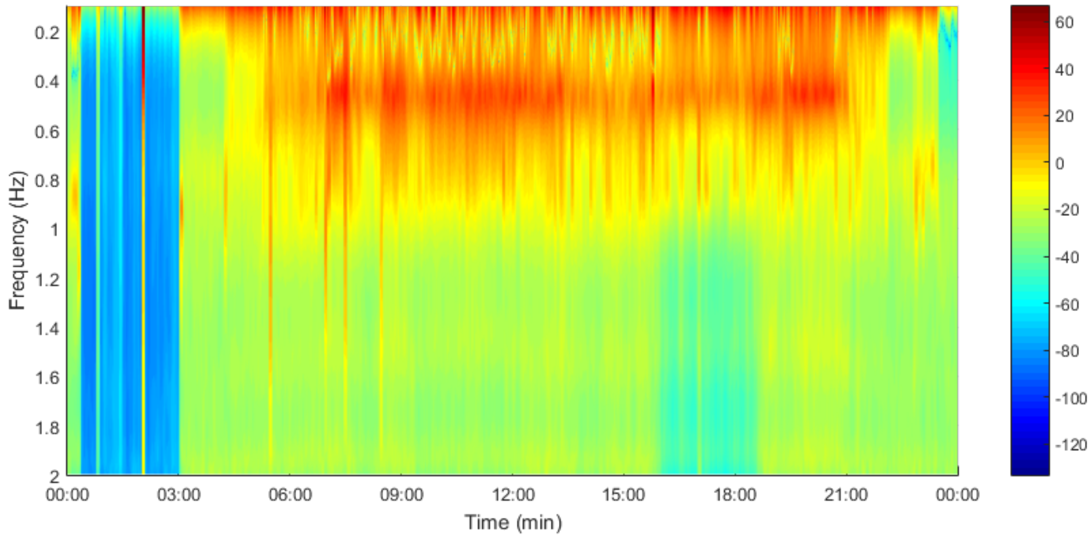

Figure 5.26: ARMA spectral estimation over time. (15 March 2015)

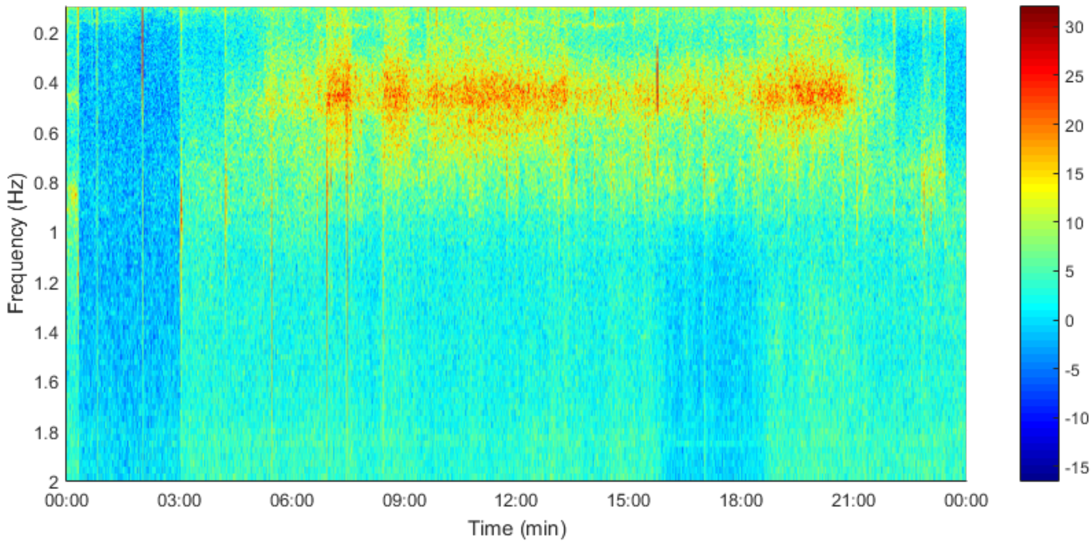

Figure 5.27: CWT coefficients over time. (15 March 2015)

Sudden increases in broad-spectrum energy are observed, that is the red vertical lines in Figure 5.26 and 5.27. Most of these occurrences coincide with sudden increases in active power transfer.

5.6.3 Mode Shape

Mode shape for 15 March 2015 at 12:00 is analysed. Figure 5.28 presents the mode shape for the ARMA and wavelet method.

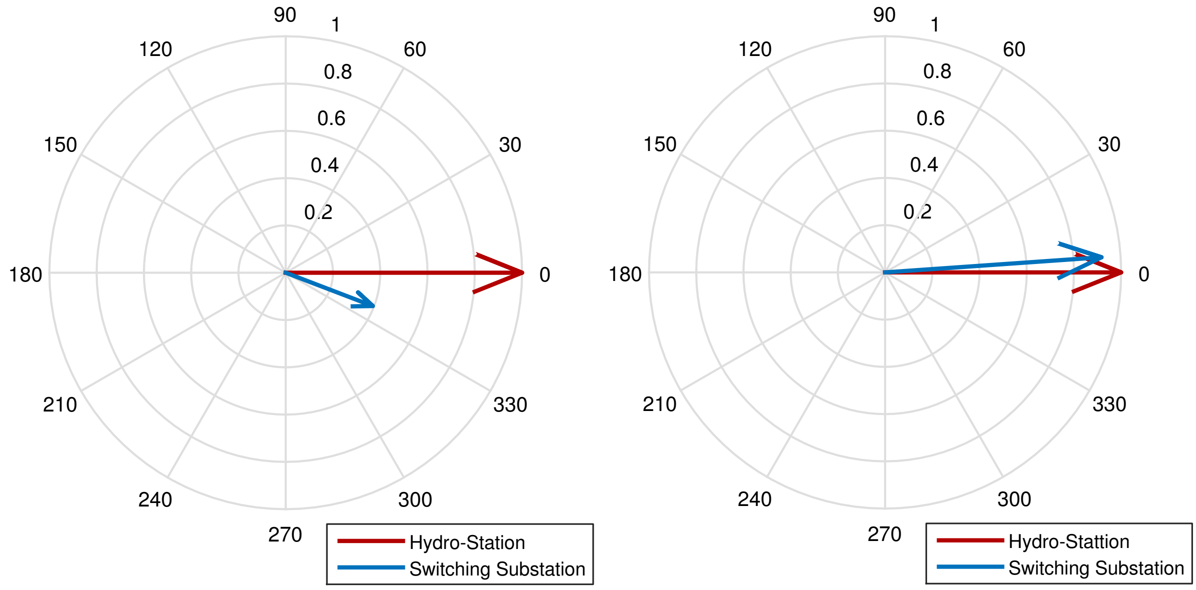

(a) ARMA method **(b)** Wavelet method

Figure 5.28: Mode shape. (15 March 2015 12:00)

The mode shape confirms the results from 1 February 2015 (see Figure 5.15). The switching substation oscillates in phase with the hydro-station.

5.7 Conclusion

The practical performance of the ARMA and wavelet methods was validated in this chapter by application to emulated field data. Simulated low frequency oscillations were generated as typical substation instrumentation signals of 110 V rms by a highly accurate CM256plus™ waveform generator. This output signals were then recorded by the same instrumentation used to record field data.

Comparison of results from the simulated and emulated datasets indicated near identical results. The synchrophasor recorders do not introduce inaccuracies that negatively influenced modal estimation performance.

It was shown that input signal selection is crucial to get accurate results from both methods. Using multiple input signals can help when little is known regarding observability of inter-area modes in measured signals. Using a combination of all the possible input signals produced results similar to that of using only signals with high observability.

Trended frequency and damping results provide detail on inter-area mode behaviour. Careful selection of window size is necessary to produce accurate results. A 2-min window used with the wavelet method produced useful results. A 5-min window was used for the ARMA method. Selecting prominent modes for the ARMA results became challenging when using smaller window lengths.

The two methods produce slightly different damping estimations. The ARMA method provides higher damping estimations than the wavelet method. Exact values for mode frequency and damping for the power system in question is unknown. It is thus not possible to determine which method provides accurate results.

Estimation of the spectral content of the measured signals provide insight into developing system conditions, especially if tracked over time. While trended frequency and damping values give detail insight for a single mode, the signal spectrum affords insight into all frequency components.

Mode shape shows which parts of the power system take part in an oscillatory condition. It was possible to determine from the field data that the switching substation oscillates in phase with the hydro-station, however without access to more points of measurement, it is not possible to investigate this interaction further over a larger geographical area.

Chapter 6

Conclusion

... where the results contained in this dissertation are reviewed and topics for future work are proposed.

6.1 Summary of Results

This research evaluated the feasibility to implement WAMS functions through versatile measurement instrumentation. Network coherent data with sufficient certainty in time-stamping to allow the recording of voltage and current synchrophasors, has become accessible to utilities without the need for the expense and sophistication associated with PMU based systems. WAMS functionality can be widely deployed at different levels of network management and control, not only at transmission level.

Small signal stability monitoring was evaluated, as it is a useful application of synchrophasor data. Two different methods of ambient modal estimation were implemented from first principles. Potential for real-time implementation was comprehensively evaluated.

Both methods were able to identify and track inter-area mode frequency and damping ratio with a delay determined by the window length of input data. Window length must be carefully considered to find an acceptable trade-off between a fast response of the method and sufficient accuracy. This trade-off determines the opportunity and operational value of this small signal stability information extracted by the different methods.

The ARMA method is more sensitive to window length of input data than the wavelet method. Accuracy of the ARMA method improves with increasing window length, while the wavelet method results are less sensitive to window length. Frequency can be determined with greater accuracy than damping ratio under all conditions.

System damping also affects result accuracy. The accuracy of both methods improves when system damping is low. Poorly damped modes contain significant energy and are easier to identify reliably.

Input signal selection is crucial to obtain accurate results. Using multiple signals as input is beneficial when little is known regarding observability of inter-area modes in measured signals.

Visualisation of signal spectral content over time support intuitive understanding of developing system conditions. The signal spectrum provides an overview of system dynamics in contrast to the detail information provided by frequency and damping ratio of a specific mode.

Mode shape is used to identify areas or components participating in an oscillation. Multiple system wide points of measurement are necessary to provide a comprehensive insight into geographical mode behaviour.

WAMS functionalities such as small signal stability monitoring can successfully be based on the versatile measurement instrumentation. Such innovation could be a valuable and cost-effective approach to additional information on network dynamic performance. The modal analysis methods evaluated require limited resources in terms of specialised software and data acquisition systems as shown in this research.

The exclusivity and expenses traditionally associated with application of WAMS for monitoring transmission systems are negated. WAMS can therefore become accessible to many other areas of power system control and operation.

6.2 Recommendations for Further Work

Outputs from small signal stability monitoring should have operational value and aid network operational decision-making. Results need to be intuitive. This can be challenging as system wide behaviour has to be monitored. It becomes especially challenging in big interconnected systems spanning a large geographical area. Further work should focus on ways to promote intuitive understanding of results in a system wide context with the number of synchrophasor recorders optimized for the level of system performance information required.

Further improvement can also be made to the methods used to estimate mode characteristics. Methods providing accurate results in ambient conditions, using smaller window lengths of input data are needed.

Bibliography

[1] M. Bollen and I. Gu, *Signal Processing of Power Quality Disturbances.* New-York: Wiley-Interscience, 2006.

[2] IEEE Standard 2030-2011, *IEEE Guide for Smart Grid Interoperability of Energy Technology and Information Technology Operation with the Electric Power System (EPS), End-Use Applications, and Loads*, 2011.

[3] IEEE/CIGRE Joint Task Force on Stability Terms And Definitions, "Definition and Classification of Power System Stability," *IEEE Transactions on Power Systems*, vol. Vol 19, pp. 1387–1388, 2004.

[4] P. Kundur, *Power System Stability and Control*, 2nd ed. New-York: McGraw-Hill, 1994.

[5] L. L. Grigsby, *The Electric Power Engineering Handbook.* Auburn, Alabama: CRC Press, 2001.

[6] T. van Rooyen, J. Rens, and J. Desmet, "Field Performance of Ambient Modal Estimation in Small Signal Stability," in *2015 IEEE International Workshop on Applied Measurements for Power Systems (AMPS) (AMPS 2015)*, Aachen, Germany, sep 2015, pp. 144 – 149.

[7] V. Venkatasubramanian and H. Khalilinia, "Modal Analysis of Ambient PMU Measurements Using Orthogonal Wavelet Bases," *IEEE Transactions on Smart Grid*, no. 99, 2015.

[8] Task Force on Identification of Electromechanical Modes, "Identification of Electromechanical Modes in Power Systems," IEEE PES, Tech. Rep. June 2012, 2012.

[9] B. Pal and B. Chaudhuri, *Robust Control in Power Systems.* New-York: Springer Science, 2005.

[10] G. Rogers, *Power System Oscillations.* New-York: Springer Science, 2000.

[11] D. J. Trudnowski, "Estimating electromechanical mode shape from synchrophasor measurements," *IEEE Transactions on Power Systems*, vol. 23, no. 3, pp. 1188–1195, 2008.

[12] N. Zhou, Z. Huang, L. Dosiek, D. Trudnowski, and J. W. Pierre, "Electromechanical mode shape estimation based on transfer function identification using PMU measurements," in *2009 IEEE Power and Energy Society General Meeting, PES '09*, 2009.

[13] L. Di Noia, D. Lauria, C. Pisani, and D. Villacci, "A Novel Procedure for Real-Time Detection of Inter-Area Oscillations," in *Energy Conference and Exhibition (ENERGYCON), 2012 IEEE International*, Florence, 2012, pp. 433 – 438.

[14] J. F. Hauer, C. J. Demeure, and L. L. Scharf, "Initial results in Prony analysis of power system response signals," *IEEE Transactions on Power Systems*, vol. 5, no. 1, pp. 80–89, 1990.

[15] J. F. Hauer, "Application of Prony analysis to the determination of modal content and equivalent models for measured power system response," *IEEE Transactions on Power Systems*, vol. 6, no. 3, pp. 1062–1068, 1991.

[16] D. J. Trudnowski, J. M. Johnson, and J. F. Hauer, "Making prony analysis more accurate using multiple signals," *IEEE Transactions on Power Systems*, vol. 14, no. 1, pp. 226–231, 1999.

[17] G. Liu, J. Quintero, and V. Venkatasubramanian, "Oscillation monitoring system based on wide area synchrophasors in power systems," in *2007 iREP Symposium-*

Bulk Power System Dynamics and Control - VII, Revitalizing Operational Reliability, 2007.

[18] J. Xiao, X. Xie, Y. Han, and J. Wu, "Dynamic tracking of low-frequency oscillations with improved Prony method in wide-area measurement system," in *IEEE Power Engineering Society General Meeting, 2004.*, 2004.

[19] L. Ding, A. Xue, F. Han, J. Li, M. Wang, T. Bi, and J. Wang, "Dominant mode identification for low frequency oscillations of power systems based on prony algorithm," in *2010 5th International Conference on Critical Infrastructure, CRIS 2010 - Proceedings*, 2010.

[20] S. Y. Sun, H. C. Shu, J. Dong, and Z. J. Liu, "Analysis of low frequency oscillation mode based on PMU and PRONY method," in *Asia-Pacific Power and Energy Engineering Conference, APPEEC*, 2009.

[21] P. Tripathy, S. C. Srivastava, and S. N. Singh, "An improved Prony method for identifying low frequency oscillations using synchro-phasor measurements," in *2009 International Conference on Power Systems, ICPS '09*, 2009.

[22] S. Navabi and A. Chakrabortty, "A Real-Time Distributed Prony-Based Algorithm for Modal Estimation of Power System Oscillations," in *American Control Conference (ACC), 2014*, 2014, pp. 729 – 734.

[23] Y. Huang, Z. Xu, and W. Pan, "A practical analysis method of low frequency oscillation for large power systems," in *IEEE Power Engineering Society General Meeting, 2005*, 2005, pp. 1–7.

[24] T. K. Sarkar and O. Pereira, "Using the matrix pencil method to estimate the parameters of a sum of complex exponentials," *IEEE Antennas and Propagation Magazine*, vol. 37, no. 1, pp. 48–55, 1995.

[25] J. Sanchez-Gasca, "Computation of power system low-order models from time domain simulations using a hankel matrix," *IEEE Transactions on Power Systems*, vol. 12, no. 4, pp. 1461–1467, 1997.

[26] ——, “Computation of Turbine-Generator Subsynchronous Torsional Modes From Measured Data Using the Eigensystem Realization Algorithm,” in *IEEE Tansactions on Power Apparatus and Systems*, no. C, 2001, pp. 1272–1276.

[27] I. Kamwa, G. Trudel, and L. Gerin-Lajoie, “Low-order black-box models for control system design in large power systems,” *Power Industry Computer Application Conference, 1995. Conference Proceedings., 1995 IEEE*, pp. 190–198, 2002.

[28] Y. Hua and T. K. Sarkar, “Matrix Pencil Method for Estimating Parameters of Exponentially Damped Undamped Sinusoids in Noise,” *IEEE Trans. Acoust., Speech, Signal Process*, vol. 38, no. 5, pp. 814–824, 1990.

[29] J. W. Pierre, “Initial results in electromechanical mode identification from ambient data,” *IEEE Transactions on Power Systems*, vol. 12, pp. 1245–1251, 1997.

[30] D. J. Trudnowski and J. W. Pierre, “Overview of algorithms for estimating swing modes from measured responses,” in *2009 IEEE Power and Energy Society General Meeting, PES ’09*, 2009, pp. 1–8.

[31] P. Stoica and R. Moses, *Spectral Analysis of Signals.* New-Jersey: Prentice Hall, 2004.

[32] J. Hauer and R. Cresap, “Measurement and Modeling of Pacific AC Intertie Response to Random Load Switching,” *IEEE Transactions on Power Apparatus and Systems*, vol. PAS-100, no. 1, 1981.

[33] D. J. Trudnowski, J. W. Pierre, N. Zhou, J. F. Hauer, and M. Parashar, “Performance of three mode-meter block-processing algorithms for automated dynamic stability assessment,” *IEEE Transactions on Power Systems*, vol. 23, no. 2, pp. 680–690, 2008.

[34] B. Friedlander and B. Porat, “The Modified Yule-Walker Method of ARMA Spectral Estimation,” *IEEE Transactions on Aerospace and Electronic Systems*, vol. AES-20, no. 2, pp. 158–173, 1984.

[35] R. W. Wies, J. W. Pierre, and D. J. Trudnowski, "Use of ARMA block processing for estimating stationary low-frequency electromechanical modes of power systems," *IEEE Transactions on Power Systems*, vol. 18, no. 1, pp. 167–173, 2003.

[36] M. G. Anderson, N. Zhou, J. W. Pierre, and R. W. Wies, "Bootstrap-based confidence interval estimates for electromechanical modes from multiple output analysis of measured ambient data," *IEEE Transactions on Power Systems*, vol. 20, pp. 943–950, 2005.

[37] J. M. Seppänen, J. Turunen, L. C. Haarla, M. Koivisto, and N. Kishor, "Analysis of electromechanical modes using multichannel Yule-Walker estimation of a multivariate autoregressive model," in *2013 4th IEEE/PES Innovative Smart Grid Technologies Europe, ISGT Europe 2013*, 2013.

[38] N. Zhou, D. J. Trudnowski, J. W. Pierre, and W. a. Mittelstadt, "Electromechanical mode online estimation using regularized robust RLS methods," *IEEE Transactions on Power Systems*, vol. 23, no. 4, pp. 1670–1680, 2008.

[39] R. Wies, J. Pierre, and D. Trudnowski, "Use of least mean squares (LMS) adaptive filtering technique for estimating low-frequency electromechanical modes in power systems," in *IEEE Power Engineering Society General Meeting, 2004.*, 2004.

[40] B. D. Rao and K. S. Arun, "Model based processing of signals: A state space approach," *Proceedings of the IEEE*, vol. 80, no. 2, pp. 283–309, 1992.

[41] G. Liu and V. Venkatasubramanian, "Oscillation monitoring from ambient PMU measurements by frequency domain decomposition," in *Proceedings - IEEE International Symposium on Circuits and Systems*, 2008, pp. 2821–2824.

[42] J. Thambirajah, N. F. Thornhill, and B. C. Pal, "A multivariate approach towards interarea oscillation damping estimation under ambient conditions via independent component analysis and random decrement," *IEEE Transactions on Power Systems*, vol. 26, no. 1, pp. 315–322, 2011.

[43] C. Xia and J. Howell, “Isolating multiple sources of plant-wide oscillations via independent component analysis,” *Control Engineering Practice*, vol. 13, no. 8, pp. 1027–1035, 2005.

[44] J. Turunen, M. Larsson, J. Thambirajah, L. C. Haarla, and T. Rauhala, “Recent developments in modal estimation of power system electromechanical oscillations,” in *2011 IEEE PES Trondheim PowerTech: The Power of Technology for a Sustainable Society, POWERTECH 2011*, 2011.

[45] H. A. Cole, “Failure detection of a space shuttle wing flutter model by random decrement,” NASA, Tech. Rep., 1971.

[46] ——, “On-line failure detection and damping measurement of aerospace structures by random decrement signatures,” NASA, Tech. Rep., 1973.

[47] C. S. Chang, “Study of Dynamic Characteristics of Aeroelastic Systems Utilizing Randomdec Signatures,” NASA, Tech. Rep., 1975.

[48] L. B. Soares, S. Bampi, C. David, and P. Crovato, “A Fast EMD-based Technique for Power Quality Signals Decomposition , Compression, and Time- Frequency Analysis,” in *Digital Signal Processing (DSP), 2013 18th International Conference on*, 2013.

[49] T. J. Browne, V. Vittal, G. T. Heydt, and a. R. Messina, “A Comparative Assessment of Two Techniques for Modal Identification From Power System Measurements,” *Power Systems, IEEE Transactions on*, vol. 23, no. 3, pp. 1408–1415, 2008.

[50] D. S. Laila, A. R. Messina, and B. C. Pal, “A refined Hilbert-Huang transform with applications to interarea oscillation monitoring,” *IEEE Transactions on Power Systems*, vol. 24, no. 2, pp. 610–620, 2009.

[51] N. Senroy, S. Suryanarayanan, and P. F. Ribeiro, “An improved Hilbert-Huang method for analysis of time-varying waveforms in power quality,” *IEEE Transactions on Power Systems*, vol. 22, no. 4, pp. 1843–1850, 2007.

[52] M. A. Andrade, A. R. Messina, C. A. Rivera, and D. Olguin, “Identification of instantaneous attributes of torsional shaft signals using the Hilbert transform,” *IEEE Transactions on Power Systems*, vol. 19, no. 3, pp. 1422–1429, 2004.

[53] A. R. Messina, V. Vittal, D. Ruiz-Vega, and G. Enríquez-Harper, “Interpretation and visualization of wide-area PMU measurements using Hilbert analysis,” *IEEE Transactions on Power Systems*, vol. 21, no. 4, pp. 1763–1771, 2006.

[54] I. Daubechies, *Ten Lectures on Wavelets.* Philadelphia, PA: SIAM, 1992, vol. 61.

[55] S. Bruno, M. De Benedictis, and M. La Scala, “”Taking the pulse” of Power Systems: Monitoring Oscillations by Wavelet Analysis and Wide Area Measurement System,” in *IEEE/PES Power Systems Conference and Exposition*, 2006.

[56] S. J. Huang, C. T. Hsieh, and C. L. Huang, “Application of Morlet wavelets to supervise power system disturbances,” *IEEE Transactions on Power Delivery*, vol. 14, no. 1, pp. 235–241, 1999.

[57] Y. Dai and J. Zhang, “Continuous wavelet transform-based estimation of modal parameters with scale selection,” in *2012 IEEE International Conference on Mechatronics and Automation, ICMA 2012*, 2012, pp. 1445–1450.

[58] J. L. Rueda and I. Erlich, “Enhanced wavelet-based method for modal identification from power system ringdowns,” in *2011 IEEE PES Trondheim PowerTech: The Power of Technology for a Sustainable Society, POWERTECH 2011*, 2011.

[59] J. L. Rueda, C. A. Juárez, and I. Erlich, “Wavelet-based analysis of power system low-frequency electromechanical oscillations,” *IEEE Transactions on Power Systems*, vol. 26, no. 3, pp. 1733–1743, 2011.

[60] J. Turunen, J. Thambirajah, M. Larsson, B. C. Pal, N. F. Thornhill, L. C. Haarla, W. W. Hung, A. M. Carter, and T. Rauhala, “Comparison of three electromechanical oscillation damping estimation methods,” *IEEE Transactions on Power Systems*, vol. 26, no. 4, pp. 2398–2407, 2011.

[61] J. Turunen, L. Haarla, and T. Rauhala, "Performance of wavelet-based damping estimation method under ambient conditions of the power system," in *2010 IREP Symposium - Bulk Power System Dynamics and Control - VIII, IREP2010*, 2010, pp. 1–9.

[62] J. Turunen, T. Rauhala, and L. Haarla, "Selecting wavelets for damping estimation of ambient-excited electromechanical oscillations," in *IEEE PES General Meeting, PES 2010*, 2010.

[63] X. Pan, F. Shang, and S. Yuan, "Wavelet-based electromechanical mode shape online identification from ambient data," in *DRPT 2011 - 2011 4th International Conference on Electric Utility Deregulation and Restructuring and Power Technologies*, 2011, pp. 1841–1847.

[64] P. M. Ashton, G. A. Taylor, A. M. Carter, and H. Renner, "Opportunities to exploit Phasor Measurement Units (PMUs) and synchrophasor measurements on the GB Transmission Network," in *Universities' Power Engineering Conference (UPEC), Proceedings of 2011 46th International*, no. September, 2011, pp. 3–8.

[65] J. F. Hauer, W. A. Mittelstadt, K. E. Martin, J. W. Burns, H. Lee, J. W. Pierre, and D. J. Trudnowski, "Use of the WECC WAMS in wide-area probing tests for validation of system performance and modeling," *IEEE Transactions on Power Systems*, vol. 24, no. 1, pp. 250–257, 2009.

[66] X. Xie, Y. Xin, J. Xiao, J. Wu, and Y. Han, "WAMS applications in Chinese power system," *IEEE Power and Energy Magazine*, vol. 4, pp. 54–63, 2006.

[67] C. L. Su and B. Y. Jau, "Visualization of wide area dynamics in power network for oscillatory stability assessment," in *2007 International Conference on Intelligent Systems Applications to Power Systems, ISAP*, 2007, pp. 1–6.

[68] A. B. Leirbukt, J. O. Gjerde, P. Korba, K. Uhlen, L. K. Vormedal, and L. Warland, "Wide Area Monitoring experiences in Norway," in *2006 IEEE PES Power Systems Conference and Exposition, PSCE 2006 - Proceedings*, 2006, pp. 353–360.

[69] J. Y. Cai, Z. Huang, J. Hauer, and K. Martin, "Current status and experience of WAMS implementation in North America," in *Proceedings of the IEEE Power Engineering Society Transmission and Distribution Conference*, vol. 2005, 2005, pp. 1–7.

[70] P. Korba, "Real-time monitoring of electromechanical oscillations in power systems: first findings," *IET Generation, Transmission & Distribution*, vol. 1, no. 1, p. 80, 2007.

[71] W. Sattinger, J. Bertsch, and P. Reinhardt, "Operational experience with wide area measurement systems," in *Cigré Session 2006*, 2006, pp. 1–8.

[72] G. Ledwich, D. Geddey, and P. O'Shea, "Phasor measurement units for system diagnosis and load identification in Australia," in *IEEE Power and Energy Society 2008 General Meeting: Conversion and Delivery of Electrical Energy in the 21st Century, PES*, 2008, pp. 1–6.

[73] D. Wilson, "Wide-Area Measurement and Control for Dynamic Stability," in *2007 IEEE Power Engineering Society General Meeting*, 2007.

[74] J. Turunen, M. Larsson, P. Korba, J. Jyrinsalo, and L. Haarla, "Experiences and future plans in monitoring the inter-area power oscillation damping," in *IEEE Power and Energy Society 2008 General Meeting: Conversion and Delivery of Electrical Energy in the 21st Century, PES*, 2008, pp. 1–8.

[75] IEEE Standard C37.118.1-2011, *IEEE Standard for Synchrophasor Measurements for Power Systems*, 2011.

[76] K. E. Martin, D. Hamai, M. G. Adamiak, S. Anderson, M. Begovic, G. Benmouyal, G. Brunello, J. Burger, J. Y. Cai, B. Dickerson, V. Gharpure, B. Kennedy, D. Karlsson, A. G. Phadke, J. Salj, V. Skendzic, J. Sperr, Y. Song, C. Huntley, B. Kasztenny, and E. Price, "Exploring the IEEE standard C37.118-2005 synchrophasors for power systems," *IEEE Transactions on Power Delivery*, vol. 23, no. 4, pp. 1805–1811, 2008.

[77] J. De La Ree, V. Centeno, J. S. Thorp, and A. G. Phadke, "Synchronized Phasor Measurement Applications in Power Systems," *Smart Grid, IEEE Transactions on*, vol. 1, no. 1, pp. 20–27, 2010.

[78] L. Dosiek, D. Trudnowski, and J. W. Pierre, “New Algorithms for Mode Shape Estimation Using Measured Data,” in *PES General Meeting 2008*, Pittsburgh, PA, 2008, pp. 1–8.

[79] S. Mallat, *A Wavelet Tour of Signal Processing.* San Diego: Academic Press, 1999.

[80] C. Torrence and G. P. Compo, “A Practical Guide to Wavelet Analysis,” *Bulletin of the American Meteorological Society*, vol. 79, no. 1, pp. 61–78, 1998.

[81] M. Hemmingson, “Power System Oscillations Detection Estimation & Control,” Ph.D. dissertation, Lund University, 2003.

[82] N. Zhou, D. Trudnowski, J. W. Pierre, S. Sarawgi, and N. Bhatt, “An Algorithm for removing trends from power-system oscillation data,” in *IEEE Power and Energy Society 2008 General Meeting: Conversion and Delivery of Electrical Energy in the 21st Century, PES*, 2008, pp. 1–7.

[83] J. Chow and K. Cheung, “A toolbox for power system dynamics and control engineering education and research,” *IEEE Transactions on Power Systems*, vol. 7, no. 4, pp. 1559–1564, 1992.

Appendix A

Research Outputs

... where research outputs produced during the duration of the study is discussed.

A.1 Conference Proceedings - Powertech 2015

A paper was submitted for the 2015 IEEE Powertech conference held in Eindhoven, Netherlands titled "Real-Time Power System Oscillation Monitoring using Synchrophasor Measurements". The paper was accepted for publication in the conference proceedings and the work presented during an oral presentation session. The full paper is attached.

In this paper the ARMA method is tested with the aim of real-time implementation. The method is applied to simulated data as well as data from a practical case study. It is shown that the method is capable of power system oscillation monitoring. This peer reviewed work validates the ARMA method implemented, simulated tests conducted and initial results from the practical case study.

Real-Time Power System Oscillation Monitoring using Synchrophasor Measurements

Tian van Rooyen, Johan Rens
School of Electrical and Electronic Engineering
Potchefstroom Campus of the North-West University
Potchefstroom, South Africa
22144153@nwu.ac.za, johan.rens@nwu.ac.za

***Abstract*—Inter-area oscillations impact negatively on power system stability and power transfer capability. Monitoring oscillations in real time can improve control of the power system. Synchrophasor data from Phasor Measurement Units (PMU) provide new options for oscillation monitoring. In this study, an oscillation monitoring method using synchrophasor data from PMUs is presented. The method is verified by power system simulation and its value illustrated by application to data from a practical case study.**

***Index Terms*—Inter-area oscillation, power system monitoring, synchrophasor measurement.**

I. Introduction

Low frequency oscillations (LFOs) in power systems limit power transfer capability and can cause system instability if oscillations become insufficiently damped. Components such as high-gain excitation systems, high-bandwidth speed governors; factors like large power flows over interconnected power systems and increased integration of renewable resources reduce LFO damping in modern power systems. LFOs are a well known aspect of small-signal stability in power systems, which refer to the ability of the power system to remain in synchronism after being subjected to a small disturbance. A disturbance can be seen as small if the response of the power system can be described by a linear set of equations around an operating point [1].

One particular group of LFOs is inter-area oscillations. These are oscillations occurring when machines in one area of the power system oscillate against machines in another area. Inter-area oscillations form when coherent groups of machines are interconnected via weak tie-lines transferring significant power [2]. Inter-area oscillations typically exist in the 0.1 - 1 Hz frequency range and are of particular concern in large interconnected networks.

Phasor Measurement Units (PMU) provide new possibilities for monitoring and control of power systems. PMU technology makes it possible to measure distributed power system parameters (like voltage angle difference over a transmission line) that are ideally suited to monitor power system oscillations. This is possible due to the high accuracy in time stamping of recorded measurements.

The paper presents a real-time power system oscillation monitoring application using synchrophasor data from PMUs. An efficient mathematical approach to this goal was identified, the fundamental principles comprehensively analysed and then tested to real-life data. The goal is to continuously extract oscillation characteristics from PMU data to make power system oscillations visible, and useful, with minimal sophistication in computing and communication requirements. The monitoring method was applied to data from a 330 kV, 521 km Southern African transmission line to validate the theoretical model.

II. Monitoring Low Frequency Oscillation

Modal analysis has traditionally been used to investigate power system small-signal stability. While modal analysis completely describes the small-signal behaviour of a power system, a detailed model of the power system is needed to perform modal analysis. For large interconnected power systems, the complexity of the model becomes immense. For such large systems, this type of analysis is not suited to perform real-time monitoring of a power system.

Many textbooks have been written on modal analysis such as [2]. A method is needed that uses real-time measured power system data and then continuously extracts the LFO information. An alternative solution to LFO monitoring, which can calculate mode frequency, mode damping and mode shape, is analysed and then tested on both simulated and field data. These parameters sufficiently characterise LFOs to enable monitoring and control of power system stability [3].

A. Mode frequency and damping

Parametric methods of spectral estimation can be used to find spectral characteristic from measured signals. Various parametric methods have been researched [4]–[6]. The approach in this paper makes use of an autoregressive moving average (ARMA) model fitted to the recorded data. The spectral characteristics of the signal can then be derived from the characteristics of the fitted model.

The ARMA modelling method has been proven to provide accurate results for power system oscillation monitoring [7]. It uses ambient power system data, and enables fast processing time. It is possible to update LFO values every second, making it suitable for real-time monitoring applications.

An ARMA model is fitted to the measured dataset $y(t)$ so that [8]:

$$y(t) = \frac{B(z)}{A(z)} e(t) \tag{1}$$

where z^{-1} is the unit delay operator $(z^{-k}y(t) = y(t-k))$ and $e(t)$ is white noise with variance of σ^2.

The ARMA model in (1) has an order of (n, m) and can be described by the difference equation [7]:

$$\begin{aligned} y(t) + a_1 y(t-1) + \cdots + a_n y(t-n) = \\ b_0 e(t) + b_1 e(t-1) + \cdots + b_m e(t-m) \end{aligned} \tag{2}$$

where a_i for $i = 1, \ldots, n$ are the coefficients of $A(z)$ and b_j for $j = 0, \ldots, m$ are the coefficients of $B(z)$.

The modified Yule-Walker equations use the relationship between the autocorrelation function of the input data and the a_i coefficients to find the mode information. The autocorrelation function is defined as:

$$r(k) = E\{y(t)y(t-k)\} \tag{3}$$

Multiplying both sides of (2) with $y(t-k)$ and taking the expected value gives the summated form [7]:

$$r(k) + \sum_{i=1}^{n} a_i r(k-i) = \sum_{j=0}^{m} b_j E\{e(t-j)y(t-k)\} \tag{4}$$

The output of the system has to be uncorrelated with future white noise input, then (4) reduces to [8]:

$$r(k) + \sum_{i=1}^{n} a_i r(k-i) = 0 \qquad \text{for } k > m \tag{5}$$

Writing (5) in matrix form for $k = m+1, m+2, \ldots, m+M$ results in:

$$R\underline{a} = -\underline{r} \tag{6}$$

In (6):

$$R = \begin{bmatrix} r(m) & r(m-1) & \cdots & r(m+1-n) \\ r(m+1) & r(m) & \cdots & r(m+2-n) \\ \vdots & & & \\ r(m+M-1) & \cdots & & r(m+M-n) \end{bmatrix} \tag{7}$$

and

$$\underline{a} = \begin{bmatrix} a_1 & a_2 & \cdots & a_n \end{bmatrix}^T \tag{8}$$

and

$$\underline{r} = \begin{bmatrix} r(m+1) & r(m+2) & \cdots & r(m+M) \end{bmatrix}^T. \tag{9}$$

Since the true values for $r(k)$ is unknown, values are estimated [8]:

$$\hat{r}(k) = \frac{1}{N} \sum_{t=k+1}^{N} y(t)y(t-k) \tag{10}$$

With M chosen so that $M > n$, (6) can now be solved to find the over-determined solution for a_i. The z-domain roots can be determined once a_i are known. The s-domain roots are found by

$$s_i = \frac{\ln(z_i)}{T} \tag{11}$$

where T is the sampling period and z_i the z-domain roots of $A(z)$. With the s_i roots known, the mode frequency and damping ratio can be calculated. The roots are complex and of the form $s_i = \sigma_i \pm j\omega_i$. The frequency in Hz is found by [2]:

$$f_i = \frac{\omega_i}{2\pi} \tag{12}$$

The damping ratio is given by:

$$\zeta_i = \frac{-\sigma_i}{\sqrt{\sigma_i^2 + \omega_i^2}} \tag{13}$$

The above method is then extended to take different power system parameters, such as RMS voltage, active power, voltage phase angle across the line and others, as inputs. Construct (6) for each of the n_0 input signals and concatenate into one matrix problem to result in the extended modified Yule-Walker equations [6]:

$$\begin{bmatrix} R_1 \\ R_2 \\ \vdots \\ R_{n_0} \end{bmatrix} \underline{a} = - \begin{bmatrix} \underline{r}_1 \\ \underline{r}_2 \\ \vdots \\ \underline{r}_{n_0} \end{bmatrix} \tag{14}$$

Voltage phase angle across a transmission line is used as the input to the method. It is an ideal parameter for oscillation monitoring since the properties of voltage phase angle across a line are similar to those of active power [9].

The nature of voltage phase angle is such that it requires measurements at different locations in the power system, producing a distributed parameter suitable for monitoring of distributed phenomena like LFOs.

B. Mode shape analysis

From modal analysis, the i$^{\text{th}}$ right-eigenvector, $\underline{u}_i$ can be found for the i$^{\text{th}}$ eigenvalue. The right-eigenvector contains information of the oscillation magnitude and phasing for states in which an oscillatory mode is visible. Information contained in the right-eigenvector is also referred to as mode shape. The k$^{\text{th}}$ element of $\underline{u}_i$, $u_{i,k}$ contains information of the i$^{\text{th}}$ oscillation mode in the k$^{\text{th}}$ state. Magnitude of $u_{i,k}$ is a measure of its observability, while the angle indicates the phasing of the oscillation.

There exists a relationship between $\underline{u}_i$ and the Power-Spectral Density (PSD) and Cross-Spectral Density (CSD) functions of a signal [10]. This relationship is used to derive mode shape from measured data. When deriving mode shape from measured data, the answer describes the contribution of a machine or coherent area towards an oscillation, in terms of its magnitude and phasing. The CSD and PSD functions are defined as follows:

$$S_{kl}(w) = \lim_{T \to \infty} \frac{1}{T} E\{Y_k^*(w) Y_l(w)\} \tag{15}$$

$$S_{kk}(w) = \lim_{T \to \infty} \frac{1}{T} E\{Y_k^*(w) Y_k(w)\} \tag{16}$$

where $S_{kl}(w)$ is the CSD function of $y_k(t)$ and $y_l(t)$, $Y_k(w)$ represents the Fourier transform of $y_k(t)$ and $Y_l(w)$ represents the Fourier transform of $y_l(t)$. Similarly, $S_{kk}(w)$ is the PSD function for $y_k(t)$.

A relationship is then established between the right-eigenvector $\underline{u}_i$, from the modal analysis, and the spectral function defined in (15) and (16). Important aspects relating to the implementation of this algorithm will be highlighted, although not all details of its derivation will be repeated in this paper. Additional detail on this relationship can be found in [10].

The following two equations result from the derivation [10]:

$$\angle S_{kl}(w_i) \cong \angle u_{i,l} - \angle u_{i,k} \tag{17}$$

and

$$S_{kk}(w_i) \cong |u_{i,k}|^2 \lim_{T\to\infty} \frac{1}{T} E\{|Z_i(w_i)|^2\} \tag{18}$$

where w_i is the mode frequency of interest.

To demonstrate the significance of (17) and (18), let the input signals be the rotor speed signals of each generator in the network. When evaluating the CSD of signal $y_l(w)$ and reference signal $y_k(w)$ at w_i, the resulting angle is the phasing of the oscillation between the generators, as given by (17). From (18), the PSD evaluated at w_i for each generator speed signal will be scaled by $|u_{i,k}|^2$, giving an indication of the observability of the mode at the generator.

The PSD and CSD functions of signals are calculated using Matlab functions "*pwelch*" and "*cpsd*", available in the Matlab Signal Processing Toolbox [11].

Machine rotor speed is not a parameter normally available from PMU data, therefore bus frequency is used as input to the mode shape calculation. This signal is suited because its properties are closely coupled to those of machine rotor speed [10].

C. Additional Calculations

Additional aspects of finding mode information from measured signals were applied but will not be discussed in the paper in detail. These include detrending, filtering and downsampling to preprocess the input data [12], mode selection [6] and calculation of the PSD of the signal from calculated ARMA parameters [8].

III. Monitoring Method Verification

In this section, the performance of the monitoring method was evaluated by application to simulated data obtained from a 4-machine, 2-area test system. The test power system was simulated using PST [13] to test the performance of the monitoring method. The test system can be seen in Fig. 1.

Fig. 1 shows the simple power system consisting of 4 machines divided into 2 coherent areas, connected via long transmission lines. This test system is frequently used for small-signal stability analysis because of its relative simplicity, whilst still being complex enough to study the fundamental nature of power system oscillations.

PST was used to simulate the system in the time domain, as well as to perform a modal analysis of the system model.

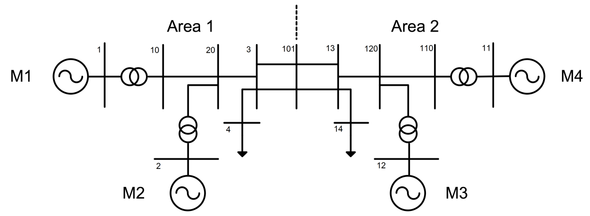

Fig. 1. 4-Machine, 2-Area test System

A. Mode frequency and damping

The accuracy of the ARMA model calculated with the modified extended Yule-Walker method is tested in this section. A number of factors can influence the accuracy of the ARMA model and the resulting mode information. Among these are parameter choice during model fitting, damping ratio of oscillations and data window size. The effect of each of these parameters is discussed.

The true model order of the system is unknown for a real-world scenario. Measured data filtered around the frequency band of interest mostly contain only a few modes, typically six or less [6], but values for n and m are chosen larger to ensure that the ARMA model order is high enough to accurately describe the data. The value for M is chosen so that $M > n$ to find the overdetermined solution for (6).

To test the effect of oscillation damping ratio, the test system was simulated for varying damping ratios. This was done by changing the amount of PSSs connected to the generators in the test system. To achieve a high damping ratio scenario each generator was fitted with a PSS. Low damping was achieved by disabling the PSS on generator 4 and generator 3. Table I summarises the results from the modal analysis of the two scenarios. Each scenario was simulated for an hour at 10 Hz sampling frequency. Data from bus 20 and bus 120 were detrended, filtered and downsampled to 5 Hz and used as input.

TABLE I
Simulation Scenarios

Scenario	Description	Frequency (Hz)	Damping (%)
1	High Damping	0.5410	16.64
2	Low Damping	0.5672	4.13

Mode information was extracted by moving the data window over each set of data. The calculation was repeated every 5 s and the data window moved accordingly. This was repeated for data window sizes ranging from 1 min to 20 min in 1 min increments. It was done to investigate the effect of the data window size on accuracy. The average and standard deviation of the results were calculated for each data window size.

Fig. 2 and 3 shows accuracy of the average values increase with increasing data window size. The dash-dot line indicates the calculated average value and the solid line shows the actual value from the modal analysis. Lines marked with a square indicates results from the high damping scenario, while the low damping scenario results are marked with an x.

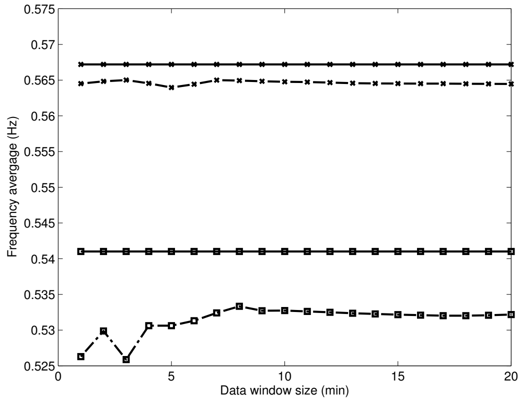

Fig. 2. Average value for frequency vs data window size. Solid lines indicate actual mode frequency values. Low damping scenario marked with an x, high damping scenario marked with a square.

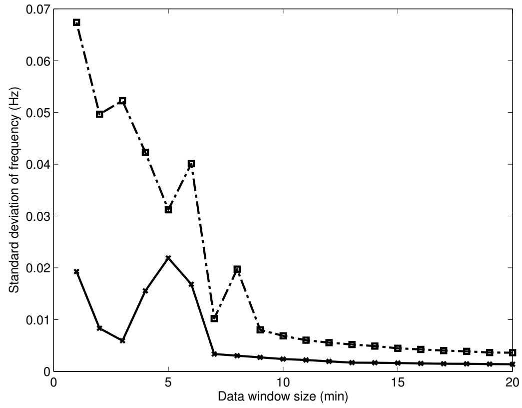

Fig. 4. Standard deviation of frequency results vs data window size. Dash-dot line indicates high damping scenario and solid line indicates low damping scenario.

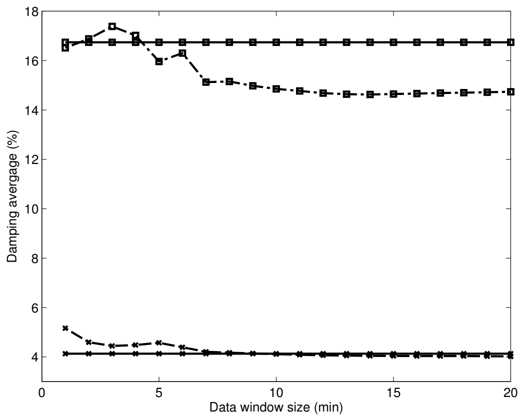

Fig. 3. Average value for damping vs data window size. Solid lines indicate actual mode damping values. Low damping scenario marked with an x, high damping scenario marked with a square.

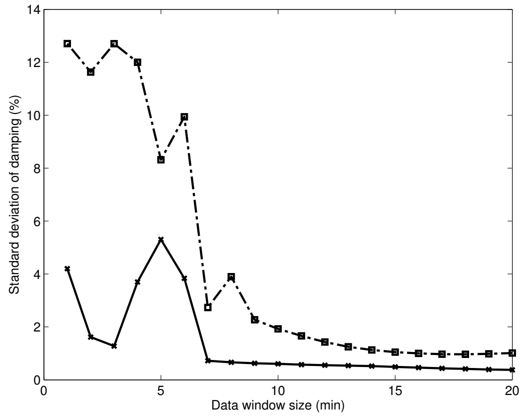

Fig. 5. Standard deviation of damping results vs data window size. Dash-dot line indicates high damping scenario and solid line indicates low damping scenario.

Fig. 4 and 5 show the standard deviations of the results from using different data window sizes. The dash-dot line indicates the high damping scenario and the solid line indicates the low damping scenario.

The accuracy of the average result for frequency and damping (Fig. 2 and 3) increase with data window size for both simulated scenarios. Standard deviation decreases with increasing data window size (Fig. 4 and 5). Accuracy increases with increasing window size as a more accurate estimation of the autocorrelation sequence in (10) is obtained. The average result and standard deviation stabilizes for data window sizes from 10 min upwards.

It is observed that lowered damping in the simulated system increase the accuracy of the result. This is observed for the average frequency and damping result (Fig. 2 and 3) as it moves closer to the actual value for the scenario with lower damping. Standard deviation for frequency and damping is also lower with lower oscillation damping in the system (Fig. 4 and 5).

In terms of (13), an increase in accuracy is found as the poles of the ARMA model move closer to the jw-axis. This results is intuitive as it is easier to identify oscillation characteristics when the oscillation is more prominent in the data, as will be the case for oscillations with low damping.

From the results are seen that the frequency can be more accurately determined than the damping. The variations in frequency result for differing data window size is much less than the variation in damping result (Fig. 2 and 3). Standard deviation for any given window size is significantly smaller for frequency result than damping result (Fig. 4 and 5).

Results found in this section are confirmed by those found in [7].

B. Mode shape

The right-eigenvector was calculated in the modal analysis of the test system. Mode shape for the rotor speed states relating to the inter-area oscillation mode was evaluated by means of a compass plot. The spectral method to determine mode shape was applied to the simulated data.

The mode shape calculation was repeated every time the oscillation mode result was refreshed. The average of all the results were taken and represented on a single compass plot. Fig. 6 presents a comparison between results from the modal analysis and the spectral analysis based method.

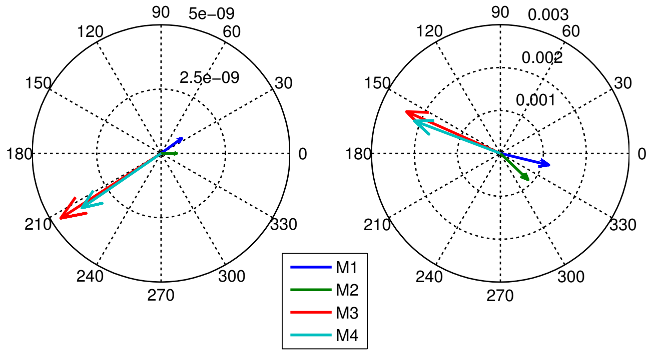

Fig. 6. Mode shape comparison: results from spectral method (left), results from modal analysis (right)

It can be seen that the spectral method accurately calculates mode shape from measured data. The difference in angles between the two methods are due to generator 2 being used as a reference generator in the spectral method, having an angle of 0°.

Relative angles and amplitudes of the calculated mode shape of each generator are similar to those obtained from the modal analysis. The absolute amplitudes of the calculated mode shapes differ from the modal analysis results, but this is expected as the spectral method used provides a scaled version of the actual value. The value of the result lies in the relative size of the mode shapes of the different generators.

The result confirms that an inter-area mode is present in the test system, since generators 1 and 2 (situated in Area 1) are oscillating against generators 3 and 4 (situated in Area 2).

IV. Practical Case Study

In this section, the monitoring method is applied to synchrophasor data recorded on a 330 kV, 521 km transmission line. The transmission line connects a hydro-generation plant to a transmission switching substation, with no loading, injection or compensation in between.

Fig. 7 shows the active power transferred over the 330 kV transmission line on 1 Feb 2015. It is observed that the generation of the hydro-station is reduced from approximately midnight to 07:00, and generation is reduced again from 21:00 onwards. This pattern is repetitive and observed every day.

Mode frequency, mode damping and mode shape analysis was applied to the data recorded on 1 Feb 2015. Fig. 8 and 9 shows the identified mode frequency and damping respectively. A dominant mode between 0.4 Hz and 0.5 Hz with damping between 10% and 20% is identified.

It is observed that the method produces inaccurate results during the early hours of the morning and again later at night.

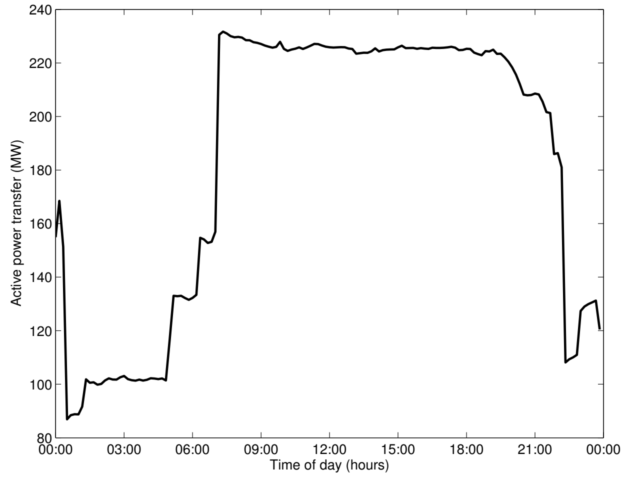

Fig. 7. Active power signal for the hydro-generation plant (1 Feb 2015)

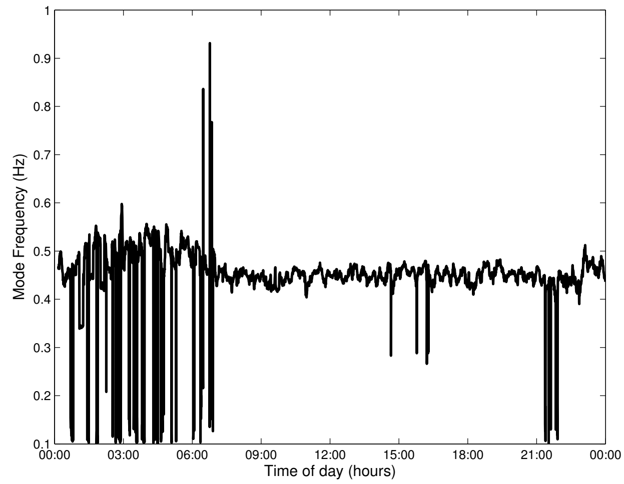

Fig. 8. Identified mode frequency (1 Feb 2015)

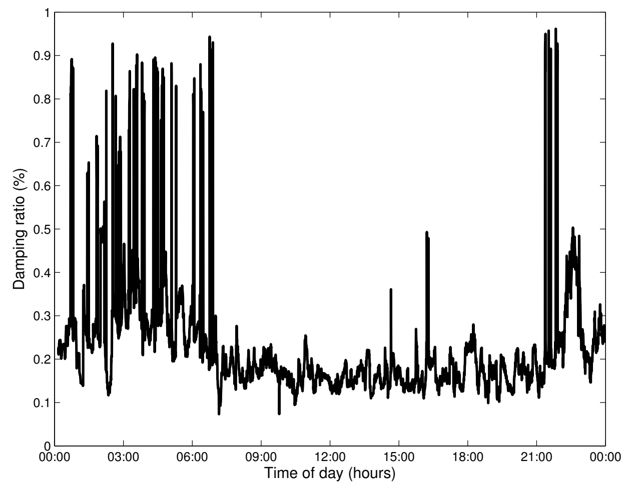

Fig. 9. Identified damping ratio (1 Feb 2015)

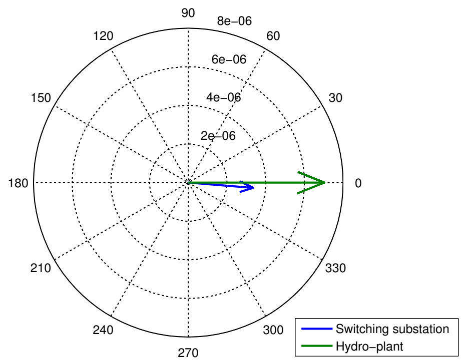

Fig. 10. Mode shape (1 Feb 2015)

This inaccuracy coincides with reduced hydro generation, as noted in fig. 7.

The reduced power transferred over the transmission line results in increased oscillation damping in the system. This is confirmed by the result of calculating the damping as shown in fig. 9. A higher damping ratio is obtained when generation is decreased. It was shown in section III-A that the accuracy of the ARMA method increases with lower oscillation damping, accounting for the reduced accuracy at high damping values.

The mode shape calculation was repeated each time the oscillation mode result was refreshed. Fig. 10 shows the average of the calculated values displayed as a compass plot. It is observed that the switching substation oscillates in phase with the hydro-station. The larger amplitude for mode shape observed at the hydro-station indicates that it is situated more towards the ends of the oscillation pathway than the switching substation.

V. Conclusion

In this paper, the theoretical principles of methods to determine inter-area oscillation characteristics in real-time were analysed and tested on both simulated and field data. These methods were verified by means of a simulated test power system containing inter-area modes. A practical case study was then presented where results from field data proved the usefulness of mode frequency, mode damping and mode shape analysis. Online application of the methods can provide valuable information for transmission system operation if obtained in near real-time.

References

[1] P. M. Anderson and A. A. Fouad, *Power System Control and Stability*, 2nd ed. New-Jersey: Wiley-Interscience, 2003.

[2] P. Kundur, *Power System Stability and Control*, 2nd ed. New-York: McGraw-Hill, 1994.

[3] Task Force on Identification of Electromechanical Modes, “Identification of Electromechanical Modes in Power Systems,” IEEE PES, Tech. Rep. June 2012, 2013.

[4] G. Liu, J. Quintero, and V. Venkatasubramanian, “Oscillation monitoring system based on wide area synchrophasors in power systems,” *2007 iREP Symposium- Bulk Power System Dynamics and Control - VII, Revitalizing Operational Reliability*, 2007.

[5] D. J. Trudnowski and J. W. Pierre, “Overview of algorithms for estimating swing modes from measured responses,” in *2009 IEEE Power and Energy Society General Meeting, PES ’09*, 2009, pp. 1–8.

[6] D. J. Trudnowski, J. W. Pierre, N. Zhou, J. F. Hauer, and M. Parashar, “Performance of three mode-meter block-processing algorithms for automated dynamic stability assessment,” *IEEE Transactions on Power Systems*, vol. 23, no. 2, pp. 680–690, 2008.

[7] R. W. Wies, J. W. Pierre, and D. J. Trudnowski, “Use of ARMA block processing for estimating stationary low-frequency electromechanical modes of power systems,” *IEEE Transactions on Power Systems*, vol. 18, no. 1, pp. 167–173, 2003.

[8] P. Stoica and R. Moses, *Spectral Analysis of Signals*. New-Jersey: Prentice Hall, 2004.

[9] M. Hemmingson, “Power System Oscillations Detection Estimation & Control,” Ph.D. dissertation, Lund University, 2003.

[10] D. J. Trudnowski, “Estimating electromechanical mode shape from synchrophasor measurements,” *IEEE Transactions on Power Systems*, vol. 23, no. 3, pp. 1188–1195, 2008.

[11] MathWorks, “Signal Processsing Toolbox.” [Online]. Available: www.mathworks.com/products/signal/

[12] N. Zhou, D. Trudnowski, J. W. Pierre, S. Sarawgi, and N. Bhatt, “An Algorithm for removing trends from power-system oscillation data,” in *IEEE Power and Energy Society 2008 General Meeting: Conversion and Delivery of Electrical Energy in the 21st Century, PES*, 2008, pp. 1–7.

[13] J. Chow and K. Cheung, “A toolbox for power system dynamics and control engineering education and research,” *IEEE Transactions on Power Systems*, vol. 7, no. 4, pp. 1559–1564, 1992.

A.2 Conference Proceedings - AMPS 2015

A paper was submitted for the IEEE AMPS 2015 conference in Aachen, Germany titled "Field Performance of Ambient Modal Estimation in Small Signal Stability". The paper was accepted for publication in the conference proceedings and presented during an oral session. The full paper is attached.

A comparison of the ARMA and wavelet methods is presented in this paper. Both methods are applied to simulated and practical data. The possibility of implementing multiple measurement functions in parallel on a single instrument is discussed in this paper. The implementation of both chosen methods are validated in this paper by peer review. Additional simulated tests based on the same methodology as in the Powertech paper (section A.1) are conducted.

Field Performance of Ambient Modal Estimation in Small Signal Stability

Tian van Rooyen, Johan Rens
Potchefstroom Campus of the North-West University
Potchefstroom, South Africa
22144153@nwu.ac.za, johan.rens@nwu.ac.za

Jan Desmet
Ghent University
Kortrijk, Belgium
janj.desmet@ugent.be

***Abstract*—Small signal stability is one focus of Wide Area Measurement Systems (WAMS). WAMS systems are becoming more widespread, driven by availability of synchrophasor data from Phasor Measurement Units (PMUs). In this paper, two methods capable of performing real-time small signal stability monitoring is evaluated by application to simulated data. Performance of the methods are tested to conditions likely to be found in practical use. The potential of both methods are further evaluated when applied to real-world data from a practical case study.**

***Index Terms*—Inter-area oscillation monitoring, synchrophasor data, Wide Area Measurement Systems (WAMS)**

I. Introduction

Modern power systems require increasingly fast and accurate monitoring to operate and control. As power systems become more interconnected and operated closer to capacity, increasingly advanced monitoring is required to ensure reliable delivery of electrical energy to consumers. Economic implications of power system blackouts further emphasize the importance of reliable operation of the power system.

The need for advanced monitoring is realised globally. A popular example is the USA blackout of 14 August 2003 and the recommendations published after an investigation into the cause of the incident [1]. A number of Wide Area Measurement Systems (WAMS) have been implemented in different countries to improve power system monitoring [2]–[8].

The focus of this paper is on monitoring small-signal stability, specifically inter-area oscillations. Inter-area oscillations limit power transfer capability in power systems and can cause system instability if they become insufficiently damped.

Modal analysis methods can be divided into ambient and ringdown methods. Ringdown methods focus on extracting modal information from data measured following a system disturbance, like a major fault or generator trip. Many ringdown methods are available that produce accurate results within a short time after the disturbance event.

Continuous real-time monitoring of inter-area oscillation characteristics dictate a need for methods designed to use ambient measured data as input. A power system is in an ambient condition when the only excitation to system response can be modelled as white noise inputs, corresponding to random load changes [9]. In comparison with results from ringdown methods, inter-area oscillation monitoring during ambient operation remain challenging due to minimal excitation of the modes [5].

Many ambient methods for modal estimation are available in the literature [10]–[15], with varying accuracy. A number of the methods have been implemented in WAMS as mentioned, and practical experience has shown that a trade-off exists between accuracy of the estimation and rate of response to changing system conditions. This is especially true in the case of damping estimation for each oscillatory mode [16].

In this paper, two different ambient methods of modal estimation will be tested according to criteria chosen to evaluate its suitability for practical use in WAMS. The methods are tested to simulated data where distinct conditions are generated that might be found in a practical power system. The two methods will also be applied to real world data measured on a 330 kV, 521 km Southern African transmission line.

II. Measurement Instrumentation in WAMS

Synchrophasor data from Phasor Measurement Units (PMUs) are used as input to monitoring algorithms in WAMS. The high accuracy time stamp of synchrophasor data make advanced monitoring applications possible. Ambient modal estimation methods also make use of synchrophasor data.

Synchrophasor measurement accuracy is defined in the IEEE C37.118.1:2011 standards document, specifying that a PMU must be equipped with a time source accurate enough to produce total vector error (TVE), frequency error (FE) and rate of change of frequency (ROCOF) error (RFE) below the specified limits. A GPS is traditionally used for this purpose. No limit value for time uncertainty is explicitly defined, rather it is contained in the definition for TVE, FE and RFE.

The accuracy of Power Quality (PQ) instruments are defined in the IEC 61000-4-30 standards document. Along with requirements on other measured parameters, Class A instruments are required to have time uncertainty of less than 20 ms for a 50 Hz system and 16,7 ms for a 60 Hz system. It is suggested that some time synchronisation procedure be used to achieve the required time uncertainty, such as a GPS receiver.

Time uncertainty much better than the IEC 61000-4-30 specification can be achieved if a PQ instrument is fitted with GPS. The addition of a GPS to a PQ instrument enable time accuracy that complies to specifications as set in the C37.118.1 standard. Class A PQ instruments with GPS time synchronisation can measure with sufficient accuracy to be used as a PMU.

Advances in instrumentation make it possible to merge functions of previously separate instruments into one. PMU functionality according to C37.118.1 specification can be implemented in parallel with IEC 61000-4-30 PQ measurement methodologies on a single instrument. PQ instruments can now measure synchrophasor data with minimal extra sophistication, whilst also providing PQ data (with high accuracy in time stamping) that can potentially further aid in power system monitoring. A similar suggestion to merge different WAMS functionalities into one instrument is made in [8].

WAMS was solely the domain of specialised devices like PMUs. Enabling PQ instruments to measure synchrophasor data makes WAMS functionality available to general network management. Operational risk and security of supply capacity in Southern African power systems is strained, and will remain so for a number of years. Opportunities exist to implement WAMS functions through synchrophasor enabled PQ instruments. WAMS systems can provide information useful for managing these risks.

This concept is shown to be feasible in this paper by applying the two methods to data measured by an instrument were synchrophasor data measurement is implemented according to C37.118.1 specifications in parallel with PQ measurements according to IEC 61000-4-30 Class A specifications.

III. Ambient Modal Estimation Methods

Two methods of ambient modal estimation is considered in this paper. The methods are explained briefly and references provided to the relevant literature for more detailed description of each method used. The two methods considered are:

1) an ARMA model fitted with the extended Modified Yule-Walker algorithm
2) Wavelet scale decomposition using orthogonal wavelet bases

A. ARMA method

The method uses the extended Modified Yule-Walker (MYW) equations to fit an Auto Regressive Moving Average (ARMA) model to measured ambient data. This is a parametric method where the spectral characteristics of the signal is derived from the fitted model. The Yule-Walker method has been applied to the problem of ambient modal analysis as early as 1997 [17] and have since been applied successfully in various other sources in the literature [11], [18]–[20].

An ARMA model fitted to the measured dataset $y(t)$ is defined [21]:

$$y(t) = \frac{B(z)}{A(z)}e(t) \tag{1}$$

The ARMA model in (1) has an order of (n, m) and can be expressed in the time domain as a difference equation [22]:

$$\begin{aligned} y(t) + a_1 y(t-1) + \cdots + a_n y(t-n) = \\ b_0 e(t) + b_1 e(t-1) + \cdots + b_m e(t-m) \end{aligned} \tag{2}$$

where a_i for $i = 1, \ldots, n$ are the coefficients of $A(z)$ and b_j for $j = 0, \ldots, m$ are the coefficients of $B(z)$.

The MYW equations use the relationship between the autocorrelation function of the input data and the a_i coefficients to find the mode information. The autocorrelation of the signal is defined as:

$$r(k) = E\{y(t)y(t-k)\} \tag{3}$$

Equation (2) can be manipulated to contain the definition of the autocorrelation of the signal and with simplification, (4) results:

$$r(k) + \sum_{i=1}^{n} a_i r(k-i) = 0 \qquad \text{for } k > m \tag{4}$$

Writing (4) in matrix form for $k = m+1, m+2, \ldots, m+M$, the over-determined solution for a_i can be found. The frequency and damping of the oscillatory modes are found by examining the poles of the ARMA model in (1). The method can easily be extended to take more than one measured signal as input, forming the extended MYW equations [19].

B. Wavelet Scale Decomposition Method

The Wavelet Scale Decomposition (WSD) method uses the Continuous Wavelet Transform (CWT) to transform a signal into wavelet scales. This is done by defining new bases using orthogonal wavelet functions [9].

WSD is a non-parametric method suitable to be applied to non-stationary signals. The wavelet transform of a signal is taken to find the wavelet coefficients, and expressed for discrete computer implementation:

$$C(s,u) = \sum_{n=0}^{N} f(n) \frac{1}{\sqrt{s}} W^* \left(\frac{n-u}{s} \right) \tag{5}$$

for $s = 0, .., S$ the number of scales, $u = 0, .., U$ the number of translations of the wavelet and $n = 0, .., N$ the number of data points considered. $W^*(t)$ is the complex form of the orthogonal wavelet chosen according to criteria set to define the new base for the signal.

The goal of the method is to reconstruct the approximate system impulse response containing modal information extracted by the wavelet transform and specifically chosen wavelet function. The time domain impulse response is found by the inverse wavelet transform, where the translation effect is ignored.

$$F(t) = \frac{1}{C_\varphi} \sum_{s=0}^{S} \widehat{C(s)} \frac{1}{\sqrt{s}} W\left(\frac{t}{s}\right) \frac{1}{s^2}, t \geq 0 \tag{6}$$

The rest of the method is focused on estimating $\widehat{C(s)}$. Equation (5) is applied to each input signal to find $C_i(s, u)$, for $i = 1, .., L$ signals. The matrix $P(s)$ is formed by considering the wavelet coefficients of each input signal:

$$P(s) = \begin{bmatrix} C_1(s,u) \\ C_1(s,u) \\ \vdots \\ C_L(s,u) \end{bmatrix} \tag{7}$$

The PSD matrix is then calculated by:

$$P_{xy}(s) = \frac{1}{U} P(s) P^*(s) \tag{8}$$

$\widehat{C(s)}$ can be estimated as the norm of the PSD matrix through singular value decomposition (SVD).

To remove the effect of random noise in the measurements, $\widehat{C(s)}$ is averaged over a number of windows before being used to find the impulse response in (6). The impulse response can easily be analysed by a method suited to analyse ringdown data, such as the Prony method [23].

Detail on the method and its implementation can be found in [9]. As an added benefit, the method also provides mode shape of the oscillatory modes in the system, in addition to frequency and damping of the mode.

IV. Testing of Methods on Simulated Data

Simulations were prepared to test the performance of the two methods under various conditions that can be expected in practical use. The following tests were conducted to evaluate the sensitivity of each method to the various parameters.

The Kundur two area system (fig. 1) was simulated in Matlab using the PST toolbox. Each simulation was done for 1 hour of simulated data. Simulated values were calculated 100 times per second.

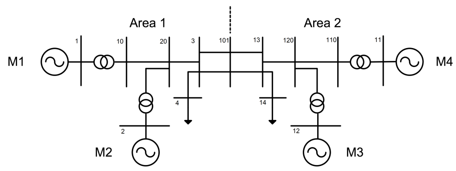

Fig. 1. Kundur 4-Machine, 2-Area test system

A. Window Length

Window length needed by each method is evaluated first. Accuracy of ambient methods tend to decrease with a decrease in window length. This is especially true for the damping result [16]. Window length will affect the response of the method to changing conditions. An algorithm with a shorter window length will react faster to changes than one with a longer window length. A trade-off exists between acceptable accuracy and fast reaction to change.

A consequence of window length for practical use is in the case of lost communication with a PMU. Window length will determine the amount of time that needs to elapse after communication has been restored, before the algorithm can produce an answer.

Each method was in turn applied to the simulated data, with window lengths from 1-min to 20-min in 1-min increments. The mean and standard deviation for results of each window length was calculated.

Fig. 2 and fig. 3 shows the average frequency values computed for each window length. Standard deviation for each window length is shown as error bars. Fig. 2 shows the result

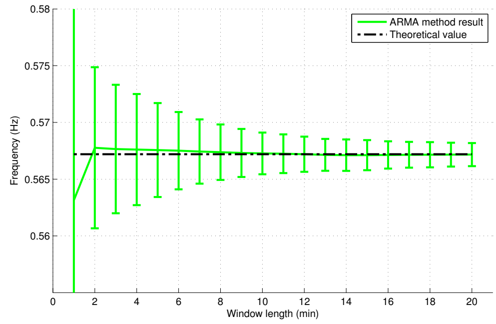

Fig. 2. ARMA method frequency result vs window length. The dash-dotted line show the actual frequency (0.5672 Hz).

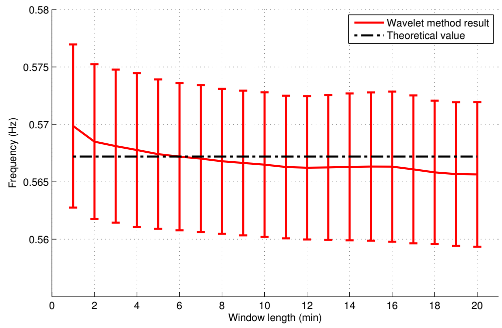

Fig. 3. Wavelet method frequency result vs window length. The dash-dotted line show the actual frequency (0.5672 Hz).

from the ARMA method and fig. 3 the results for the wavelet method.

Note that the standard deviation for the ARMA results (fig. 2) at 1-min window length falls outside the range of values shown. This is done by choosing the displayed y-axis values equal to that of the wavelet results (fig. 3) to enable visual comparison.

Both methods deliver accurate results for mode frequency (note the fine scale for frequency result). The accuracy of the ARMA method is seen to increase with an increase in window length. Standard deviation decreases with increasing window length for the ARMA method. Window length has a much smaller impact on the accuracy of the wavelet method. While still providing a frequency mean close to the actual value, very little change in standard deviation is noticed when increasing window length.

Fig. 4 and fig. 5 follow the same methodology as above to show results for mode damping. Fig. 4 shows the results for the ARMA method and fig. 5 shows the results for the wavelet method. Once again, the range of y-axis values for the ARMA method (fig. 4) is restricted for visual comparison of results.

The ARMA method (fig. 4) again shows an increase in mean damping accuracy and decrease in standard deviation with increasing window length. Mean damping accuracy for the wavelet method (fig. 4) remain largely unaffected by window length, however an increase in standard deviation is observed as window length increases.

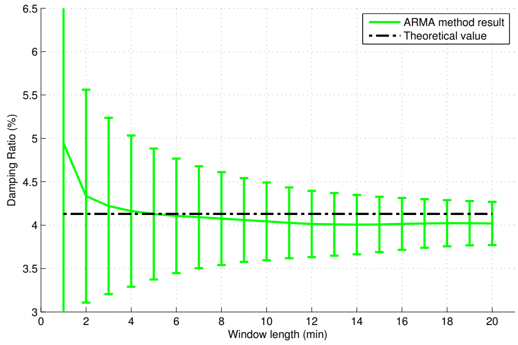

Fig. 4. ARMA method damping result vs window length. The dash-dotted line show the actual damping ratio (4.13 %).

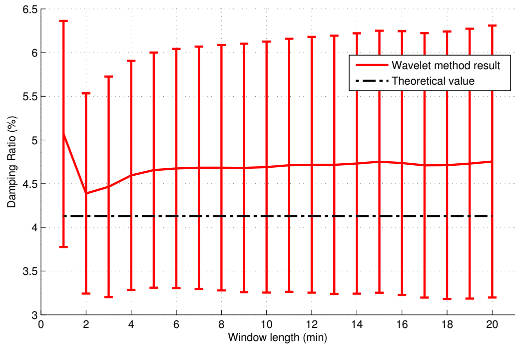

Fig. 5. Wavelet method damping result vs window length. The dash-dotted line show the actual damping ratio (4.13 %).

Being a time domain method, it is expected that a change in window length could have a larger effect on the ARMA method, rather than the wavelet method were all calculations are performed in the wavelet domain.

By comparing the results for frequency and damping for the two methods, it is observed that results with a similar mean accuracy and standard deviation are found when a 2-min window length is used. For all tests that follow a 2-min window length will be used for both methods as comparative results are expected.

B. System Damping Level

The damping of oscillations in a power system affects the accuracy of ambient methods. The Kundur system was used to simulate a power system with different damping ratios. This was achieved by varying the amount of PSS's connected to the machines in the system. The Kundur system was simulated for three scenarios with different damping ratios. Table I summarises the inter-area characteristics for each scenario.

Both methods were applied to each of the datasets using a 2-min window length. The frequency and damping calculation error for each set of results was calculated. The error is taken as the difference between the mean of the results and the actual value.

Fig. 6 shows mean frequency and damping error plotted against system damping for both methods. Results for the ARMA and wavelet method are shown by the green and red lines respectively. The error for both methods increase approximately linearly with system damping, in both frequency and damping.

TABLE I
SIMULATION SCENARIOS

Scenario	Damping (%)	Frequency (Hz)
1	4.13	0.5672
2	9.67	0.5598
3	16.64	0.5410

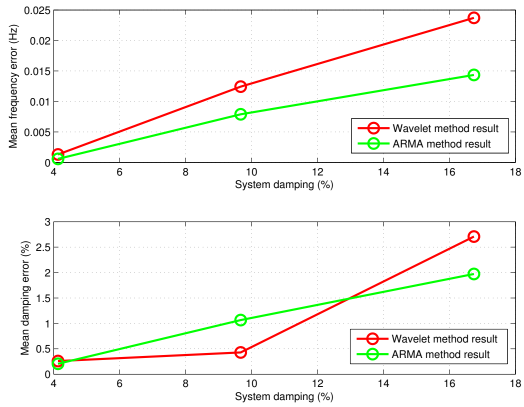

Fig. 6. Mean frequency and damping error vs system damping.

C. Ability to Track Changing Conditions

It is important for each method to track changes in system conditions to be of practical use. The tracking performance of each method is evaluated in this section. A single pole system excited by a Gaussian noise input was simulated. The parameters of the system was altered to produce changing frequency and damping values, similar to what might be found in a practical power system. Table II shows the conditions created in the simulation.

TABLE II
SIMULATION WITH RAMPED CHANGE IN FREQUENCY AND DAMPING

Time (min)	Damping (%)	Frequency (Hz)
0 - 15	7	0.3
15 - 30	7 - 2	0.3 - 0.7
30 - 45	2	0.7

Fig. 7 and fig. 8 shows the frequency and damping result respectively. The ARMA method results are shown in green, and the wavelet results in red.

Both methods are capable of tracking changes in frequency and damping. Frequency can be tracked accurately by both methods. Damping estimation is less accurate, especially in the region where damping is high (0 to 15-min). Both methods show a delay between the change in system conditions and change in the result. This delay is equal to the 2-min window length used.

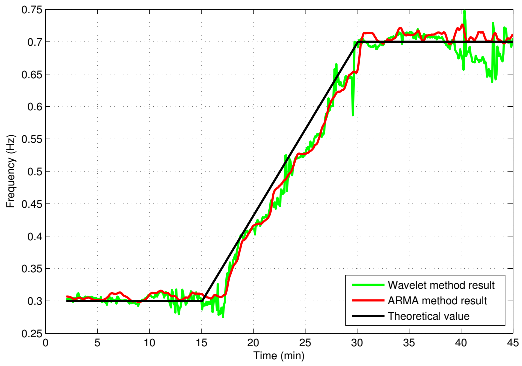

Fig. 7. Frequency tracking test. Green line: ARMA method. Red line: wavelet method.

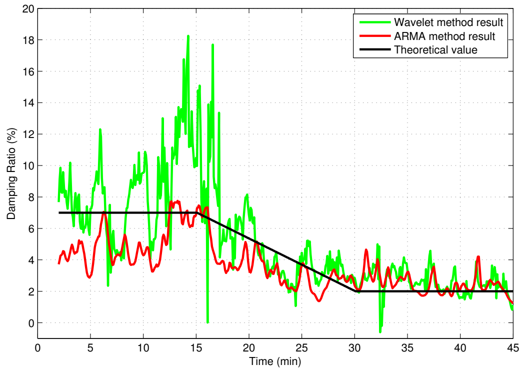

Fig. 8. Damping tracking test. Green line: ARMA method. Red line: wavelet method.

The wavelet method is less prone to the influence of random noise than the ARMA method. ARMA method results show larger changes over a short period of time. The averaging process of the wavelet coefficients over a number of windows act to filter out sudden changes in result (section III-B).

V. Testing on Real World Data

In this section, both methods are applied to synchrophasor data recorded on a 330 kV, 521 km transmission line. The transmission line connects a hydro-generation plant to a transmission switching substation, with no loading, injection or compensation in between.

Fig. 9 shows the active power transferred over the 330 kV transmission line on 1 Feb 2015. It is observed that the generation of the hydro-station is reduced from approximately midnight to 07:00, and generation is reduced again from 21:00 onwards. This pattern is repetitive and observed every day.

Both methods were applied to the data from 1 Feb to find mode frequency and damping. Fig. 10 and 11 show the frequency and damping result respectively. Both methods identify a dominant mode between 0.4 - 0.5 Hz at 10 - 20 % damping during the period of high generation at the hydro-station.

A 2-min window length was used when the wavelet method was applied to real world data, as previous tests on simulated

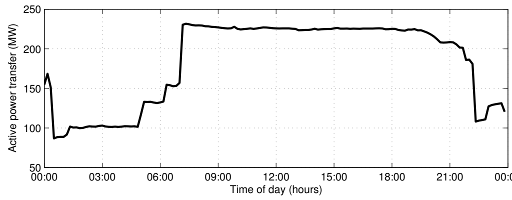

Fig. 9. Practical data test: Active power signal for the hydro-station (1 Feb 2015)

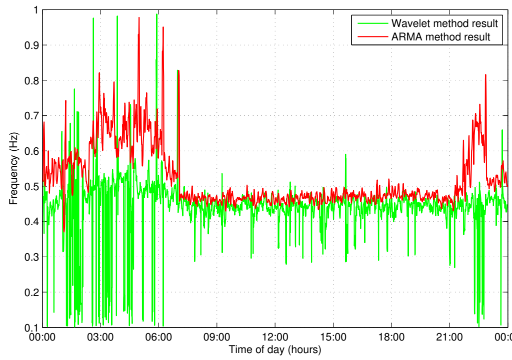

Fig. 10. Practical data test: Mode frequency. Green line: ARMA method. Red line: wavelet method. (1 Feb 2015)

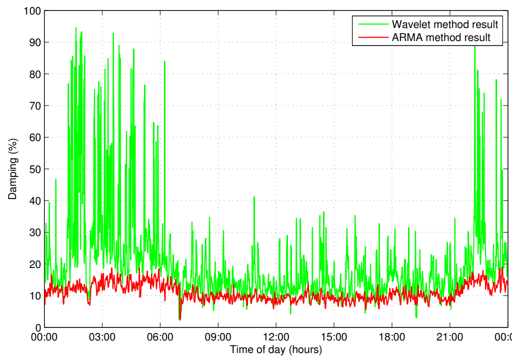

Fig. 11. Practical data test: Mode damping. Green line: ARMA method. Red line: wavelet method. (1 Feb 2015)

data used this window length. A 4-min window was applied to the real world data for the ARMA method. Real world results from the ARMA method with a 2-min window varied so much that mode frequency and damping identification became impractical. Window length in practical use will depend on operational use of the small signal results, as well as accuracy and monitoring response requirements.

Instantaneous frequency measured according to C37.118.1 specifications are used as input to the methods. Data is captured at 10 samples per second, and downsampled to 5 samples per second during preprocessing.

It is observed that the results are inaccurate and differ greatly during the early hours of the morning and again later at night. During these times the results from the ARMA method are erratic. The wavelet method results are also erratic, although less than the ARMA method. The inaccurate results coincide with reduced hydro-station generation, as shown in fig. 9.

The reduced power transferred over the transmission line results in increased oscillation damping in the system. This is confirmed by the damping result shown in fig. 11. A higher damping ratio is obtained when generation is decreased. It was shown in section IV-B that the accuracy of both methods decreases with higher oscillation damping, accounting for the reduced accuracy at high damping values.

The ARMA method seems more sensitive to random noise than the wavelet method. Results from the wavelet method are more stable than the ARMA method results.

VI. CONCLUSION

Two different methods for modal estimation from ambient measured data is evaluated. The performance of the two methods are compared for various simulated test setups and also tested to real-world data.

Both methods are capable of calculating mode frequency and damping. Damping result is less accurate than frequency result for both methods. Accuracy is further influenced by system damping. Accuracy of both methods improves as inter-area modes become less stable.

The ARMA method is much more sensitive to window length than the wavelet method. Accuracy of the ARMA method increases with increasing window length, while the wavelet method results display little change for different window lengths.

Both methods are capable of tracking changing system conditions, with a lag in results equal to the window length.

The wavelet method produces less variance in results than the ARMA method. ARMA method results can vary significantly over a short time.

It was shown that WAMS functions like small signal stability monitoring is possible from PQ instruments fitted with GPS and configured to measure synchrophasor data in parallel with PQ measurements. Validation of practical results over a longer period is ongoing, in cooperation with the transmission system operator. Ambient modal estimation methods can successfully be applied to synchrophasor data measured on enabled PQ instruments.

REFERENCES

[1] U.S.-Canada Power System Outage Task Force, "Final Report on the August 14, 2003 blackout in the United States and Canada: Causes and Recommendations," Tech. Rep., 2004.

[2] G. Ledwich, D. Geddey, and P. O'Shea, "Phasor measurement units for system diagnosis and load identification in Australia," in *IEEE Power and Energy Society 2008 General Meeting: Conversion and Delivery of Electrical Energy in the 21st Century, PES*, 2008, pp. 1–6.

[3] W. Sattinger, J. Bertsch, and P. Reinhardt, "Operational experience with wide area measurement systems," in *Cigré Session 2006*, 2006, pp. 1–8.

[4] J. F. Hauer, W. A. Mittelstadt, K. E. Martin, J. W. Burns, H. Lee, J. W. Pierre, and D. J. Trudnowski, "Use of the WECC WAMS in wide-area probing tests for validation of system performance and modeling," *IEEE Transactions on Power Systems*, vol. 24, no. 1, pp. 250–257, 2009.

[5] J. Turunen, M. Larsson, P. Korba, J. Jyrinsalo, and L. Haarla, "Experiences and future plans in monitoring the inter-area power oscillation damping," in *IEEE Power and Energy Society 2008 General Meeting: Conversion and Delivery of Electrical Energy in the 21st Century, PES*, 2008, pp. 1–8.

[6] C. L. Su and B. Y. Jau, "Visualization of wide area dynamics in power network for oscillatory stability assessment," in *2007 International Conference on Intelligent Systems Applications to Power Systems, ISAP*, 2007, pp. 1–6.

[7] P. Korba, "Real-time monitoring of electromechanical oscillations in power systems: first findings," *IET Generation, Transmission & Distribution*, vol. 1, no. 1, p. 80, 2007.

[8] P. M. Ashton, G. A. Taylor, A. M. Carter, and H. Renner, "Opportunities to exploit Phasor Measurement Units (PMUs) and synchrophasor measurements on the GB Transmission Network," in *Universities' Power Engineering Conference (UPEC), Proceedings of 2011 46th International*, no. September, 2011, pp. 3–8.

[9] V. Venkatasubramanian and H. Khalilinia, "Modal Analysis of Ambient PMU Measurements Using Orthogonal Wavelet Bases," *IEEE Transactions on Smart Grid*, no. 99, 2015.

[10] D. J. Trudnowski and J. W. Pierre, "Overview of algorithms for estimating swing modes from measured responses," in *2009 IEEE Power and Energy Society General Meeting, PES '09*, 2009, pp. 1–8.

[11] M. G. Anderson, N. Zhou, J. W. Pierre, and R. W. Wies, "Bootstrap-based confidence interval estimates for electromechanical modes from multiple output analysis of measured ambient data," *IEEE Transactions on Power Systems*, vol. 20, pp. 943–950, 2005.

[12] J. Turunen, J. Thambirajah, M. Larsson, B. C. Pal, N. F. Thornhill, L. C. Haarla, W. W. Hung, A. M. Carter, and T. Rauhala, "Comparison of three electromechanical oscillation damping estimation methods," *IEEE Transactions on Power Systems*, vol. 26, no. 4, pp. 2398–2407, 2011.

[13] J. C. H. Peng, N. K. C. Nair, J. Zhang, and A. K. Swain, "Detection of lightly damped inter-area power oscillations using extended complex Kalman Filter," in *IEEE Region 10 Annual International Conference, Proceedings/TENCON*, 2009.

[14] G. Liu and V. Venkatasubramanian, "Oscillation monitoring from ambient PMU measurements by frequency domain decomposition," in *Proceedings - IEEE International Symposium on Circuits and Systems*, 2008, pp. 2821–2824.

[15] H. Ghasemi, S. Member, C. Cañizares, S. Member, and A. Moshref, "Oscillatory Stability Limit Prediction Using Stochastic Subspace Identification," *IEEE Transactions on Power Systems*, vol. 21, no. 2, pp. 736–745, 2006.

[16] J. Turunen, L. Haarla, and T. Rauhala, "Performance of wavelet-based damping estimation method under ambient conditions of the power system," in *2010 IREP Symposium - Bulk Power System Dynamics and Control - VIII, IREP2010*, 2010, pp. 1–9.

[17] J. W. Pierre, "Initial results in electromechanical mode identification from ambient data," *IEEE Transactions on Power Systems*, vol. 12, pp. 1245–1251, 1997.

[18] Task Force on Identification of Electromechanical Modes, "Identification of Electromechanical Modes in Power Systems," IEEE PES, Tech. Rep. June 2012, 2012.

[19] D. J. Trudnowski, J. W. Pierre, N. Zhou, J. F. Hauer, and M. Parashar, "Performance of three mode-meter block-processing algorithms for automated dynamic stability assessment," *IEEE Transactions on Power Systems*, vol. 23, no. 2, pp. 680–690, 2008.

[20] T. van Rooyen and J. Rens, "Real-Time Power System Oscillation Monitoring using Synchrophasor Measurements," in *PowerTech, 2015 IEEE Eindhoven*, Eindhoven, 2015.

[21] P. Stoica and R. Moses, *Spectral Analysis of Signals*. New-Jersey: Prentice Hall, 2004.

[22] R. W. Wies, J. W. Pierre, and D. J. Trudnowski, "Use of ARMA block processing for estimating stationary low-frequency electromechanical modes of power systems," *IEEE Transactions on Power Systems*, vol. 18, no. 1, pp. 167–173, 2003.

[23] G. Liu, J. Quintero, and V. Venkatasubramanian, "Oscillation monitoring system based on wide area synchrophasors in power systems," in *2007 iREP Symposium- Bulk Power System Dynamics and Control - VII, Revitalizing Operational Reliability*, 2007.

A.3 Journal Article - AMPS 2015 Special Edition

After the presentation of the work for the IEEE AMPS 2015 conference, an upgraded version of the conference proceedings was submitted for review to be included in the AMPS 2015 Special Edition of the IEEE Transactions on Instrumentation and Measurement. The manuscript is still in the process of being reviewed.

The extension of the manuscript beyond the scope of the original conference proceeding included:

- Visualisation of signal spectral content over time to aid small signal monitoring, applied to simulated and field data.

- Discussion regarding input signal selection for practical use of small signal stability monitoring methods without prior knowledge of observability of inter-area modes in measured signals.

- Improved small signal stability results are found using multiple signals as input to the methods considered.

The manuscript is attached as it was submitted for review.

Field Performance of Ambient Modal Estimation in Small Signal Stability

Tian van Rooyen, Johan Rens
Potchefstroom Campus of the North-West University
Potchefstroom, South Africa
22144153@nwu.ac.za, johan.rens@nwu.ac.za

Jan Desmet
Ghent University
Kortrijk, Belgium
janj.desmet@ugent.be

***Abstract*—Small signal stability monitoring is one focus of Wide Area Measurement Systems (WAMS). WAMS are becoming more widespread, driven by availability of synchrophasor data from Phasor Measurement Units (PMUs). In this paper, two methods capable of performing real-time small signal stability monitoring is evaluated by application to simulated data. Performance of the methods are tested to conditions likely to be found in practical use. The potential of both methods are further evaluated when applied to field data from a practical case study.**

***Index Terms*—Inter-area oscillation monitoring, synchrophasor data, Wide Area Measurement Systems (WAMS)**

I. Introduction

Modern power systems require increasingly fast and accurate monitoring to operate and control. As power systems become more interconnected and operated closer to capacity, increasingly advanced monitoring is required to ensure reliable delivery of electrical energy to consumers. Economic implications of power system blackouts further emphasize the importance of reliable operation of the power system.

The need for advanced monitoring is realised globally. A popular example is the USA blackout of 14 August 2003 and the recommendations published after an investigation into the cause of the incident [1]. A number of Wide Area Measurement Systems (WAMS) have been implemented in different countries to improve system wide power system monitoring [2]–[6].

The focus of this paper is on evaluating the performance of small-signal stability monitoring methods for modal estimation of inter-area oscillations. Inter-area oscillations limit power transfer capability in power systems and can cause system instability if they become insufficiently damped.

Modal analysis methods can be divided into ambient and ringdown methods. Ringdown methods focus on extracting modal information from data measured following a system disturbance, like a major fault or generator trip. Many ringdown methods are available that produce accurate results within a short time after the disturbance event.

Continuous real-time monitoring of inter-area oscillation characteristics dictate a need for methods designed to use ambient measured data as input. A power system is in an ambient condition when the only excitation to system response can be modelled as white noise inputs, corresponding to random load changes [7]. In comparison with results from ringdown methods, inter-area oscillation monitoring during ambient operation remain challenging due to minimal excitation of the modes [4].

Many ambient methods for modal estimation are available in the literature [8]–[12], with varying success in accuracy. A number of the methods have been implemented in WAMS as mentioned, and practical experience has shown that a trade-off exists between accuracy of the estimation and rate of response to changing system conditions. This is especially true in the case of damping estimation for each oscillatory mode [13].

In this paper, two different ambient methods of modal estimation are tested according to criteria chosen to evaluate its suitability for practical use in WAMS. The methods are tested to simulated data where distinct conditions are generated that might be found in a practical power system. The two methods are also applied to field data measured on a 521 km transmission line.

II. Measurement Instrumentation in WAMS

Synchrophasor data from Phasor Measurement Units (PMUs) are used as input to monitoring algorithms in WAMS. The high accuracy time stamp of synchrophasor data make advanced monitoring applications possible. Ambient modal estimation methods also make use of synchrophasor data.

Synchrophasor measurement accuracy is defined in the IEEE C37.118.1:2011 standards document, specifying that a PMU must be equipped with a time source accurate enough to produce total vector error (TVE), frequency error (FE) and rate of change of frequency (ROCOF) error (RFE) below the specified limits. A GPS is traditionally used for this purpose. No limit value for time uncertainty is explicitly defined, rather it is contained in the definition for TVE, FE and RFE.

The accuracy of Power Quality (PQ) instruments are defined in the IEC 61000-4-30 standards document. Class A instruments are required to have time uncertainty of less than 20 ms for a 50 Hz system and 16.7 ms for a 60 Hz system.

Time uncertainty much better than the IEC 61000-4-30 Class A specification can be achieved if a PQ instrument is fitted with GPS. It enables a PQ instrument to achieve time accuracy that complies with specifications of the C37.118.1 standard. PQ instruments can now measure synchrophasor data with minimal extra sophistication, in parallel with PQ parameters. A similar suggestion to merge different WAMS functionalities into a single power system instrument is made in [6].

WAMS were solely the domain of specialised devices like PMUs. Enabling PQ instruments to also record synchrophasor data presents the opportunity to deploy the powerful features of WAMS to more role players in network control and operation. Opportunities exist to implement WAMS functions through synchrophasor enabled PQ instruments.

This concept is shown to be feasible in this paper by applying the two modal analysis methods to data recorded by an instrument where synchrophasor measurement capability is implemented according to C37.118.1 specifications in parallel with PQ recordings according to IEC 61000-4-30 Class A specifications.

III. Ambient Modal Estimation Methods

Two methods of ambient modal estimation is briefly presented in this paper. The two methods are:

1) an ARMA model fitted using the extended Modified Yule-Walker algorithm.
2) Wavelet scale decomposition using orthogonal wavelet bases.

A. Modified Yule-Walker ARMA method

The method uses the extended Modified Yule-Walker (MYW) equations to fit an Auto Regressive Moving Average (ARMA) model to measured ambient data. This is a parametric method where the spectral characteristics of the signal is derived from the fitted model. The Yule-Walker method has been applied to the problem of ambient modal analysis as early as 1997 and have since been applied successfully in various other sources in the literature [9], [14], [15].

An ARMA model fitted to the measured dataset $y(t)$ is defined [16]:

$$y(t) = \frac{B(z)}{A(z)}e(t) \tag{1}$$

The ARMA model in (1) has an order of (n, m) and can be expressed in the time domain as a difference equation [17]:

$$\begin{aligned} y(t) + a_1 y(t-1) + \cdots + a_n y(t-n) = \\ b_0 e(t) + b_1 e(t-1) + \cdots + b_m e(t-m) \end{aligned} \tag{2}$$

where a_i for $i = 1, \ldots, n$ are the coefficients of $A(z)$ and b_j for $j = 0, \ldots, m$ are the coefficients of $B(z)$.

The MYW equations use the relationship between the autocorrelation function of the input signal and the a_i coefficients to find the mode information. The autocorrelation of the signal is defined as:

$$r(k) = E\{y(t)y(t-k)\} \tag{3}$$

Equation (2) can be manipulated to contain the definition of the autocorrelation of the signal and with simplification, results in:

$$r(k) + \sum_{i=1}^{n} a_i r(k-i) = 0 \qquad \text{for } k > m \tag{4}$$

Writing (4) in matrix form for $k = m{+}1, m{+}2, \ldots, m{+}M$, the over-determined solution for a_i can be found. The frequency and damping of the oscillatory modes are found by examining the poles of the ARMA model in (1). The method can easily be extended to accept more than one measured signal as input, resulting in the extended MYW equations [14].

The process so far has determined the AR part of the ARMA model. The spectrum of the signal described by the ARMA model can be found if the MA part is also known. The covariance sequence of the MA part can be estimated from the a_i coefficients and the AR covariances $r(k)$ [16]. The spectral content of the signal is then visible.

B. Wavelet Scale Decomposition Method

The Wavelet Scale Decomposition (WSD) method uses the Continuous Wavelet Transform (CWT) to transform a signal into wavelet scales. This is done by defining new bases using orthogonal wavelet functions [7].

WSD is a non-parametric method suitable to be applied to non-stationary signals. The wavelet transform of a signal is taken to find the wavelet coefficients, and expressed for discrete computer implementation:

$$C(s,u) = \sum_{n=0}^{N} f(n)\frac{1}{\sqrt{s}}W^*\left(\frac{n-u}{s}\right) \tag{5}$$

for $s = 0, .., S$ the number of scales, $u = 0, .., U$ the number of translations of the wavelet and $n = 0, .., N$ the number of data points considered. $W^*(t)$ is the complex form of the orthogonal wavelet chosen according to criteria set to define the new base for the signal.

The goal of the method is to reconstruct the approximate system impulse response containing modal information extracted by the wavelet transform and specifically chosen wavelet function. The time domain impulse response is found by the inverse wavelet transform, where the translation effect is ignored.

$$F(t) = \frac{1}{C_\varphi}\sum_{s=0}^{S}\widehat{C(s)}\frac{1}{\sqrt{s}}W\left(\frac{t}{s}\right)\frac{1}{s^2}, t \geq 0 \tag{6}$$

The rest of the method is focused on estimating $\widehat{C(s)}$. Equation (5) is applied to each input signal to find $C_i(s,u)$, for $i = 1, .., L$ signals. The matrix $P(s)$ is formed by considering the wavelet coefficients of each input signal:

$$P(s) = \begin{bmatrix} C_1(s,u) \\ C_1(s,u) \\ \vdots \\ C_L(s,u) \end{bmatrix} \tag{7}$$

The Power Spectral Density (PSD) matrix is then calculated by:

$$P_{xy}(s) = \frac{1}{U}P(s)P^*(s) \tag{8}$$

$\widehat{C(s)}$ can be estimated as the norm of the PSD matrix through singular value decomposition (SVD).

To remove the effect of random noise in the measurements, $\widehat{C(s)}$ is averaged over a number of windows before being used to find the impulse response in (6). The impulse response can easily be analysed by a method suited to analyse ringdown data, such as the Prony method [18].

Detail on the method and its implementation can be found in [7]. As an added benefit, the method also provides mode shape of the oscillatory modes in the system, in addition to frequency and damping of the mode.

IV. Testing of Methods on Simulated Data

Simulations were used to test the performance of the two methods under various conditions that can be expected in practical cases.

The Kundur two-area system (fig. 1) was simulated in Matlab using the PST toolbox. Each simulation was completed for 1 hour of simulated operation. The simulation used a refresh rate of 100 Hz.

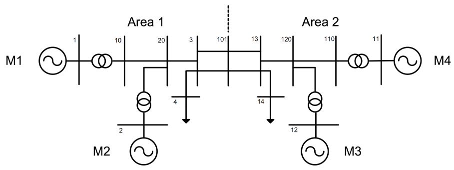

Fig. 1: Kundur 4-Machine, 2-Area test system

A. Window Length

Window length used by each method is evaluated first. Accuracy of ambient methods tend to degrade with a decrease in window length. This is especially true for the result on mode damping [13]. Window length affects the response of the method to changing system conditions. An algorithm with a shorter window length will react faster to system changes than an algorithm with a longer window length. A trade-off exists between acceptable accuracy and fast reaction to system change.

A consequence of window length for practical use is in the case of lost communication with a PMU. Window length will determine the amount of time that needs to elapse after communication has been restored, before the algorithm can produce an answer.

Each method is applied to the simulated data, with window lengths ranging from 1 min to 20 min in 1 min increments. The mean and standard deviation for results of each window length is then calculated.

Fig. 2 and fig. 3 show the average frequency values computed for each window length. Standard deviation for each window length is shown as error bars. Fig. 2 shows the result from the ARMA method and fig. 3 the results for the wavelet method.

Note that the standard deviation for the ARMA results (fig. 2) at 1 min window length falls outside the range of values shown. This is done by choosing the displayed y-axis values equal to that of the wavelet results (fig. 3) to enable visual comparison.

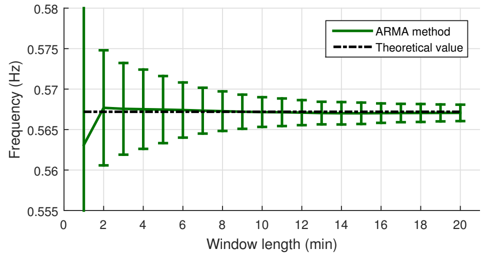

Fig. 2: ARMA method frequency result vs window length. The dash-dotted line show the actual frequency (0.5672 Hz).

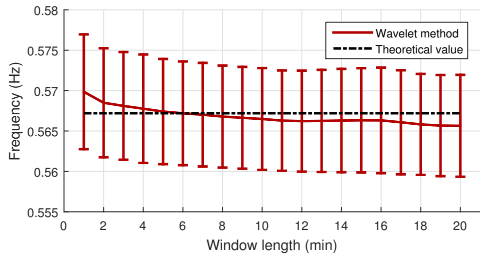

Fig. 3: Wavelet method frequency result vs window length. The dash-dotted line show the actual frequency (0.5672 Hz).

Both methods deliver accurate results for mode frequency (note the fine scale for frequency). The accuracy of the ARMA method improves with an increase in window length. Standard deviation decreases with increasing window length for the ARMA method. Window length has a much smaller impact on the accuracy of the wavelet method. While still providing a frequency mean close to the actual value, very little change in standard deviation is noticed when increasing window length.

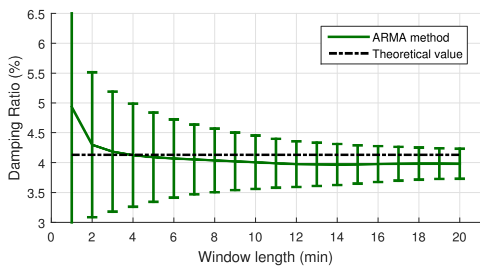

Fig. 4: ARMA method damping result vs window length. The dash-dotted line show the actual damping ratio (4.13 %).

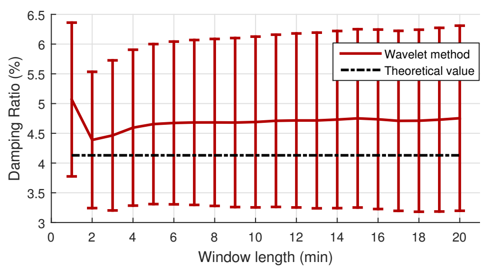

Fig. 5: Wavelet method damping result vs window length. The dash-dotted line show the actual damping ratio (4.13 %).

Fig. 4 and fig. 5 follow the same methodology as above to show results for mode damping. Fig. 4 presents the results for the ARMA method and fig. 5 the results for the wavelet method. Once again, the range of y-axis values for the ARMA method (fig. 4) is restricted for visual comparison of results.

The ARMA method (fig. 4) again shows an increase in mean damping accuracy and decrease in standard deviation with increasing window length. Mean damping accuracy for the wavelet method (fig. 4) remain largely unaffected by window length, however an increase in standard deviation is observed as window length increases.

Being a time domain method, it is expected that a change in window length could have a larger effect on the ARMA method, rather than the wavelet method were all calculations are performed in the wavelet domain.

By comparing the results for frequency and damping for the two methods, it is observed that results with a similar mean accuracy and standard deviation are found when a 2 min window length is used. For all tests that follow a 2 min window length will be used for both methods as comparative results are expected.

B. System Damping Level

The damping of oscillations in a power system affects the accuracy of ambient methods. Different damping ratios in the power system is simulated using the Kundur system. This is achieved by varying the number of PSS's connected to the machines in the system. The Kundur system is simulated for three scenarios with different damping ratios. Table I summarises the inter-area characteristics for each scenario.

TABLE I: Simulation Scenarios

Scenario	Damping (%)	Frequency (Hz)
1	4.13	0.5672
2	9.67	0.5598
3	16.64	0.5410

Both methods are applied to each of the datasets using a 2 min window length. The frequency and damping calculation error for each set of results is calculated. The error is taken as the difference between the mean of the results and the actual value.

Fig. 6 shows mean frequency and damping error plotted against system damping for both methods. Results for the ARMA and wavelet method are shown by the green and red lines respectively. The error for both methods increase approximately linearly with system damping, in both frequency and damping.

The effect of increased system damping is further investigated by inspecting the ARMA spectral estimation and CWT coefficients for the three simulated cases. Fig. 7 presents the spectral estimates from the ARMA model fitted to the data. Similarly, fig. 8 presents the wavelet coefficients from the wavelet transformation. If the values are comparatively large, it indicates energy identified in the specific frequency component. The figures show the spectral estimates for increasing damping from left to right.

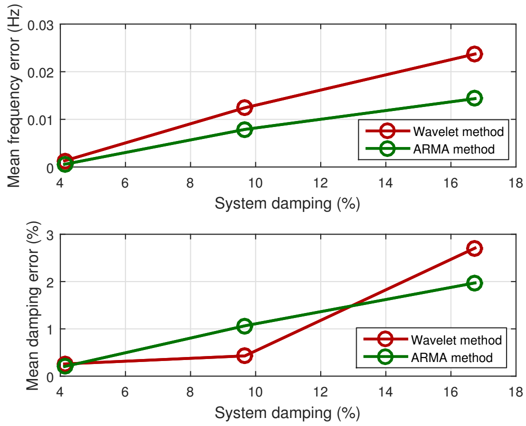

Fig. 6: Mean frequency and damping error vs system damping.

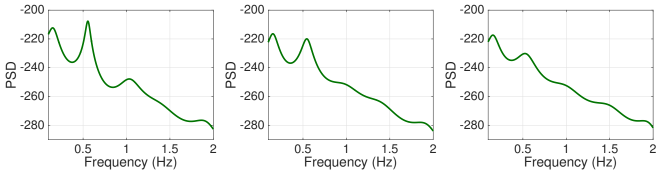

Fig. 7: ARMA spectral estimation: 4.13 % damping scenario (left), 9.67 % damping scenario (middle), 16.64 % damping scenario (right)

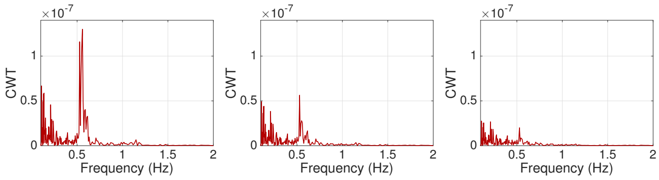

Fig. 8: Wavelet transform coefficients: 4.13 % damping scenario (left), 9.67 % damping scenario (middle), 16.64 % damping scenario (right)

Energy near the 0.5 Hz component is identified by both methods. It is observed that increased damping reduces the energy in the 0.5 Hz range. Both methods will have increasing difficulty in reliably identifying the inter-area mode characteristics when mode energy reduces.

C. Ability to Track Changing System Conditions

It is important for each method to track changes in system conditions in near real-time to be of practical use. The tracking performance of each method is evaluated in this section. A single pole system excited by a Gaussian noise input is simulated. The parameters of the system are altered to produce changing frequency and damping values, similar to what might be found in a practical power system. Table II lists the simulated conditions.

TABLE II: Simulation with ramped change in frequency and damping

Time (min)	Damping (%)	Frequency (Hz)
0 - 15	7	0.3
15 - 30	7 - 2	0.3 - 0.7
30 - 45	2	0.7

Fig. 9 and fig. 10 presents the frequency and damping result respectively. The ARMA method results are shown in green, and the wavelet results in red.

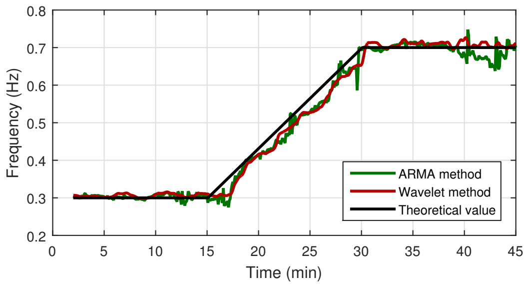

Fig. 9: Frequency tracking test. Green line: ARMA method. Red line: wavelet method.

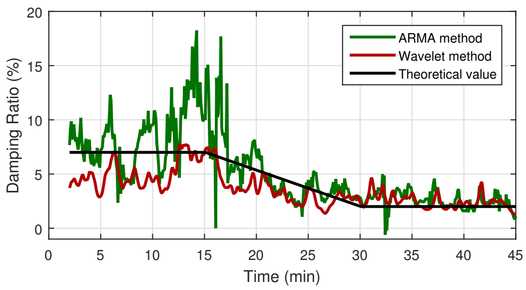

Fig. 10: Damping tracking test. Green line: ARMA method. Red line: wavelet method.

Both methods are capable of tracking changes in frequency and damping. Frequency can be tracked accurately by both methods. Damping estimation is less accurate, especially in the region where damping is high (0 to 15 min). Both methods show a delay between the change in system conditions and change in the result (easy to observe in frequency result). This delay between result change and system condition change is equal to the 2 min window length used.

The wavelet method is less prone to the influence of random noise than the ARMA method. ARMA method results show larger changes over a short period of time. The averaging process of the wavelet coefficients over a number of windows act to filter out sudden changes in result (section III-B).

V. Testing on Field Data

In this section, both methods are applied to synchrophasor data recorded across a 521 km transmission line. The transmission line connects a hydro-generation plant to a transmission switching substation, with no loading, injection or compensation in between.

Fig. 11 shows the active power transferred on a specific day. It is observed that the generation of the hydro-station is reduced from approximately midnight to 07:00, and again from 21:00. This is a daily pattern.

Input signals to the modal analysis methods must be selected. Active power is an obvious choice as the mechanism for power system oscillations are the exchange of active power

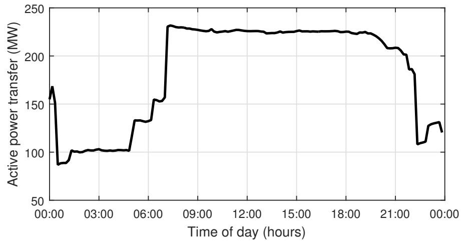

Fig. 11: Field dataset: Daily production

between different components or areas. Active power relates directly to the phenomena of interest. The nonlinear nature of the power system could hold disadvantages to using active power, especially when angular separation becomes large [19].

Alternatively, the voltage phase angle difference across the line can be used as input. This angular separation between the two areas directly relates to active power transfer. Angular separation has the advantage of exhibiting less nonlinear behaviour for large power transfers than active power [19].

Frequency and angular separation share most properties. Frequency, similar to angular separation is well suited for oscillation monitoring. An added advantage is that jumps in angular separation and active power are not observed in frequency measurement due to the integral relationship of frequency and angular separation [19].

The best signal to use as input will depend on the dynamics of the power system. This will determine which signal will have the best observability of a mode.

Both methods can use multiple signals as input. Results from each of the input signals are compared. Three sets of results are based on a single input signal. The fourth set of results use a combination of all the possible input signals. Fig. 12 and fig. 13 present the frequency and damping results for the ARMA method, while fig. 14 and fig. 15 are the results for the wavelet method.

Results using angular separation, active power and the combination input show similar results for both methods. Both methods identify a dominant mode between 0.4 - 0.5 Hz at 5 - 10 % damping during the period of high generation at the hydro-station. The frequency input signal consistently produces higher results than the other input signals. Fig. 16 shows the PSD of frequency and active power input signals. The active power signal contains energy at approximately 0.4 Hz. The frequency signal does not contain significant energy in this band. Observability of inter-area oscillations in the frequency signal is limited.

It is a challenge selecting an input signal without prior knowledge of the observability of inter-area modes in each measured signal. By using multiple inputs, signals with good observability of a mode enable accurate results. Results from using a combination of input signals in fig. 12 to fig. 15 shows this approach is feasible. The combination input signal produces results similar to signals with high observability. Result accuracy is improved from [20] by using multiple signals as input, instead of a single signal.

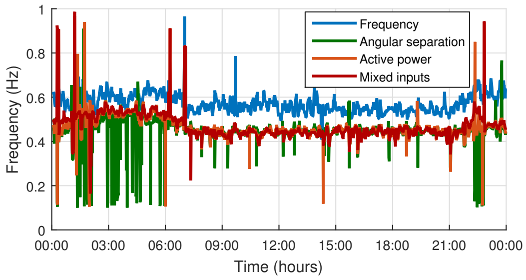

Fig. 12: ARMA method frequency results for different input signals.

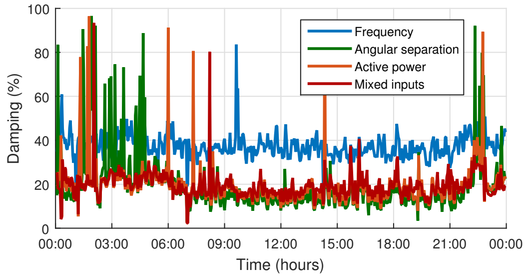

Fig. 13: ARMA method damping results for different input signals.

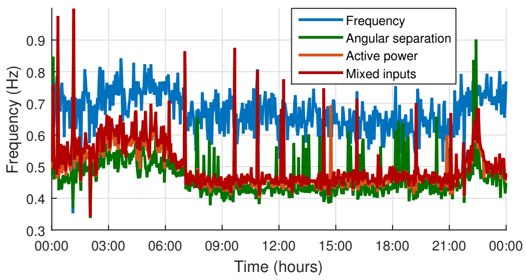

Fig. 14: Wavelet method frequency results for different input signals.

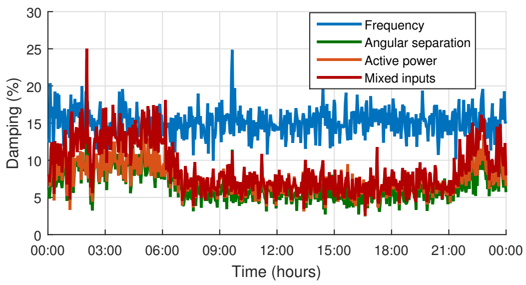

Fig. 15: Wavelet method damping results for different input signals.

A 2 min window length was used when the wavelet method was applied to field data, as previous tests on simulated data used this window length. A 5 min window was used on the field data for the ARMA method. Practical results from the ARMA method with a 2 min window varied so much that mode frequency and damping identification became unreliable. Choice of window length in practical cases depend on operational use of the small signal results, as well as accuracy and monitoring response requirements.

The periods of greatest inaccuracy in the results coincide

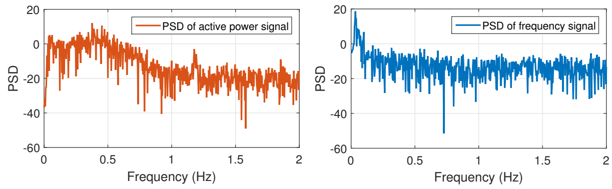

Fig. 16: PSDs of frequency and active power input signals. Active power PSD left. Frequency PSD right.

with periods of reduced generation at the hydro-station, shown in fig. 11. The reduced power transferred over the transmission line results in increased oscillation damping in the system. This is confirmed by the damping result shown in fig. 13 and fig. 15. A higher damping ratio is obtained when generation is decreased. It was shown in section IV-B that the accuracy of both methods degrade with higher oscillation damping, accounting for the reduced accuracy at high damping values.

The frequency content of the measured signals tracked over time can aid the understanding of developing conditions. Increasing energy in a frequency component can be a visually intuitive indication of unstable modes. For the ARMA method, the ARMA spectral estimation is calculated for each window and displayed over time in a surface plot in fig. 17. For the wavelet method, the coefficients from the CWT are similarly plotted over time in fig. 18.

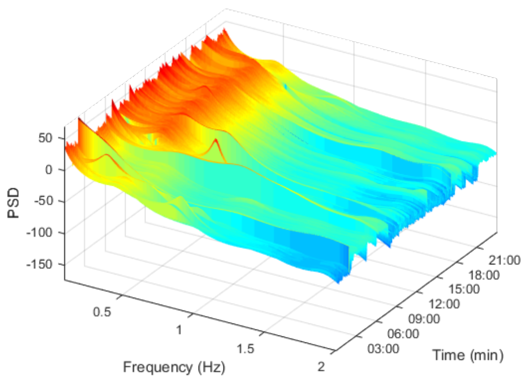

Fig. 17: ARMA spectral estimation over time

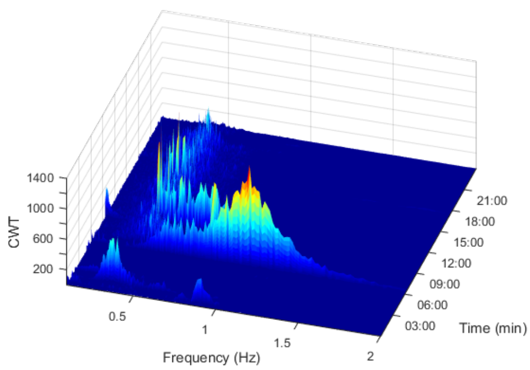

Fig. 18: CWT coefficients over time

The ARMA spectral estimation and the CWT coefficients show the absence of significant energy between 0.1 Hz and 2 Hz when hydro-generation is reduced (early morning). As soon as generation is increased, the inter-area mode is excited at 0.4 Hz. The inter-area mode remains excited when active power transfer is high.

Observe the peak at 1 Hz occurring around 06:00. Both methods identify energy over a large range of frequencies during this time. The energy in these frequency components decay quickly. A rapid increase in active power transfer (see fig. 11), due to the sudden energisation of hydro-generators, lead to a transient behaviour. Due to the damping ability of this power system, the decay is relatively fast.

VI. Conclusion

Two different methods for modal estimation from ambient measured data was evaluated. The performance of the two methods are compared for various simulated reference cases based on the Kundur test system and then subjected to field data.

Both methods identify mode frequency and damping ratio with a delay determined by the window length. The window length requires careful consideration to enable the generation of results, fast enough but still sufficiently accurate, for operational use. Damping result is less accurate than frequency result for both methods. Accuracy is also affected by system damping. Accuracy of both methods improves as inter-area modes become less stable, due to increased energy of the mode.

The ARMA method is much more sensitive to window length than the wavelet method. Accuracy of the ARMA method improves with increasing window length, while the wavelet method results display less sensitivity for different window lengths.

Practical performance of both methods were evaluated by application to field data. Input signal selection is crucial to produce accurate and reliable results. Using multiple signals can help when little is known regarding observability of inter-area modes. Three-dimensional visualisation of inter-area behaviour support the understanding of a change in the dynamic character of the network under observation.

WAMS functionality such as small signal stability monitoring can also be based on PQ instruments with the ability to record synchrophasor data in parallel with PQ parameters. Such innovation could be a valuable and cost-effective approach to additional information on network dynamic performance. The modal analysis methods evaluated requires limited resources in terms of specialised software and data acquisition systems as shown in this paper.

The exclusivity and expenses traditionally associated with application of WAMS for monitoring transmission systems are negated. WAMS can therefore become accessible to many other areas of power system control and operation.

References

[1] U.S.-Canada Power System Outage Task Force, "Final Report on the August 14, 2003 blackout in the United States and Canada: Causes and Recommendations," Tech. Rep., 2004.

[2] G. Ledwich, D. Geddey, and P. O'Shea, "Phasor measurement units for system diagnosis and load identification in Australia," in *IEEE Power and Energy Society 2008 General Meeting, PES*, 2008, pp. 1–6.

[3] J. F. Hauer, W. A. Mittelstadt, K. E. Martin, J. W. Burns, H. Lee, J. W. Pierre, and D. J. Trudnowski, "Use of the WECC WAMS in wide-area probing tests for validation of system performance and modeling," *IEEE Transactions on Power Systems*, vol. 24, no. 1, pp. 250–257, 2009.

[4] J. Turunen, M. Larsson, P. Korba, J. Jyrinsalo, and L. Haarla, "Experiences and future plans in monitoring the inter-area power oscillation damping," in *IEEE Power and Energy Society 2008 General Meeting, PES*, 2008, pp. 1–8.

[5] P. Korba, "Real-time monitoring of electromechanical oscillations in power systems: first findings," *IET Generation, Transmission & Distribution*, vol. 1, no. 1, p. 80, 2007.

[6] P. M. Ashton, G. A. Taylor, A. M. Carter, and H. Renner, "Opportunities to exploit Phasor Measurement Units (PMUs) and synchrophasor measurements on the GB Transmission Network," in *Universities' Power Engineering Conference (UPEC), Proceedings of 2011*, no. September, 2011, pp. 3–8.

[7] V. Venkatasubramanian and H. Khalilinia, "Modal Analysis of Ambient PMU Measurements Using Orthogonal Wavelet Bases," *IEEE Transactions on Smart Grid*, no. 99, 2015.

[8] D. J. Trudnowski and J. W. Pierre, "Overview of algorithms for estimating swing modes from measured responses," in *2009 IEEE Power and Energy Society General Meeting, PES '09*, 2009, pp. 1–8.

[9] M. G. Anderson, N. Zhou, J. W. Pierre, and R. W. Wies, "Bootstrap-based confidence interval estimates for electromechanical modes from multiple output analysis of measured ambient data," *IEEE Transactions on Power Systems*, vol. 20, pp. 943–950, 2005.

[10] J. Turunen, J. Thambirajah, M. Larsson, B. C. Pal, N. F. Thornhill, L. C. Haarla, W. W. Hung, A. M. Carter, and T. Rauhala, "Comparison of three electromechanical oscillation damping estimation methods," *IEEE Transactions on Power Systems*, vol. 26, no. 4, pp. 2398–2407, 2011.

[11] J. C. H. Peng, N. K. C. Nair, J. Zhang, and A. K. Swain, "Detection of lightly damped inter-area power oscillations using extended complex Kalman Filter," in *IEEE Region 10 Annual International Conference, Proceedings/TENCON*, 2009.

[12] G. Liu and V. Venkatasubramanian, "Oscillation monitoring from ambient PMU measurements by frequency domain decomposition," in *Proceedings - IEEE International Symposium on Circuits and Systems*, 2008, pp. 2821–2824.

[13] J. Turunen, L. Haarla, and T. Rauhala, "Performance of wavelet-based damping estimation method under ambient conditions of the power system," in *2010 IREP Symposium*, 2010, pp. 1–9.

[14] D. J. Trudnowski, J. W. Pierre, N. Zhou, J. F. Hauer, and M. Parashar, "Performance of three mode-meter block-processing algorithms for automated dynamic stability assessment," *IEEE Transactions on Power Systems*, vol. 23, no. 2, pp. 680–690, 2008.

[15] T. van Rooyen and J. Rens, "Real-Time Power System Oscillation Monitoring using Synchrophasor Measurements," in *PowerTech, 2015 IEEE Eindhoven*, Eindhoven, 2015.

[16] P. Stoica and R. Moses, *Spectral Analysis of Signals*. New-Jersey: Prentice Hall, 2004.

[17] R. W. Wies, J. W. Pierre, and D. J. Trudnowski, "Use of ARMA block processing for estimating stationary low-frequency electromechanical modes of power systems," *IEEE Transactions on Power Systems*, vol. 18, no. 1, pp. 167–173, 2003.

[18] G. Liu, J. Quintero, and V. Venkatasubramanian, "Oscillation monitoring system based on wide area synchrophasors in power systems," in *2007 iREP Symposium*, 2007.

[19] M. Hemmingson, "Power System Oscillations Detection Estimation & Control," Ph.D. dissertation, Lund University, 2003.

[20] T. van Rooyen, J. Rens, and J. Desmet, "Field Performance of Ambient Modal Estimation in Small Signal Stability," in *2015 IEEE International Workshop on Applied Measurements for Power Systems (AMPS 2015)*, Aachen, Germany, sep 2015.

A.4 Conference Proceedings - AMPS 2014

A paper was submitted for the IEEE AMPS 2014 conference in Aachen, Germany titled "Where is the power of the IEEE 1459-2010?". The paper was accepted for publication in the conference proceeding and presented. The full paper is attached.

The paper explores the possibility of including the IEEE 1459 power definition parameters with the parameters measured according to the IEC 61000-4-30 PQ standard. It is shown that the IEEE 1459 parameters can easily be calculated from already available parameters of the IEC 61000-4-30 measurement methodology. Practical benefit to the use of these parameters are illustrated.

The topic of this paper does not have the same focus as the work done in the research, however the data used in this paper was measured by the same instrumentation as was used here. The versatility of the measurement instrument is illustrated by calculating the IEEE 1459 parameters.

Where is the power of the IEEE 1459-2010?

Johan Rens
School for Electrical and Electronic Engineering
Potchefstroom Campus of the North-West University
Potchefstroom, South Africa
johan.rens@nwu.ac.za

Tian van Rooyen, Francois de Jager
School for Electrical and Electronic Engineering
Potchefstroom Campus of the North-West University
Potchefstroom, South Africa

***Abstract*— The integration of the IEEE 1459-2010 power definitions with the IEC 61000-4-30 PQ standard is investigated. A Class A PQ instrument, which record network coherent data with an absolute time uncertainty of less than 100 ns, is used to analyse and evaluate this opportunity. This paper then propose how the usefulness of the IEEE 1459-2010 parameters to better understand the performance of a modern power system in addition to PQ characterisation.**

Keywords—Power definitions, IEEE 1459-2010; IEC 61000-4-30; network coherent data; synchrophasors, PQ

I. INTRODUCTION

The contribution to power theories have been well documented in literature with the first examples starting nearly a century ago. With better understanding of the fundamental physical phenomena, some concepts have been discredited and others improved.

A well-known example is the 1927 Budeanu [1] reactive power definition under non-sinusoidal waveform conditions. L.S Czarnecki [2] demonstrated the deficiencies in the Budeanu theory in 1987. Similar disclaimers and alternatives to the Budeanu approach followed, but the summation of reactive powers in all harmonic components are still in widespread use although the constraints to the usefulness thereof to engineers is known.

Emanuel [5] has (and still does) for many decades advocated the importance of the positive sequence reactive power by explanation of underlying theoretical principles and by practical examples. Evidence of commercial instrumentation recognising this important aspect and of engineers applying the principles, are still not seen.

The operation of a power system requires network performance information to be used by engineers for operational requirements (to manage Quality of Supply for example) whilst the business processes need this information for the billing/financial information. Different instrumentation with different measurement class specification is used by electrical utilities to measure Quality of Supply and energy.

Billing instruments will not inform the user on the mathematical detail on for example, how reactive power and power factor were calculated, the user has only to ascertain the certification of class performance as required by local authorities, and then accept that value as a true reflection of the useless power. The quality, by which that electrical power was supplied, is made visible by Power Quality (PQ) instrumentation. It can be certified to record data according to IEC 61000-4-30 (for example) requirements.

This IEC 61000-4-30 standard was historically a Quality of Supply (QoS) standard for the measurement of voltage based parameters to be used in the assessment of the compatibility between supply conditions and user equipment. The same standard can also address the measurement of current parameters and is proposed to be included in the latest draft version [6]. It will enable the production of voltage and current data that are repeatable and comparable, regardless of the instrument manufacturer (if the instrument in use is certified to be a Class A PQ instrument, for example).

Engineers require a practical approach to the operational performance of a power system. It should include both PQ parameters and power phenomena. PQ and energy has to be analysed simultaneously, and in context, to fully understand the physical phenomena pertaining.

A power theory, which can support the above, has to allow simple implementation by industrial measurement equipment. Modern PQ instrumentation (and energy meters) could provide that visibility on both the PQ and energy performance of the power system.

The IEEE 1459-2010 [5] sets a practical approach to the definition of power under nonsinusoidal and asymmetrical waveform conditions. Literature has confirmed the usefulness of this approach but no evidence is seen that energy billing, PQ instrumentation or related technical standards are recognising or promoting the IEEE 1459-2010 approach, although the power definitions are simple and straightforward.

Most industrial measurement platforms should have the memory and processing power to include the IEEE 1459-2010 parameters. The IEEE 1459-2010 can be a useful universal agreed-upon approach for inclusion by both PQ and billing standards.

In this paper, an instrument designed as a Class A IEC 61000-4-30 voltage and current PQ recorder was used to investigate the possibility of implementing the IEEE 1459-2010 power definitions as an additional option to engineers when analysing a practical power quality problem.

II. THE IEEE 1459-2010: A PRACTICAL APPROACH

Sound physical explanation of power phenomena in a modern 3-phase power system under non-sinusoidal and asymmetric waveforms conditions were done by means of the electromagnetic laws. The Poynting vector was shown by Emmanuel *et al* [3] to be helpful in understanding physical phenomena. Sophisticating in mathematical analysis of 4-conductor 3-phase systems was enhanced by a space-vector transform proposed by Ferrero et al [4].

The IEEE 1459-2010 [5] describes a less mathematical intense but practical approach to the definition of powers in a power system with non-sinusoidal asymmetrical supply voltages and unbalanced non-linear load currents, for both 4-wire and 3-wire cases. The principles and mathematical formulation enables straightforward implementation in digital instrumentation.

A high resolution in time-stamping digital samples of voltage and current present the opportunity to a different understanding of power phenomena as traditional Phasor Measurement Unit (PMU) functionalities can now be extended to the harmonic frequencies and integrated with the IEC 61000-4-30 parameters. The ability to calculate the IEEE 1459-2010 parameters coherently at different points in the network should further innovative application of the results.

III. IEC 61000-4-30 CAN INCLUDE THE IEEE 1459-2010

Data acquisition, calculation and time aggregation of PQ parameters by a Class A PQ instrument is specified by IEC 61000-4-30 standards document. Although utilities sell "voltage", the management of minimum standards in Quality of Supply (QoS) is not possible in a modern power system without understanding the withdrawal of current.

Users increasingly make use of the sophistication in equipment made possible by the direct conversion and control of electrical energy. The principle of operation of the solid-state electronics that interface with the electrical network is inherently non-linear which do affect the sinusoidality of voltage waveforms as the harmonic load currents are withdrawn through non-zero supply impedances. Nonsinusoidal and asymmetrical waveform conditions in a power system are characteristic of a modern power system, especially at distribution voltage levels.

With the latest draft version of the IEC 61000-4-30 acknowledging current parameters, comprehensive characterization of a 3-phase power system can be done by the approach of the IEEE 1459-2010 in addition to the IEC PQ parameters. It is straightforward due to the signal acquisition and processing principles used in modern PQ, billing and Phasor Measurement Units (PMU's).

A. The 3-phase power system as a single entity

The "effective" values in voltage (V_e), current (I_e), apparent power (S_e), power factor (PF_e), Total Harmonic Distortion in Voltage (THD_V) and Total Harmonic Distortion in Current (THD_I) recognise the 3-phase power system as a single entity [6]. It qualifies and quantifies the impact of nonsinusoidal and asymmetrical waveform conditions on the quality of electrical energy in a practical manner.

The basic measurement principle of the IEC 61000-4-30 [6] is based on digital samples representing 10 or 12 fundamental cycles of the voltage waveform for 50 or 60 Hz respectively to attain a 200 ms window of data. It is referred to as the 10/12 cycle block principle.

Rules to attain 1280 samples per 10/12-cycle block of data inclusive of possible changes in instantaneous frequency [7] of the voltage signal (position of zero crosses can change cycle by cycle) is acknowledged in the IEC standard. Frequency content of the voltage (and current) waveform obtained by this 10/12 cycle block principle is a "best", but also practical, representation of the real-life phenomena in a power system.

With harmonic content of both voltage and current now available, the calculation of rms values per phase for voltage and current is specified by the IEC 61000-4-30. The calculation of effective 3-phase voltage, current and other IEEE 1459-2010 values per 10/12-cycle block requires minimal additional computational effort. A summary of the parameters proposed (in addition to the IEC 61000-4-30 and shown for the 3-wire case only) is listed in Table I.

A comprehensive resolution of effective apparent power [5] in a modern power system is depicted in Fig. 1. Observe the resolution of the non-active apparent power (S_{eN}) into distortion power due to current harmonics (D_{eI}), distortion power due to voltage harmonics (D_{eV}) and the harmonic apparent power (S_{eH}) due to the interaction of both voltage and current harmonics.

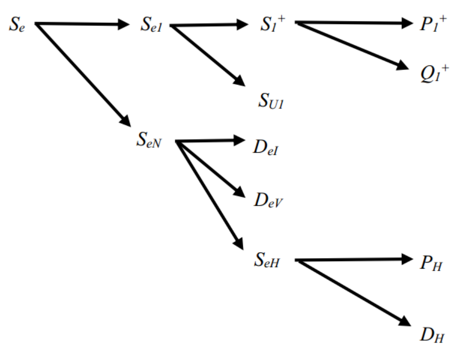

Fig. 1. IEEE 1459-2010 resolution of three-phase effective apparent power

With QoS management being complimented by the inclusion of the IEEE 1459-2010 parameters listed in Table I, the reason for QoS management can change. It will not only be in the measurement of QoS parameters to report on the compliance to regulatory requirements. QoS management can become an operational risk management tool in the day-to-day operation of the power system, as the PQ performance of the network in context of the energy phenomena has to be valuable.

Billing instruments will also benefit as the IEEE 1459-2010 energy resolution will enable a "true" reflection of energy phenomena; specifically the correct measurement of useless (reactive) power.

TABLE I. IEEE 1459-2010 PARAMETERS TO COMPLIMENT PQ AND ENERGY PARAMETERS[1]

V_e	$V_e = \sqrt{\frac{\sum_h(V_{abh}^2 + V_{bch}^2 + V_{cah}^2)}{9}}$
V_{e1}	$V_{e1} = \sqrt{\frac{V_{ab1}^2 + V_{bc1}^2 + V_{ca1}^2}{9}}$
$\boldsymbol{V}_1^+$ $\boldsymbol{I}_1^+$	Positive sequence voltage and current phasor of the 50/60 Hz 3-phase voltage and current phasors
V_{eH}	$V_{eH} = \sqrt{V_e^2 - V_{e1}^2}$
I_e	$I_e = \sqrt{\frac{\sum_h(I_{ah}^2 + I_{bh}^2 + I_{ch}^2) + \sum_h I_{nh}^2}{3}}$
I_{e1}	$I_e = \sqrt{\frac{I_{a1}^2 + I_{b1}^2 + I_{c1}^2}{3}}$
I_{eH}	$I_{eH} = \sqrt{I_e^2 - I_{e1}^2}$
THD_V	$THD_V = \frac{V_{eH}}{V_e}$
THD_I	$THD_I = \frac{I_{eH}}{I_e}$
S_e	$S_e = 3V_eI_e$
S_{e1}	$S_{e1} = 3V_{e1}I_{e1}$
S_{eN}	$S_{eN} = \sqrt{S_e^2 - S_{e1}^2}$
D_{eV}	$D_{eV} = THD_V S_{e1}$
D_{eI}	$D_{eI} = THD_I S_{e1}$
S_{eH}	$S_{eH} = THD_V THD_I S_{e1}$
S_1^+	$\boldsymbol{S}_1^+ = \boldsymbol{V}_1^+ \boldsymbol{I}_1^+ = P_1^+ + jQ_1^+$
PF_e	$PF_e = \frac{P_{3\Phi}}{S_e}$
PF_1^+	$PF_1^+ = \frac{P_1^+}{S_1^+}$
S_{u1}	$S_{u1} = \sqrt{S_e^2 - (S_1^+)^2}$

IV. THE POWER OF THE IEEE 1459-2010

It is expected that the resolution of the effective apparent power will help engineers to better understand the effect of voltage and current waveform distortion, asymmetry between the phase voltages and in unbalance of load currents withdrawn. Also, with the different power components and PQ parameters measured coherently all over the network, the assessment of emission (harmonics, unbalance) should benefit.

A. *Demonstration on the usefulness of D_{eV}, D_{eI} and S_{eH}*

A high-level sensitivity analysis of the voltage distortion power (D_{eV}), current distortion power (D_{eI}) and harmonic apparent power (S_{eH}) was done under controlled experimental conditions. A CMC 256plus™ instrument was configured to generate voltage and current waveforms. An IEC 61000-4-30 Class A PQ instrument measured the 10/12 cycle block parameters of both voltage and current. The IEEE 1459-2010 parameters listed in Table I was calculated in addition to the IEC 61000-4-30 parameters and aggregated to 3-second values.

Test 1 and 2 are hypothetical as a purely sinusoidal supply voltage is rare at distribution voltage level in an industrial area and the withdrawal of purely sinusoidal load currents when supplied by a nonsinusoidal voltage, is also not possible. It serves only to demonstrate the principles at discussion.

Test 3 and 4 make use of both distorted voltages and currents. The maximum effective apparent power S_e with V_e at 110 V and I_e at 5 A, is 1650 VA.

B. *Measurement results*

Minimal additional computational effort was required to find the IEEE 1459-2010 values for D_{eI}, D_{eV} and S_{eH} as the IEC 61000-4-30 parameters calculated every 10/12-cycle block can be directly used in Table I.

Test 1: Current distortion power (D_{eI}): With phase voltages perfectly sinusoidal and symmetrical in both amplitude (110 V rms) and phase displacement, THD_I (in each phase) was emulated as the characteristic current harmonics withdrawn by a 6-pulse diode rectifier. With harmonic currents introduced, the total rms current had to be less than 5 A. The rms values of the individual current harmonics and the fundamental were changed from 0.2 to 1.0 p.u. Harmonic currents withdrawn by a 6-pulse rectifier (resistive load) will result in a THD_I of 30.2% when supplied by a pure sinusoidal voltage.

The results shown in Fig. 2 are expected, as the linear relation between D_{eI} and current harmonics is evident in the calculation ($D_{eI} = THD_I S_{e1}$) thereof. THD_I remain fixed as both the fundamental and harmonic currents changed when the loading of the 6-pulse rectifier is adjusted. Harmonic apparent power S_{eH} and voltage distortion power D_{eV} remained zero.

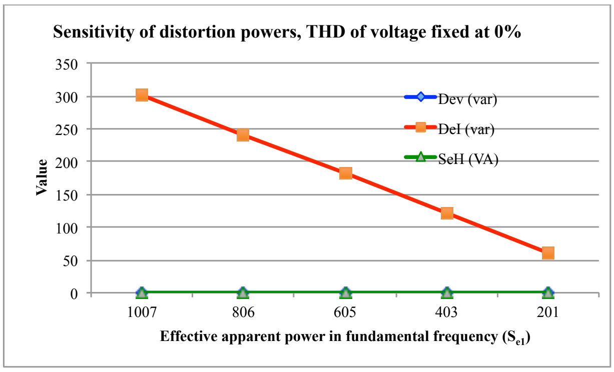

Fig. 2. THD_I and S_{e1} dictate D_{eI}

Test 2: Voltage distortion power (D_{eV}): With line currents perfectly sinusoidal (50 Hz current at 5 A rms per phase) and symmetrical in both amplitude and phase displacement, THD_V was adjusted by the variation of voltage harmonics (in each phase) up to the maximum values allowed by the IEC 61000-3-6 for individual harmonics. The 50 Hz component was fixed at 110 V rms. The harmonic voltages were then changed relative to the 50 Hz voltage and to not result in a maximum THD_V of more than 8%, a limit value in voltage waveform distortion for networks operated up to 33 kV in Southern Africa.

Similar to Fig. 2, the results in Fig. 3 are expected; D_{eV} is linearly related to the voltage waveform distortion with S_{eH} and D_{eI} zero.

[1] An italic symbol indicates a variable. If bold, it is a complex value such as a phasor with magnitude and phase angle.

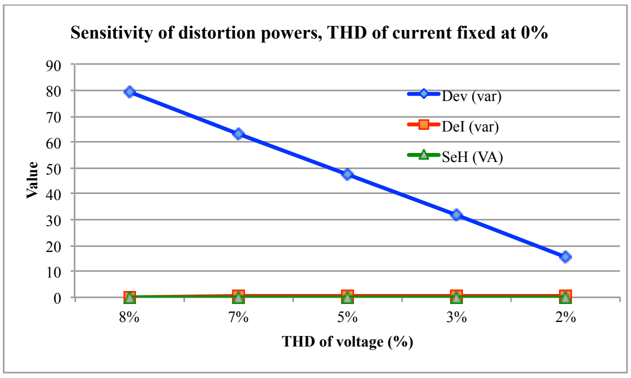

Fig. 3. Voltage waveform distortion linearly relate to D_{eV}

Distortion in both voltage and current can be expected in practical distribution systems, as the supply impedance sustaining harmonic load currents will result in voltage harmonics. Distortion power in current, voltage and harmonic apparent power will result.

Test 3: With THD_V first fixed at 8%, the loading was changed from 0.2 to 1.0 p.u. As both the fundamental and harmonic currents changed, THD_I did not change.

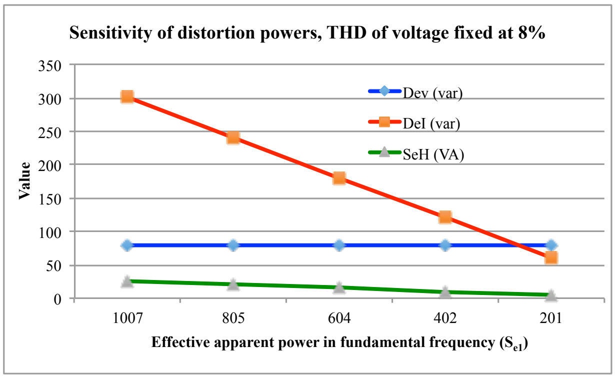

Fig. 4. D_{eI} are only dictated by S_{e1}

Test 4: With THD_I and loading fixed, THD_V (in each phase) changed from 2% to 8% with the individual voltage harmonics within the IEC 61000-3-6 compatibility levels.

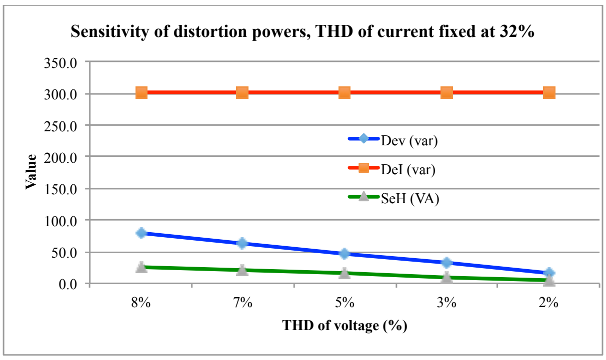

Fig. 5. The relation between THD_V, D_{eV} and S_{eH}

Although the variation in THD_V is relatively small, a variation in D_{eV} and S_{eH} is detectable in Fig. 5.

V. Discussion of Results

The resolution of effective apparent power into the components contributing is straightforward if the measurement rules of the IEC 61000-4-30 are applied. A detectable change in current distortion power (D_{eI}), voltage distortion power (D_{eV}) and in harmonic apparent power can support the better understanding of harmonic emission as both the supply and loading system can contribute to the THD_V at a Point of Common Coupling (PCC). The IEEE 1459-2010 resolution of apparent power isolates the contribution of voltage and current harmonics (harmonic pollution) in a practical manner.

Minimal additional computing power was required to calculate the IEEE 1459-2010 parameters in addition to the IEC 61000-4-30 parameters. Similarly, minimal additional requirements on memory and communication bandwidth result by the aggregation to 3-sec and 10-min values.

If the measurements are taken coherently all over the network, the analysis of the IEEE 1459-2010 energy parameters in context of the IEC 61000-4-30 PQ parameters seems to enable a valid conclusion on the relative contribution by distorting sources to THD_V. It is expected that the analysis of asymmetrical voltage conditions will also benefit as both the supply system and the unbalance in loading contribute. S_{u1} in Table I can be helpful in such analysis.

VI. Conclusion: The Power of the IEEE 1459-2010

If instrumentation is distributed all over a network producing network coherent data, many possibilities arise. The accurate time-stamping of a modern PMU integrated with a Class A PQ recorder which also record IEEE 1459-2010 parameters will fully exploit the value of PQ and energy parameters. The performance of different points in the network can be analysed in geographical and chronological context to better understand cause and effect.

For example, the management of emission (harmonics and unbalance) by sources should benefit by the synchronous measurement of D_{eI}, D_{eV} and S_{u1}. It is common practice in PQ management to allocate a level of emission to a source known to have the ability to contribute to voltage harmonics and asymmetry. Standards documents do propose methodologies on how to do the allocation, but a scientific sound method to isolate the contribution of a single source of distortion or unbalance with these sources distributed all over the network, requires network coherent data [10].

When emission has been allocated, the utility has to verify and monitor the agreement. A measurement methodology based on network coherent data in the assessment of PQ (IEC 61000-4-30) and complimented by a practical resolution of the energy phenomenon pertaining (IEEE 1459-2010), should be useful to the utility in assessing the emission. PQ and energy measurement standards can therefore exploit the power of the IEEE 1459-2010.

VII. References

[1] Budeanu G., "Reactive and Fictitious powers", *Rumanian National Institute, (Bucharest, Rumania),* 1927, *publication no* 2. Also, "The different options and conceptions regarding active power in non-

sinusoidal systems”, 1927, *Rumanian National Institute, publication no* 4

[2] Czarnecki L.S., “What is wrong with the Budeanu Concept of Reactive Power and Distortion Power and why it should be Abandoned” IEEE Transactions on Instrumentation and Measurement; Vol. IM-36, no. 3, September 1987, pp. 834-837.

[3] Čakareski Ž., Emanuel A., “Poynting Vector and the Quality of Electric Energy.”, ETEP, vol. 11, no. 6, November/December 2001, pp. 375–382

[4] Ferrero A., Giuliani G., Willems L., “A New Space-Vector Transformation for Four-Conductor Systems”, ETEP, vol. 10, no. 3, May/June 2000, pp. 139-144

[5] Emanuel, A., “Power definitions and the physical mechanism of power flow”, *Wiley*, 2010

[6] IEC 61000-4-30, Power quality measurement methods, in preparation

[7] M.H. Bollen, I.Y.H Gu, Signal Processing of Power Quality Disturbances, New York: Wiley, 2007

[8] R. Neuman, “The importance of IEC 61000-4-30 Class A for the Coordination of Power Quality Levels”, in Proc. 2007 Electrical Power Quality and Utilisation Conf.

[9] M. Albu, G.T. Heydt, "On the use of RMS values in power quality assessment" IEEE Transactions on Power Delivery, vol. 18, pp. 1586 – 1587, 2003

[10] APJ Rens, PH Swart; “On Techniques for the Localisation of multiple distortion sources in three-phase networks: time domain verification”, European Transactions on Electrical Power, Vol. 11, No. 5, September/October 2001, pp. 317 – 322.